Fabrication of cantilever chip with complementary micro channel system in SU-8 for biochemical detection

Tenje, Maria

2004

Fabrication of Cantilever Chip with Complementary Micro Channel System in SU-8 for Biochemical Detection

M.Sc. Thesis

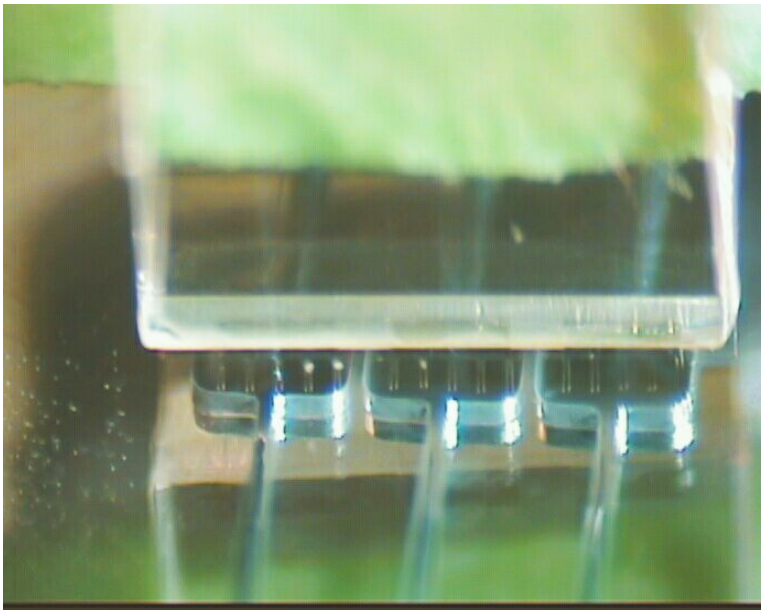

Maria Nordström

Supervisor: Dr. Montserrat Calleja, MIC, DTU
Lektor Carl-Erik Magnusson, Fysicum, Lund University

January 2004

Abstract

This thesis presents the works on fabrication and measurements done with micro cantilevers and a micro channel system, fabricated in the photo-resist SU-8. SU-8 is a polymer patterned by UV lithography which offers a cheap and fast processing and is an interesting alternative to standard Si techniques. For the structures intended here, it proved to be a well suited material and promising results were obtained.

The project involved the design of one cantilever chip with arrays of cantilevers structured into three sections of five cantilevers each and one micro channel chip, which were batch fabricated. The cantilevers are used for biochemical detection by surface stress measurements with optical read-out. Together, the two chips can be used for specific molecular detection for research oriented or medical purposes. The cantilevers proved to be very sensitive and DNA immobilisation detection was achieved. The channels are an essential component in this system for easy handling of the solutions to be investigated and sensitising of the cantilevers prior to the measurements.

To achieve the above results, several experiments were performed, investigating the surface properties of SU-8. Little has until this point been known about the surface properties of the the photo-resist and several key pieces of information were obtained, which proved to be crucial in the project.

Here, the work involved in the design and fabrication of both chips is described in detail. Also, the work on the surface investigations is presented and indications of necessary further work is given. A brief description of the measurements done is also included in the Thesis.

Preface

This Master Thesis represents the work of my project to obtain a Master of Science degree at Lund University. I carried out the work, as a guest student, at MIC - Institute of Micro and Nanotechnology at the Technical University of Denmark, DTU.

The project was built on three separate but intertwined courses. The major part of the project was the course FYS292 entitled 'Fabrication of polymeric cantilever array', corresponding to 30 ECTS points and representing the essential project work to obtain a Swedish Master's degree. Secondly, the project continued with the course entitled 'Polymeric micro channels for biomedical applications', FYS291, corresponding to 15 ECTS points. Finally, the course 'A study of wettability properties of SU-8', FYS293, also corresponding to 15 ECTS points was taken. The project was completed in a period of 40 weeks, between April 2003 and January 2004.

The courses were closely related and all work is presented in this thesis. As a guideline, Chapter 2 provides general background to the complete work where the material SU-8 is discussed. Chapter 3 represents the major part of the course FYS292 and Chapter 4 represents the major part of the course FYS291. The work involved in FYS293 is presented in Chapter 5. The final results of the work contributed to by all three courses is seen in Chapter 6, where the two chips have been used in combination for actual measurements.

Throughout the project, in all courses, both theoretical calculations as well as practical work was included. Equal amount of clean room work was involved in all three courses.

In my work, I had the opportunity to be a part of the Bioprobes group at MIC, with group leader Lektor Anja Boisen. I would like to thank all people in the group for a fantastic working environment. Particularly, I would like to thank Alicia Johansson and Lauge Gammelgaard for sharing the experiences with SU-8, it was always very helpful to draw upon each others' experiences. I would like to thank Peter Rasmussen for help with the theoretical approach to SU-8 and Maria Holmberg for helping me with AFM measurements. A Thank You goes to Rodolphe Marie for invaluable help with the chemistry side of the project, as well as equipment for the fluorescence measurements.

I also greatly appreciate all the help with the analysis of the XPS measurements and the time put in for Matematica programming. I would also like to thank Esko Forsén for making the train journeys between Malmö and Lyngby enjoyable and Anja Boisen for keeping such a stimulating working atmosphere in the group and helping me out whenever it was needed. Most of all, I thank Dr. Montserrat Calleja for being a fantastic and supportive supervisor, full of ideas at all times.

I would also like to thank Lektor Carl-Erik Magnusson at Fysicum, Lund University, for pointing me in the right direction and helping me with many administrative tasks during this period of time.

For my surface investigations of SU-8 I had the chance to work with people at different departments to myself at DTU. I would like to start with thanking Brian Bilenberg for help with preparing the bond strength samples and getting me in touch with Associate Professor Bjarne Clausen at IPL, whom I would like to thank for helping me with the actual pull-test experiments done.

Also, I would like to thank Institute Leader Ib Chorkendorff and Lab Technician John Larsen at ICAT for helping me with XPS measurements and analysis.

I also thank Project Leader Henrik Bruus and his group, Microfluidics Theory and Simulation, for clarifying discussions on micro fluidics in the initial stage of the project.

I also owe thanks to the staff at MIC, both administrative and scientific. The Cleanroom Technicians always encountered any of my wishes with a friendly approach, and for that I am very greatful. For the good working environment, I would like to thank the MSc students in student room 115, especially Mathias Lunde, with invaluable EPS/PDF support and all the rest of you for some good laughs and Danish lessons.

Lastly, I thank Niklas for always being great.

Maria Nordström
January 9th, 2004
Lyngby

Contents

List of Figures

List of Tables

Chapter 1

Introduction

1.1 Cantilevers for biochemical detection

Cantilevers were first developed as components of the scanning force microscope (SFM) and atomic force microscope (AFM) used to investigate the typography of samples on the nano scale [1, 2]. The interaction between the cantilever tip and the substrate surface is monitored via laser beam reflection and an informative image can be built up, scanning over a specific area, Figure (1.1).

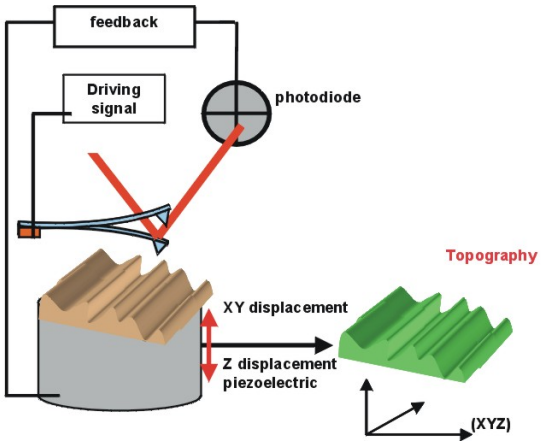

Figure 1.1: The cantilever scans over the sample surface and the reflection of the laser off the back of the cantilever generates an image of the typography of the surface.

Later, this technique was developed to be used for surface stress measurements on the cantilever [3]. The measurements can be of either dynamic or static kind. In dynamic measurements the change in resonance frequency upon the addition of masses is detected [4, 5]. Systems like these are most commonly used for gas detection [6]. In static measurements, the bending of

the cantilever due to changes in surface stress upon heat changes or chemical reactions is detected. This technique is used for chemical detection in liquid solutions. The advantages of biomolecular detection by cantilever motion is that the detected molecules do not need to be labelled by fluorescence or radioactive tags or any other method, Figure (1.2). Different approaches have been developed for the read-out method of the detected results and mostly the laser beam reflection detection method from the AFM technique, Figure (1.1), is used. Within the Bioprobes group, piezo-resistive read-out has been designed and realised as an alternative [7].

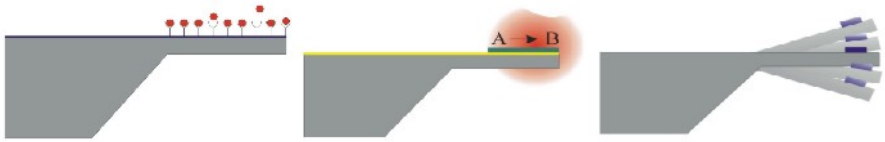

Figure 1.2: The cantilevers can be used for biochemical detection by different principles. In static detection the bending of the cantilever is measured as a result of surface stress changes. *Left:* This can arise from the binding of molecules. *Center:* It can also arise from temperature changes due to chemical reactions. *Right:* In dynamic measurements the change in resonance frequency is observed. [8].

The cantilevers fabricated in this project are all intended for surface stress measurements in a set-up with optical read-out. The measurements performed with the chips are described in detail in Chapter 6.

When molecules bind to a surface, they induce a surface stress. To achieve a difference in the surface stress on the cantilever, the two surfaces must be different. This can be obtained by sensitising one of the surfaces of the cantilever with a different molecule. Upon introducing complementary molecules, these will only bind to the sensitised side of the cantilever, resulting in a surface stress change and in turn a bending of the cantilever. The cantilever can also be coated with a specific material which the introduced molecules will bind to, for example; the self-assembly of thiolated alkanes on Au surfaces or the selective binding of mercury to Au [9, 10]. By using a bimetallic cantilever, heat fluxes caused by chemical reactions can be detected by the bending of the cantilever, due to the different co-efficients of thermal expansion, of the two metals [11]. In these types of measurements, it is important to use *reference cantilevers*, as small changes in pH, ion concentration, refractive index or temperature of the measuring solutions can dramatically influence the deflection signal [12]. Therefore, the aim of the project is to fabricate an array of cantilevers on the same chip where some can serve as reference cantilevers.

1.1.1 Origin of surface stress

The assembly of molecules often causes compressive stress on the surface in question [6]. H.-J. Butt has done serious work on the surface stress detection [13]. If the surface stress of one side of the cantilever increases, this side will contract.

Free-hanging micro cantilevers are well suited for these type of measurements as the deflection is directly proportional to changes in surface stress and they have a very high resonance frequency. Due to the high resonance frequency, the cantilevers will not be actuated by vibrations from external equipment and human noise [14]. The spring constant of the cantilever is directly proportional to the Young's modulus of the material and the dimensions. Fabricating micro sized cantilevers in a material with a low Young's modulus greatly increases the sensitivity.

The reports discussed above have been produced on the molecular detection, but the origin of the surface stress is not investigated. Wu *et al.* have done work on this with hybridisation of DNA on cantilevers and conclude that the surface stress is a result of the interplay between changes in configurational entropy and intermolecular energetics induced by specific biomolecular interactions [15]. From their measurements they show that repulsive interactions between single-stranded DNA (ssDNA) immobilised on the top of the cantilever, create a compressive stress which bends the cantilever downwards. After the injection of complementary ssDNA strands and hybridisation the cantilever bends upwards, showing the release of the compressive stress generated in the first step. Upon immobilisation, each ssDNA strand is forced to occupy a region of space smaller than its natural size and to minimise the clustering effect, the DNA makes the cantilever bend downwards to increase the surface area available. After hybridisation, the cantilever bends upwards as double-stranded DNA (dsDNA) requires a smaller region of space due to its more rigid structure. They also conclude that electrostatic repulsion between neighboring DNA molecules play a role in the cantilever motion. These findings can be applied also to other molecules such as antigen-antibody or protein-ligand reactions.

By the use of an array of cantilevers, some of the cantilevers can be sensitised with the complementary molecule and thereby, only those will react with the introduced detection molecule.

Using a laser set-up with multiple lasers, the bending of each cantilever can be detected separately. This means the out-put signal generated can be greatly enhanced as the effects of noise and laser drift can be subtracted. It proved very hard to fabricate cantilevers with no initial bending and even harder to fabricate a chip with all cantilevers perfectly aligned. With advances in the fabrication procedures, there are good hopes for a perfectly

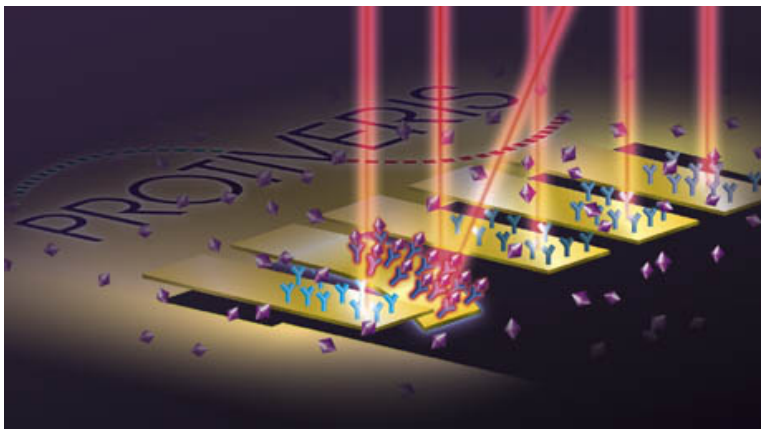

Figure 1.3: By using a set-up with multiple lasers, the bending of several cantilevers can be detected simultaneously [16].

aligned array to be fabricated in the near future. Some cantilevers will then be used for the biochemical detections and the contribution of noise to the signal can be subtracted from the reference cantilevers.

1.1.2 Previous work in the area

Cantilever detection has been used for DNA analysis [17], antigen-antibody detection [18] and protein-ligand detection [19]. The cantilever can be used both for detection in liquid (as the examples above) and in gases [6]. For measurements in liquids, it is more favorable to use changes in surface stress than resonance frequency, due to the high degree of damping of the cantilever [20].

Fritz *et al.* were among the first to report on DNA detection on cantilevers. They have reported on hybridisation of DNA resulting in a surface stress of 5 mNm^{-1} [17]. By the measurements they can detect a single base pair mismatch in a 12-base pair sequence. Meyer *et al.* have reported on a technique were bending of 10^{-4} Å can be detected by laser beam deflection [21].

In our measurements, the antibody of the pesticide Carbaryl was detected; work that has never been done before.

1.2 Micro channel system

The micro channel chip is fabricated to be used in sensitising the cantilevers for specific detections. Biochemical detection with cantilevers is very efficient and only requires small amounts of detection sample, these channels comprise 10 µL for reliable detection results.

1.2.1 Previous work in the area

Most micro channel systems are evolved within the Micro Total Analysis System, μTAS, and Lab-on-a-chip areas. Chips of that kind are intended to handle and analyse different fluids and specific chemical reactions, including every step from sample pre-treatment to final results, on a single chip. The read-out method is incorporated in the chip, usually as some micro fluidic devices. These developments were initiated by the works of A. Manz [22].

Systems for electrophoretic separation of DNA, diffusion-based extraction and micro mixers have all been realised [23, 24, 25]. To fabricate such devices, complicated process procedures are needed. Here, a simple and purpose oriented micro channel system should be fabricated. To my knowledge, no such chip - with this specific function - has been fabricated before.

1.3 Goals of project

The goals of this Master project is to design and fabricate a microchip with one or more arrays of cantilevers. The cantilevers should be used for biochemical detection by surface stress measurements with optical read-out. The measurements will be done in collaboration with the Optoelectronics and Nanomechanics Biosensor Group at CNM-CSIS, Madrid.

Also, a micro channel system should be designed and fabricated on another chip. This system will be used to sensitise the cantilevers for the intended measurements.

Here the new material SU-8 is presented. SU-8 is a low-cost polymer with a low Young's modulus which offers a good alternative to conventional Si_3N_4 cantilevers. Both the cantilever chip and the micro channel system will be fabricated in SU-8. In the project, properties of SU-8 will need to be investigated to better understand the processing and final results.

1.3.1 Outline of thesis

In Chapter 2 the general properties of the structuring material, SU-8, is presented, along with the fabrication sequence. In Chapter 3, the exact fabrication sequence of the cantilever chip and the principle behind surface stress measurements with cantilevers using optical read-out is described. In Chapter 4, the design and fabrication of the channel chip is analysed and the importance of the contact angle of the material is highlighted. In Chapter 5, the difference surface investigations of SU-8 are presented. These involved both work in the clean room at MIC but also collaborations with different institutes at DTU. The measurements done with the final fabricated chips are presented in Chapter 6. Chapter 7 provides a conclusion on this work and an outlook of the future of SU-8 as structuring material for cantilevers and micro channels.

Chapter 2

SU-8

This chapter will introduce and describe the material with which this work has been carried out.

SU-8 is a polymer developed by IBM for the semiconductor industry [26]. It is a negative photo-resist which cross-links upon UV exposure. As SU-8 is very chemically resistent, it can be used not only as a patternable layer but as a component material. The use of polymers as component materials has gained an enormous interest due to its fast processing and reduction in fabrication costs. It offers a flexible platform for component design and has wide applications, which makes it very interesting as it is also compatible with standard Si processing equipment. Previously, cantilever probes for scanning force microscopy (SFM) have been fabricated in SU-8 [27]. Here; work on fabricating cantilevers for biochemical detection in SU-8 will be presented.

The chemistry of the polymer and its mechanical properties will be described in Section (2.1). The different steps involved in the fabrication of the polymer will be run through in Section (2.2). The issue of stress will be discussed in Section (2.3).

2.1 Chemistry and properties of SU-8

The chemical name of SU-8 is glycidyl ether of bisphenol A, which is a derivative of EPON® available from Shell Chemical [26]. The monomer offers the highest epoxy functionality commercially available, of eight epoxy groups per monomer, Figure (2.1). It is the epoxy groups that are involved in the cross-linking process, initiated by UV exposure. The high epoxy density increases the cross-linking density and thereby the hardness of the final, hard baked polymer. It is possible to dilute the polymer to get different viscosities. We have worked with controlled concentrations of SU-8, commercially available from MicroChem [28]. SU-8 is developed in two forms;

the 50-series, which uses the solvent γ-butyrolacetone and the 2000-series, which is based on the solvent cyclopentanone. In this project, all work has been carried out with SU-8 from the 2000-series, due to its improved coating and adhesion properties [28]. Three different SU-8 dilutions have been used; SU-8 2002 with 29 %, SU-8 2005 with 45 % and SU-8 2075 with 74 % SU-8 in solvent.

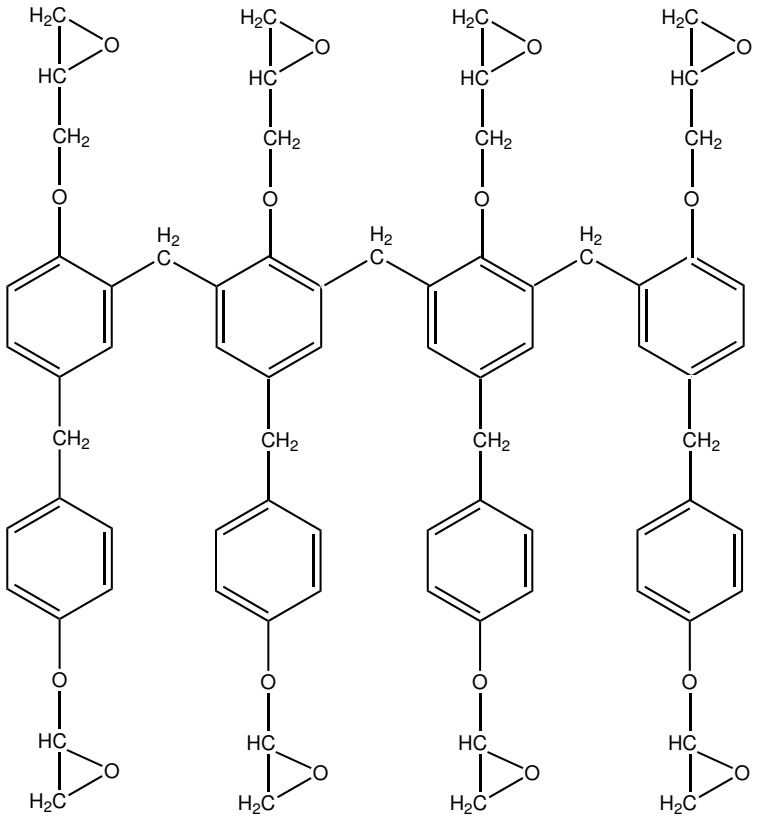

Figure 2.1: The chemical structure of the SU-8 monomer. It is the epoxy groups (–CH–O–CH_2–) at the ends which are involved in the cross-linking of the polymer, forming a ladder-like structure.

SU-8 is a chemically amplified resist where the onium salt triaryl sulfonium, Figure (2.2), is added. This salt disintegrates upon UV exposure and generates an acid which initiates cross-linking of the polymer when heated. The non-cross-linked SU-8 can dissolve in Propylene Glycol Methyl Ether Acetate (PGMEA).

The polymer is structured by standard Si processing after spin-coating onto a substrate. It can be patterned by Lithography, Galvanoforming and Abformung process (LIGA; German acronym for deep X-ray lithography,

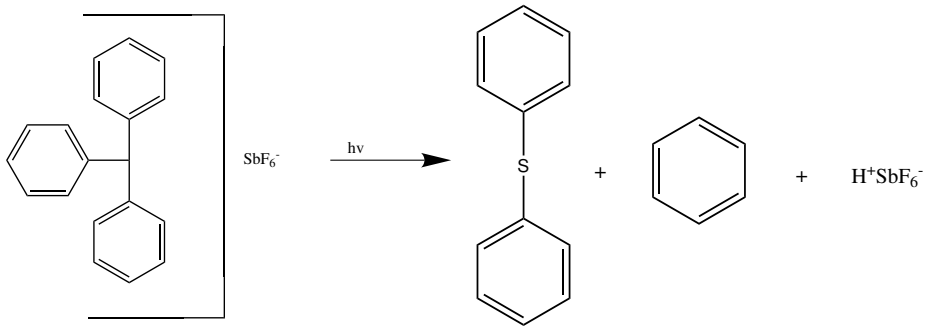

Figure 2.2: Upon UV exposure the salt is disintegrated. Upon heat treatment the radicals formed are involved in cationic ring-opening polymerization of the epoxy resin.

electroplating and molding), electron beam technology or UV exposure. Electroplating with Ni, using SU-8 as a mould has been reported by Dellmann *et al.* [29]. The SU-8 can also be used as master in hot-embossing [45]. LIGA and e-beam need very expensive equipment and as an alternative, near UV exposure can be used. In this project, exposure at 365 nm in a standard Aligner, was employed. Hard baking of the polymer increases the mechanical strength due to further cross-linking of the polymer. SU-8 is chemically resistent which makes it suitable for fabrication of structures intended for biological, chemical and medical detection systems as it will not interfere with the analysis substances. Biocompatibility studies done, show SU-8 to be a good material for medical implants [30]. This also shows SU-8 to be a good material to fabricated structures intended for medical analysis with. SU-8 is also suitable for fabrication of micro electrical mechanical systems (MEMS) as very high aspect-ratios[1] can be obtained. Aspect ratios of 15 and 18 have been reported [31, 34]. Another advantage of SU-8 is its high thermal stability. This prevents the resist from degrading and it can be used as an etch mask for Si in reactive ion etching [35]. The chemical and mechanical properties of SU-8 are summarised in Table (2.1).

The chemical resistance of SU-8 is enormous and it has been known to be able to withstand nitric acid, pH 13 sodium hydroxide solutions at 90 °C, ammonium fluoride, hydrofluoric acid and ferric chloride [36].

Khoo *et al.* have carried out investigations of variations in Young's modulus and hardness with depth penetration of SU-8 [38]. They showed that the properties greatly reduce with increased depth penetration of the micro posts fabricated for the investigations. The Young's modulus varied between 7 GPa at the top layer down to 3.5 GPa at 50 µm penetration. The hardness varied between 1.1 GPa at the top layer to 0.3 GPa at 50 µm penetration. This can be explained by the fact that the surface of the SU-8 structures will have had more solvent evaporated and will have been exposed to greater

[1]The aspect-ratio is found by dividing height by width.

From literature:	
Young's Modulus, E	4.02 GPa [36] 4.95 ± 0.42 GPa [37]
Maximum stress, σ_{max}	34 MPa [29]
Maximum shear stress, on Si substrate	∼ 6.6 MPa [38]
Poisson's ratio, ν	0.22 [39]
Co-efficient of thermal expansion, α	52×10^{-6} K^{-1} [31]
Refractive index, n, non-cross-linked	1.66 [28]
Refractive index, n, cross-linked	1.8 [32, 33]
Glass transition temperature, T_g non-cross-linked	49.5 °C [41] 50 °C [42]
Glass transition temperature, T_g cross-linked	>200 °C [34] 238 °C [41]
Decomposition temperature, T_d, fully cured	∼ 380 °C [42]
Friction co-efficient, μ	0.19 [36]
Reduction after cross-link	7.5 % [43]
Experimental results:	
Reduction after cross-link	2 ± 0.1 %
Contact angle, θ_c	90 ± 2 °
Surface roughness, cross-linked	0.4 ± 0.2 nm

Table 2.1: Mechanical properties of SU-8 as reported in literature and from own experiments.

amount of energy, which would mean that the cross-linking density is greater at the top layer. This cannot be avoided but the process steps need to be carefully monitored to minimise the difference.

2.2 Fabrication

In this section, the general fabrication steps of SU-8 will be explained. Here, the exact fabrication sequences of the chips are not described. They will be described in shorter terms in the respective chapters.

2.2.1 Release layer

The SU-8 is structured upon 4" ⟨100⟩ Si wafers used as support. Prior to starting the processing of the SU-8, the wafers need to be prepared with a layer enabling the SU-8 structures to be released in the final step. The structures fabricated are strong enough to support themselves and they only need the wafer during the processing.

As release layer, an Enhanced Sacrifical Layer is used [44]. The wafers are

coated with a 50 Å layer of Cr followed by 500 Å of Au and thereafter 500 Å of Cr. The first Cr layer is deposited to increase the adhesion between the Si wafer and the Au. After the processing of the SU-8 structures, the wafer is placed in a Cr etch and the 500 Å layer of Cr is etched away, releasing the SU-8 from the wafer. Due to the presence of the Au, the speed of this etch step is greatly increased, where the two metal layers act as an internal battery, due to the large difference in electronegativity of the two metals. The electronic properties of the metals is discussed in Chapter 5. Still, a great variation in the times of the etching was experienced, where the process could last between 45 min and 4 days. The etch rate was greatly reduced with the presence of an oxide layer on the Cr, which was something that was only discovered at the end of the project. Initially, recommendations of dehydrating the wafers in a 200 °C oven prior to processing was applied. Later, it was understood that heating the Cr generates oxide and therefore the process was planned in such a way as to be able to take the wafers directly from the metal deposition machine and onto the spinner.

Other groups have used other release layers, such as Polystyrene or Kapton films from which the SU-8 can be peeled off once processing is finished [40, 41]. These techniques were not used in this project, but could well be interesting alternative release layers.

2.2.2 Spin-coating

For the spin-coating process a KS Spinner (Karl Süss, Switzerland) is used with a spin program in two stages. The solution of SU-8 used and the spin speed and acceleration determines the final thickness of the polymer film. Recommendations from MicroChem are available but they did not compare very well with achieved thicknesses [28].

When thicker layers are spun, it is advisable to use special equipment, which reduces the air turbulence effects during the spinning [29]. This was always applied when spinning SU-8 to a thickness above 10 µm. Thicker layers of SU-8 should be allowed to rest for a few hours before the next step in the process. This is to allow the SU-8 to re-flow and planarise over the whole wafer as it tends to form a thicker layer at the edges after the spin-coating. Layers with a thickness above 160 µm are spin-coated in multiple steps of 160 µm layers at the time. The resulting thickness is never a multiple of 160, but usually slightly less.

Spin speeds and resulting thicknesses are listed in Table (2.2). The values only apply for wafers with the previously discussed release layer. It was seen that for spin-coated Si wafers, which did not have this layer, the resulting thickness was decreased. This is explained by the lower adhesion between SU-8 and Si compared to SU-8 and Cr, Chapter 5.

SU-8	Stage 1 (15 s)	Stage 2 (30 s)	Thickness (μm)
2002	3000 rpm 400 rpm/s	5000 rpm 600 rpm/s	1.6
2005	200 rpm 100 rpm/s	500 rpm 100 rpm/s	9.1
2005	500 rpm 100 rpm/s	1000 rpm 200 rpm/s	10.5
2075	3000 rpm 400 rpm/s	5000 rpm 600 rpm/s	35
2075	500 rpm 100 rpm/s	1000 rpm 200 rpm/s	160

Table 2.2: Different spin speeds and accelerations used in the processing with resulting thicknesses.

2.2.3 Soft bake

After the spin-coating, the SU-8 is soft baked. During this stage, the solvent present in the SU-8 is evaporated. Therefore, the baking should take place on a hotplate, and not in an oven, to allow the solvent to completely diffuse out of the SU-8 film. In an oven, the surface of the SU-8 may cure first, preventing solvents within from escaping and resulting in a non-uniform cure rate through the film thickness. Dellmann *et al.* claim oven soft baking to be superior as it rather heats the upper SU-8 layer and prevents over treatment of the lower SU-8 layer [37]. The complete solvent evaporation was considered to be more important in this work and a hotplate was used.

The soft bake is a two-step-cycle where the temperature is slowly ramped both in the increasing and decreasing stages to reduce the stress induced in the SU-8 film. Depending on the thickness of the film, the time at the relevant temperatures is adjusted as seen in Table (2.3).

Thickness (μm)	60 °C	90 °C
1.6	1 min	1 min
10.5	5 min	5 min
35	10 min	15 min
160	15 min	30 min
310	20 min	45 min

Table 2.3: Soft baking times at different temperatures for different thicknesses of SU-8.

It has been discussed by Zhang *et al.* that it is the soft bake step in the process that is the most important factor for good resolution and to achieve high aspect-ratios of SU-8 [45]. They analysed the resolutions and aspect-

ratios obtained for six different thicknesses of SU-8 films, with the Taguchi statistical method [46]. From their findings they propose that high aspect-ratios only correspond to a fixed solvent content. Their proposed optimal times were all slightly longer than the times applied in this process. This is because their work was carried out with SU-8 from the 50-series and the vapor pressure is lower of γ-butyrolacetone than of cyclopentanone (1.5 mmHg compared to 9.1 mmHg at 20 °C [39]). Adjusting for this, the times noted above correspond well to the optimal times.

2.2.4 Exposure

The SU-8 is exposed in a KS Aligner (Karl Süss, Switzerland) with an i-line lamp and a filter blocking out all light with a wavelength lower than 365 nm. The intensity of the lamp varied between 7.0-9.0 mW/cm^2 and was measured prior to exposure so the time could be adjusted to achieve a constant energy exposure. To limit the light, masks are used and the areas which are exposed cross-link, as shown in Figure (2.4). The smallest structures that can be produced by this technique lies around 1 µm. It is limited by the line width of the masks used. The optical absorption of SU-8 is very low in the near UV region (350-400 nm), Figure (2.3), which allows for high aspect-ratio structuring and minimises scattering. It also limits the patterns possible. Subsequent layers can be spin-coated and structured, the only limitation is that the areas cross-linked need to be smaller in the top layer than in the bottom layer, as it is a negative resist.

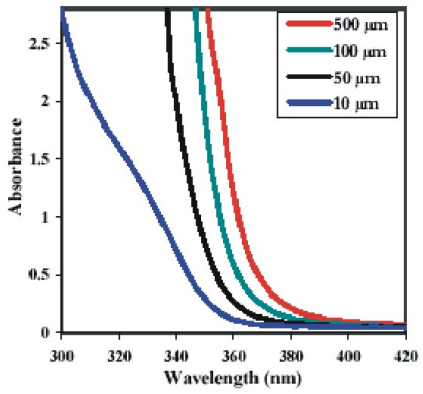

Figure 2.3: The optical absorption of SU-8 in the near UV region is very low [28].

The energy dosages applied for different thicknesses is noted below in Table (2.4). The energy dosage applied is much higher than the recommended values from MicroChem. The minimum dosage needed was determined experimentally and it was seen that a too low energy dosage resulted in very

bad adhesion between the SU-8 and the Si wafer.

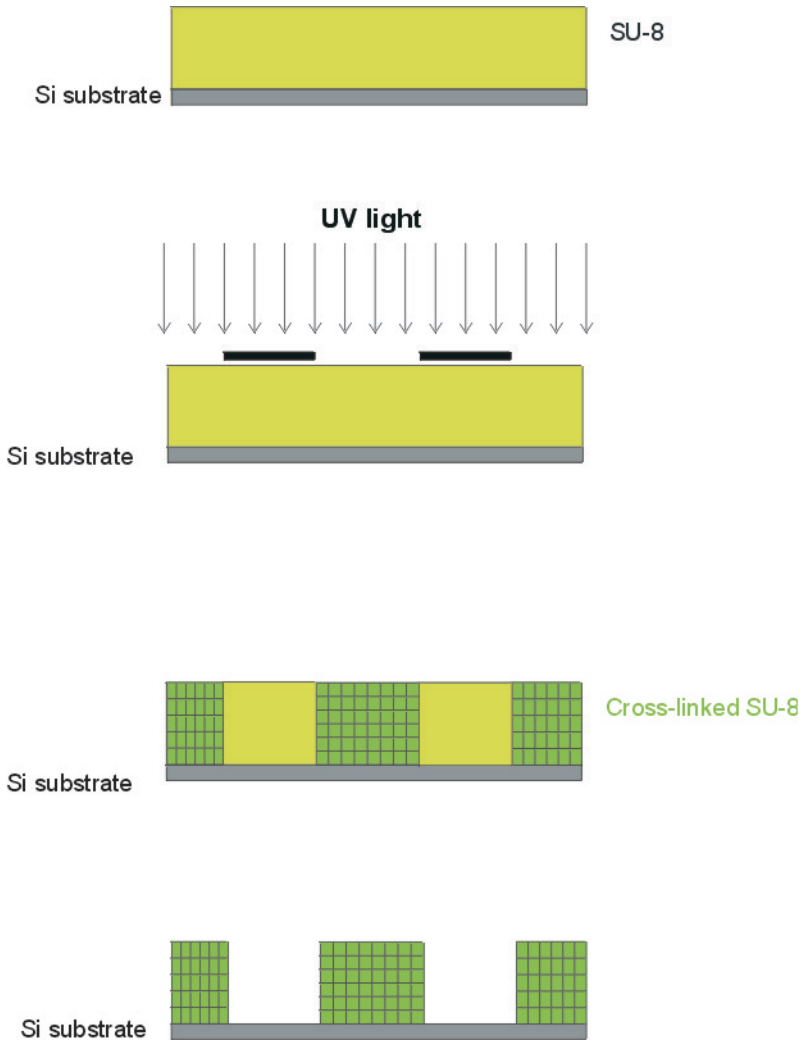

Figure 2.4: The exposed areas of the SU-8 cross-link and the un-exposed areas can be developed in PGMEA. Subsequent layers need to be of smaller size as all SU-8 exposed will cross-link.

Feng *et al.* have shown by statistical analysis that SU-8 exposed to higher UV dosages are more homogenous than if exposed to low UV dosages [41]. This is because the cross-linking is dependent on the acid catalyst formed during the UV degradation of the onium salt. At low UV dosages, not enough catalyst is generated and an in-homogenous cross-linking occurs in the sample. This also explains the lack of adhesion at low energy dosages; the bottom parts of the SU-8 structures are not fully cross-linked and can be developed in the solvent.

The reflectivity of the substrate is also of concern when the optimal exposure dosage should be determined. The reflectivity is found by Equation (2.1).

$$R = \left(\frac{n_1 - n_2}{n_1 + n_2}\right)^2 \tag{2.1}$$

Where R is the reflectivity and n_1 and n_2 represents the refractive indices of the different materials.

It has been reported by Chuang *et al.* that by using an anti-reflection coating on the substrate the thickness of SU-8 cross-linked could be controlled, leaving non-cross-linked SU-8 underneath [47]. They claim the reflected light has a major influence on the cross-linking density and by using a thin film, preventing any light being reflected off the Si wafer, top-wall structures as thin as 14 µm can be fabricated.

The anti-reflection coating they used is a resist named CK-6020L, which is unfortunately nowadays impossible to get hold of after the company producing it realised that it was being used for un-intended purposes, such as microfabrication [39]. Attempts were made to mimic their fabrication idea and these are presented in detail in Chapter 4.

Thickness (µm)	Energy dosage (mJ/cm^2)	MicroChem (mJ/cm^2)
1.6	455	100
10.5	1820	200
35	2730	300
160	3185	630
310	4550	n/a

Table 2.4: Energy dosage for exposure for different thicknesses. Compared to the recommended values from MicroChem, much higher values were used.

It is very important that the mask is as close as possible to the top of the SU-8 film during exposure to avoid light entering areas that should be covered by the mask. Some scattering will always occur in the SU-8 which can contribute to non-vertical side walls.

Chuang *et al.* have proposed a technique where a layer of glycerol is added on top of the SU-8 film to reduce the Fresnel diffraction in the air gap between the mask and the SU-8 [48]. They claim standard spin-coating of thick films (t = 0.1-1 mm) can produce un-even layers with air gaps of 30-100 µm. They show that a 156 µm high and 25 µm wide structure had a 45 % pattern-width-error without the use of the glycerol film. The ap-

plication of the glycerol film accomplished a straight resist wall without appreciable error.

No such precautions were taken in this work, as it proved not to be necessary, but soft-contact mode was always used in the Aligner and the masks were cleaned regularly to prevent any remains of SU-8 to cause air gaps.

The KS Aligner used has a set stage for the wafer chuck, which cannot be moved more than horisontally to load and un-load the wafer. This means only vertical structures can be patterned. New set-ups designed have shown the use of multi-angle exposure. This work was originally started in 1994 by Beuret *et al.* but no good results were obtained at that point [49]. They worked with the positive resist AZ4562 and integrated Ti masks on glass wafers but never managed to produce any structures with impressive definition.

Sato *et al.* have fabricated micro-mesh structures by back-side exposure of SU-8 spin-coated onto a Pyrex glass substrate patterned with metal [50]. The metal serves as the mask and by turning the substrate up-side-down, and keeping it at different angles during exposure, micro-filters can be fabricated. Yoon *et al.* have applied the same technique, also for the fabrication of micro-filter systems [51], Figure (2.5). They have incorporated the micro-filters into a channel and shown how particles, down to the size of 6 μm can be hindered to pass through the channel by the use of the filters. Han *et al.* have designed a home-made set-up with a tilting stage an a turntable [52], Figure (2.5). With this equipment, they have shown the possibilities of fabricating cylindrical structures, at an angle to the substrate.

These techniques mentioned are limited by the diffraction of the light at the air/glass and glass/SU-8 interfaces. The theoretical limit of the fabricated structure angle θ_s is 38.7° [51], calculated from Snell's law. This means that the final SU-8 structures can only range between 51° to 90° measured to the substrate [52].

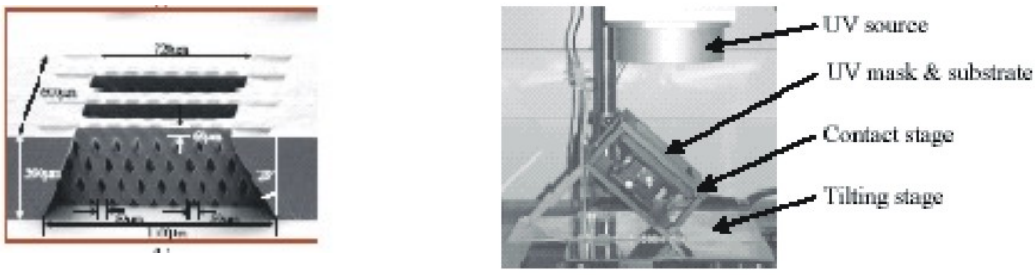

Figure 2.5: *Left:* The micro-filters structured in a channel [51]. *Right:* The home-made set-up with a tilting stage and a turntable [52].

2.2.5 Post exposure bake

The post exposure bake (PEB) is also done on a hotplate at two set temperatures with a slow ramping. During the PEB the acid generated in the exposure step, cross-links the SU-8 structure. Therefore, it is very important to place the SU-8 on the hotplate quickly after the exposure, to prevent the acid from diffusing into non-exposed areas of the polymer. The final amounts of solvent are also evaporated. It is during this step in the process that the largest amount of stress is induced in the structures. This is discussed in detail in Section (2.3).

Thickness (μm)	60 °C	90 °C
1.6	1 min	1 min
10.5	5 min	5 min
35	10 min	15 min
160	15 min	30 min
310	20 min	45 min

Table 2.5: PEB times at different temperatures for different thicknesses of SU-8.

Feng *et al.* have shown that the Young's modulus of SU-8 reaches a maximum after a certain time at PEB [41]. For a 130 μm thick layer the time was 20 min at 95 °C. They argue that the cross-linking reactions are only active when the baking temperature is higher than the glass transition temperature, T_g[2], of the SU-8. The T_g increases with increased amount of cross-linking and therefore the reaction will slow down and reach a maximum. They also show it is very important to keep the temperature of the PEB above the T_g of the SU-8 to achieve any cross-linking at all. T_g of SU-8 before cross-linking is ∼50 °C.

During cross-linking SU-8 has been reported to decrease by 7.5 % in volume [43]. The method used for that determination can be questioned as it relies on measuring the height difference of non-cross-linked SU-8 and cross-linked SU-8 with a profilometer. Before cross-linking, SU-8 is very soft and the tip of the profilometer would easily sink into the resist and thereby report on a large height difference. Attempts were made to repeat the measurements but with a new approach. An ellipsometer was used where the height can be measured without any mechanical contact with the polymer. Light is passed through the film and the diffraction is detected. From this, the thickness of the film can be calculated by the software. From these measurements, a 2 % decrease in thickness was seen after cross-linking of the SU-8.

[2] T_g is the temperature at which the polymer is liquid above and solid below.

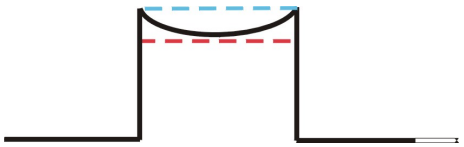

Figure 2.6: The edges of cross-linked SU-8 tend to raise, as indicated by black line. This could either be a sign of shrinkage or expansion, where the blue and red lines represents the initial positions of the SU-8 surface in either case.

The edges of the cross-linked structures tend to show a larger height at the edges than at the center of the structure. This could both indicate on a shrinkage as well as an expansion of the SU-8 after cross-linking, Figure (2.6). Either, simply the SU-8 reduces in size and shrinks, or it actually expands.

2.2.6 Develop

The non-cross-linked parts of the SU-8 are finally developed. This is done in Propylene Glycol Methyl Ether Acetate (PGMEA) and the wafers are kept in the solution where magnetic stirring is applied. The developer is kept in two different bottles; 'First' and 'Final' where the second is slightly cleaner than the first. Finally, the wafers are rinsed in iso-propanol and dried with N_2 flow. The times in the different solutions are found in Table (2.6).

Thickness (μm)	'First' (min)	'Final' (min)
1.6	1	1
10.5	10	5
35	15	5
160	20	10
310	20	20

Table 2.6: The times needed in the two different PGMEA solutions for well-developed structures. The 'Final' solution is slightly cleaner than the 'First'.

Zhang *et al.* found in their statistical analysis that with increasing thicknesses of the SU-8, the develop time became more crucial as the developer will have difficulties reaching the bottom of the photo-resist structures [45]. As seen above, Tabel (2.6), the time is greatly increased with increasing thickness.

2.2.7 Hard bake

Once the structures have been developed, they are hard baked on a hotplate at 120 °C to fully cross-link the SU-8. This increases further the mechanical strength of the structures.

2.2.8 Release

The wafer is left in Cr etch overnight and the structures are released. To remove the etch, the chips are rinsed in water and left on a cloth to dry. The cantilevers proved prone to deform in this step and the difficulties encountered are described in detail in Chapter 3.

2.2.9 Stripping

Due to the chemical resistance of SU-8, it is very hard to remove SU-8 once it has been cross-linked. It has been proposed that a hot 1-methyl-2-pyrrolidinone (NMP), H_2SO_4/H_2O_2 or fuming HNO_3 could be used [34]. Plasma ashing with O_2 has also been suggested, but was not successful, as described in Chapter 5. None of the above methods are commonly used. A definitive solution has not been found yet, that removes the SU-8 and that would not be damaging to the other structures.

2.3 Stress

One of the major problems in the fabrication of both the cantilevers and the channel system is the amount of stress easily induced in SU-8. The stress is of both intrinsic and extrinsic character [53]. Intrinsic stress is mostly the stress generated from the movement of the monomer in the cross-linking process. Stress of extrinsic type is the major cause of stress and it is the thermal stress arising during PEB. In the case of channel fabrication the large amount of stress makes the chips prone to crack and it reduces the adhesion to the Si wafers. In the fabrication of the cantilevers, the stress results in bending of the cantilevers. Residual stress in the cantilevers after fabrication is very undesirable and understanding the mechanisms and causes of stress in the polymer is very important to improve the fabrication process.

The amount of stress in a film of resist can be calculated by Stoney's formula, Equation (2.2).

$$\sigma_f = \frac{E_s}{6(1-\nu_s)} \frac{t_s^2}{t_f} \frac{1}{R} \tag{2.2}$$

Where E and ν are the Young's modulus and Poisson's ratio of the substrate, t_s and t_f are the thickness of the substrate and the film respectively and R is the radius of curvature.

2.3.1 Thermal stress

Cross-link of SU-8 occurs at a temperature of 90 °C, as described previously in Section (2.2). Before the cross-linking, the SU-8 is stress-free as the monomers are not constrained to move by the polymer lattice. At an elevated temperature SU-8 cross-links and the monomers are locked into position in the polymer structure. During the cooling stage, stress is induced due to a mis-match of the co-efficient of thermal expansion, α, of the substrate and the SU-8 film. The stress induced by this mis-match, σ_{th}, can be calculated from Equation (2.3). This equation applies only to thin films with thicknesses negligible compared to the thickness of the substrate.

The constant α determines how much the material will change in size with changes in temperature. Since the substrate is much thicker ($t_s = 525$ µm) than the resist film ($t_f \simeq 1.5$ µm) and the film is attached to the wafer, it will be the properties of the substrate that determine the behavior of the system.

$$\sigma_{th} = (\alpha_s - \alpha_f)\Delta T \left(\frac{E}{1-\nu}\right) \tag{2.3}$$

Where α_s and α_f are the co-efficient of thermal expansion for the substrate and the film respectively, ΔT is the temperature interval, E is the Young's modulus of the substrate and ν is the Poisson's ratio of the substrate. In the case of $\alpha_s < \alpha_f$ the stress induced in the resist is tensile. For the opposite case the stress induced is compressive.

The co-efficient of thermal expansion for Si is $\alpha_{Si} = 2.6 \times 10^{-6} K^{-1}$ and the co-efficient of thermal expansion for SU-8 is $\alpha_{SU-8} = 52 \times 10^{-6} K^{-1}$. This imples that the stress in the SU-8 is tensile as the polymer is not allowed to contract as much as it would prefer during the cooling stage.

After release the structure is not limited by the substrate any longer and it will be able to release the stress. Strictly speaking, the images in Figure (2.7) only represents the surface of the SU-8 in contact with the Si wafer. For the fabrication of cantilevers, the release of the induced stress results in a bending, as the surface which was in contact with the wafer will release its tensile stress. The chips comprising the channels are too large for deformation and the release of stress is seen as cracking.

2.3.2 Deviations from 'Thin film' assumption

Stoney's equation, Equation (2.2), only applies to thin films. The revised formula, Equation (2.4), should be applied for films with $t \geq 2$ µm. This formula has been evolved by Ole Hansen [54].

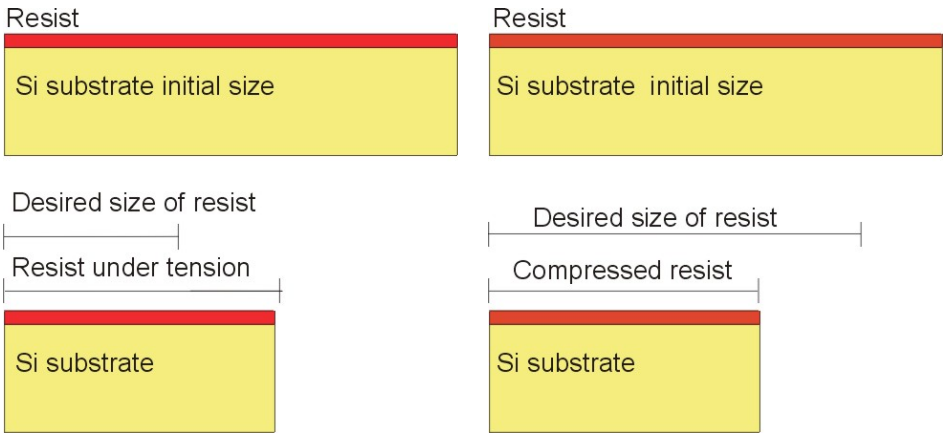

Figure 2.7: *Left:* In the case of $\alpha_s < \alpha_f$ the film experiences a tensile stress. *Right:* For $\alpha_s > \alpha_f$ the stress is compressive. In the case of SU-8 structures fabricated on Si wafers, the stress is tensile. The dimensions of this figure are not to scale.

$$\sigma_f = -\frac{E_s}{1-\nu_s}\frac{t_s^3}{6Rt_f(t_s+t_f)}\left(1+4\frac{E_f(1-\nu_s)}{E_s(1-\nu_f)}\frac{t_f}{t_s}\right) \tag{2.4}$$

Where E_s and ν_s is the Young's modulus and Poisson's ratio of the substrate, t_s and t_f are the thicknesses of the substrate and the film respectively and R is the radius of curvature.

Calculations were done on the theoretical amount of stress in different thicknesses of SU-8 due to the aforementioned thermal mis-match. Measurements were then done to find the total amount of stress in the SU-8 using the Tencor profilometer.

Thickness (µm)	σ_{th} (MPa)	$\sigma_{measured}$ (MPa)
1.6	17	19.8
10.5	17	5.2
250	17	9.9

Table 2.7: Comparison between calculated and measured values of stress for SU-8 cross-linked at 90 °C. Equation (2.2) was used for the thin film and Equation (2.4) was used for the two thicker films.

R is found by measurements using a profilometer, scanning over the whole wafer. The radius of curvature is found both on the wafer initially and after processing. The value for R used in Equation (2.2) and Equation (2.4) is found by calculating $\delta(1/R)$.

It is seen that for a thin film of SU-8 the measured total amount of stress compares very well with the calculated value from Equation (2.3). This confirms that it is the mis-match of α_{Si} and α_{SU-8} that is the major cause of

stress. For the thicker films, there is a large deviation. This can be explained by the break-down of the 'thin film' assumption. When the thickness of the film approaches the thickness of the substrate, the behavior of the system will not be fully determined by the properties of the substrate any longer. For thicker films, the stiffness of the film cannot be ignored and the position of the neutral axis has been shifted [31]. Equation (2.4) does compensate for the thickness of the film by shifting the neutral axis, but it can still be seen that other contributors to stress are more relevant.

At the same time it is seen that when comparing the 10.5 µm SU-8 to the 250 µm SU-8, the thicker film incorporates greater amount of stress. This is explained by the fact that the thicker layer will have more intrinsic stress, there will be greater amount of stress due to the cross-linking of the polymer.

2.3.3 Practical concerns

The stress discussed above is of great concern in the clean room process.

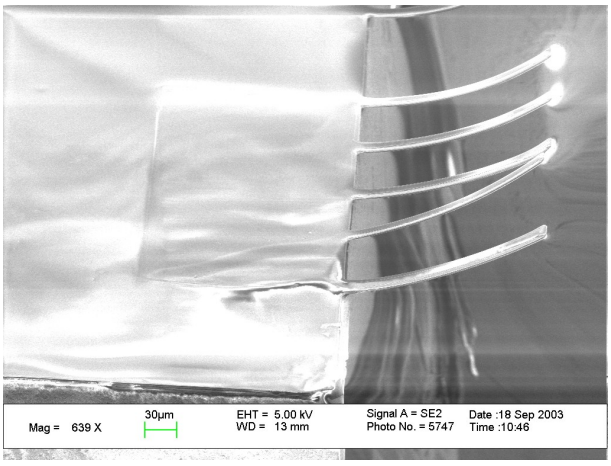

Figure 2.8: 1.6 µm thin and 200 µm long cantilevers after release.

It is important to understand the causes of stress as to overcome the problem. The cantilevers were seen to bend upwards after processing and release. The problem with the Si wafers used is the large difference in coefficient of thermal expansion, α, between Si and SU-8 and the bending of the cantilevers was attributed to this.

To overcome this problem, preferably a substrate with a value of α closer to SU-8 should be used. The possibility to use different polymers, PMMA or Topas for example, has been proposed but was never investigated in greater detail in this project. Another precaution taken at a later stage in the project was to do the PEB at a lower temperature. The SU-8 was baked at 60 °C

instead of 90 °C. This results in lower amount of stress generated but still, the difference is not that large to outweigh the longer processing time.

Lorentz *et al.* discussed that the stress induced is related to the percentage area that is exposed on the wafer [34]. It was clearly seen this is true and on occasions when a whole wafer was illuminated and cross-linked, the SU-8 film had a tendency to crack or even make the Si wafer break. On the wafers where the cantilevers are fabricated, ∼20 % of the wafer is exposed and for the wafers with the channels, just over 50 % of the total wafer area is exposed. The fact that the channel chips are so large was of major concern in the process and several times, the chips were seen to come off the Si wafers as a result of this. Actions taken to reduce the effects of stress and the results of that are described in Chapter 4.

The cantilevers that were slightly thicker, 2.3 µm, did not seem to bend as much as the thinner ones. Here, 200 µm long cantilevers have been released and it is almost possible to focus over the whole length of the cantilevers, indicating they are not very bent.

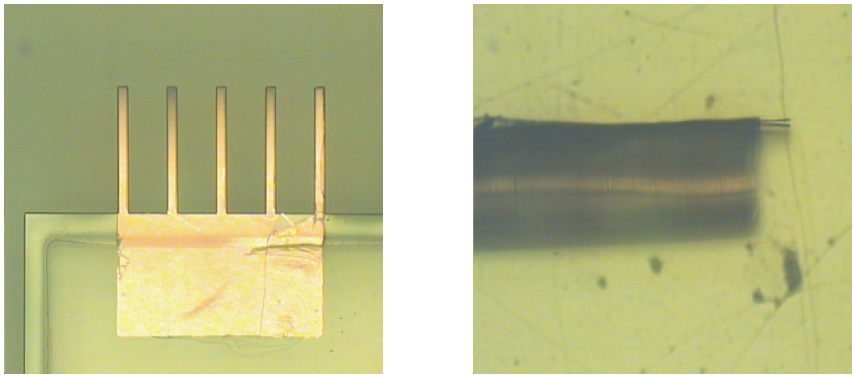

Figure 2.9: 2.3 µm thin and 200 µm long cantilevers after release. *Left:* Optical image where it is possible to focus over the major part of the cantilevers. *Right:* The chip has been placed on the side and it can be seen that the cantilevers are straight.

Chapter 3

Cantilever Chip

In this chapter the work concerning the cantilever chips will be described. The reasoning behind the design is discussed in Section (3.1) and the fabrication sequence is described in Section (3.2). The theory of surface stress measurements is discussed in Section (3.3). In Chapter 6, the actual measurements done with these chips are presented.

3.1 Design

The work for this project was initiated as a 3-week-course by Dr. M.Calleja at MIC, DTU, [55]. In that project, cantilevers with various dimensions were fabricated. The idea of this project was to continue the work started and develop the design of the cantilevers, making them suitable for the measurements intended.

3.1.1 Cantilever chip design

In Table (3.1) the dimensions of the cantilevers fabricated in the 3-week-course can be seen. All were fabricated to a thickness of 1.7 µm.

Length (µm)	Width (µm)	k (N/m)	f_{res} (kHz)
200	20	0.015	15.2
200	50	0.038	15.2
200	70	0.053	15.2
100	20	0.122	60.7

Table 3.1: Dimensions and characteristics of cantilevers fabricated in the initial 3-week-course.

In surface stress measurements it is important to use a flexible cantilever, with a low spring constant and a high resonance frequency. From this work

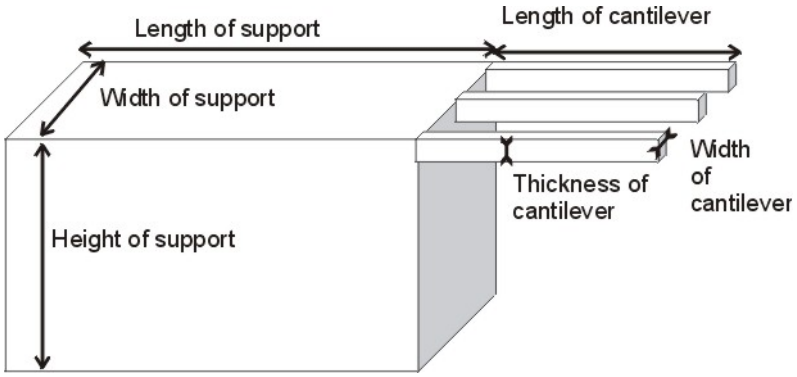

Figure 3.1: The dimensions listed in Table (3.1) represent the above marked distances. The drawing is not to scale and each seen cantilever is an array of five separate cantilevers on the actual chip.

it was concluded that the cantilevers with a 20 µm width were the most suitable ones and cantilevers of both 100 µm and 200 µm in length were designed.

We chose to make the cantilevers beam-like but V-shaped cantilevers have previously been fabricated and used. The V-shaped cantilevers were given this design to avoid twisting due to turbulence during measurements in liquid [13]. No such problems would arise during the measurements with these cantilevers, as the channels fabricated for that purpose don't induce turbulent flow, Chapter 4.

The aim was to design and fabricate an array of cantilevers which would be used for simultaneous measurements, were a few of them can be used as reference cantilevers. To use a reference cantilever is very important as the quality of the signal can be greatly increased as the effect of external noise can be subtracted. Three arrays of five cantilevers each were placed on every chip. This makes five cantilevers available for two different measurements and five cantilevers can be used as references. The aim is to have a chip with an multiple arrays of 100 cantilevers or more, but a lower number was chosen at this early stage.

3.1.2 Mask design

For the fabrication four masks were used, structuring the different layers. As subsequent layers of structured SU-8 need to be smaller, the cantilevers are the first thing that needs to be patterned. The first mask was used for this, Figure (3.2). This is also the structure of each chip from a top view.

After the cantilevers have been structured, a mask is needed for patterning the Au which should cover the cantilevers. The Au was made to also cover a small part of the chip, to make it easier to see on which side of the chip the

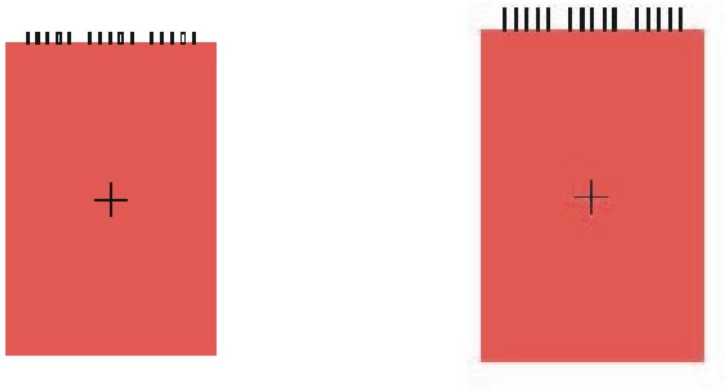

Figure 3.2: The mask used for patterning the cantilevers included one design for 100 µm long and one for 200 µm long cantilevers. The dimensions of the chip itself was 2000 x 3000 µm.

cantilevers were, without the need of a microscope. The Au did not cover the whole chip as this could easily lead to delamination of the two SU-8 layers, as the adhesion between SU-8 and Au is not as good as between SU-8 and SU-8. One of the masks shown in Figure (3.3) was used for every chip.

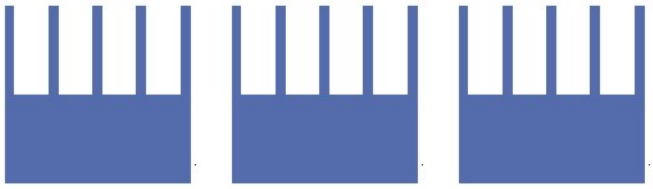

Figure 3.3: The mask used for patterning the Au covering the cantilevers. This mask was used for the 200 µm cantilevers and a similar mask was used for the shorter cantilevers. The dimensions of the piece on the chip are 400 x 200 µm.

To simplify handling the chips once they had been released from the wafer, a network was designed. Before the chips are taken out of the etch, they tend to float into each other damaging the cantilevers. This was also prevented with the network. The network was made strong enough to support at least five chips and weak enough to easily be broken once the chips needed to be separated. Each wafer included 208 chips in total and keeping them together in this network greatly decreased the time needed for transferring them from one container to another.

Finally a last mask was needed to define the support structure. The cantilevers are very thin and to be able to handle them by tweezers, they need to have a thick support. The support was just patterned by a square mask with the same dimensions as the cantilever chip, 2000 µm x 3000 µm.

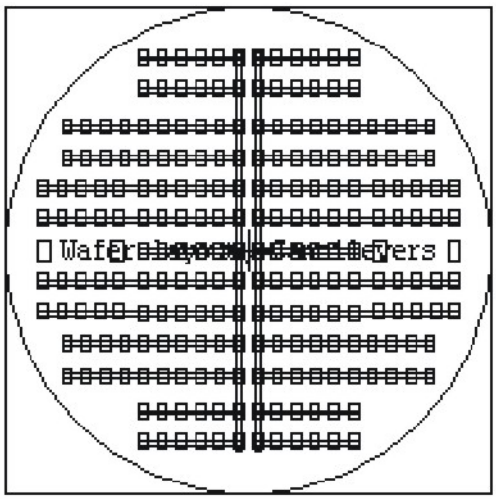

Figure 3.4: This picture shows the whole wafer layout which was used for the network. The cantilevers were kept in place by this. The width of the network is 1000 µm.

All masks were designed with the software L-Edit and fabricated as standard Cr/Glass masks.

3.2 Fabrication sequence

Here the exact fabrication sequence is described for the cantilever chips, Figure (3.5). The parameters for spin speeds, baking temperatures, baking times and exposure dosage can be found in Chapter 2, where each step of the fabrication sequence was described in detail.

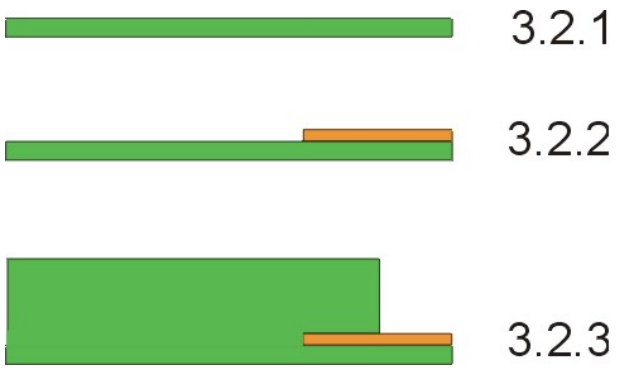

Figure 3.5: Side view of fabrication sequence of the cantilever chip. The numbers corresponds to the relevant sections.

3.2.1 Cantilever layer

The cantilevers are structured by a 1.6 µm thick layer of SU-8 and soft baked. This layer is patterned by the masks shown in Figure (3.2). After PEB the cantilever layer is developed in PGMEA and hard baked. The hard bake is done to increase the strength of the SU-8 and they are developed to ease the Au patterning.

3.2.2 Au patterning

The cantilevers are then covered with Au. There are two reasons for having this extra metal layer on top of the cantilevers: (i) For a surface stress difference to be present, the surfaces of the cantilever must consist of two different materials which will react differently to the introduction of test molecules. (ii) The set-up for the measurements uses optical read-out where a laser light is reflected off the back of the cantilevers, the Au is deposited to provide a stronger reflected signal.

There are two ways of patterning Au on the SU-8; it can be done by either covering the whole wafer and etching the unwanted Au or by a process called *Lift-off*. In both cases the resist AZ5214E is used as a mask. For the first batch etching was done but as can be seen in the SEM picture, Figure (3.6), a huge under-etch resulted and in the following batches the lift-off process was used.

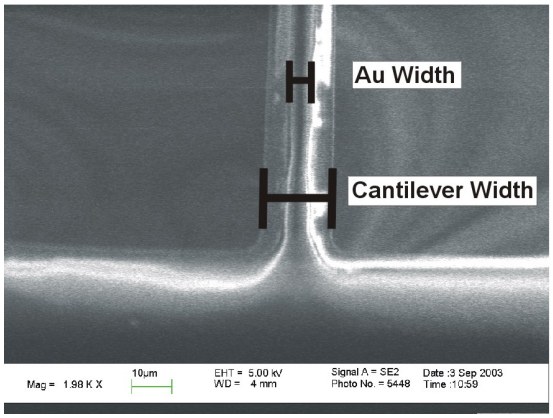

Figure 3.6: It can be seen that the Au has been greatly under etched and only covers a small section of the cantilever.

To pattern Au with the lift-off process, first a 1.5 µm layer of AZ5214E is spun onto the SU-8 structures. This resist is positive by nature but can be made negative, as needed for the lift-off process. The resist is exposed with the second mask, Figure (3.3), for 14 s and then baked on a 120 °C hotplate for 80 s. After this, the whole wafer is exposed again for 30 s without a

mask. Exposing the resist un-cross-links it, but baking it afterwards initiates a chemical reaction which makes the resist cross-link again upon another exposure. This leaves the areas exposed twice cross-linked and the areas only exposed once soluble in a NaOH based solvent. The wafer is then treated to the solvent AZ-351B at 22 °C for 2 min whilst being stirred, which finally leaves the areas where the Au should be present clean and the rest of the chip covered with resist.

The wafer is treated to a O_2/N_2 plasma to increase the adhesion between the SU-8 and the Au just prior to being placed in the Alcatel where Au is deposited to a thickness of 100 Å by electron beam evaporation at a base pressure of 2.0 x 10^{-6} mbar. A 20 Å thick Ti layer was deposited as an adhesion promoter. Afterwards the wafer is left in PGMEA overnight which dissolves the AZ5214E resist. The resist is removed by sonication and the Au deposited on top comes off with the resist. This leaves perfectly patterned cantilevers. It is the time for the first exposure of the AZ5214E resist that is the most crucial parameter, Figure (3.7).

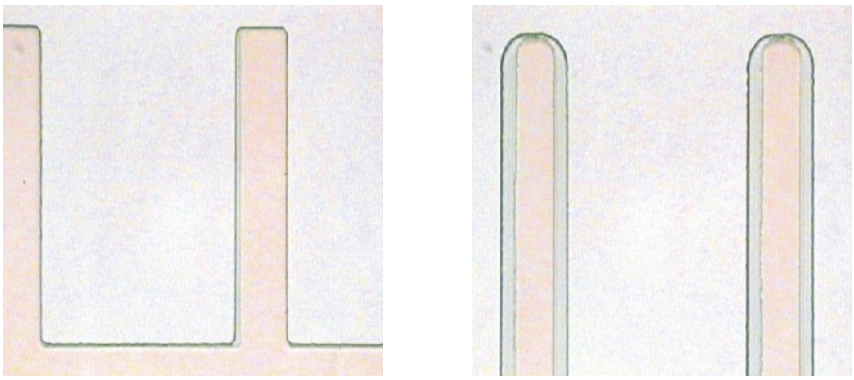

Figure 3.7: Optical images of the cantilevers. *Left:* The resist was exposed for 14 s which gives a perfect definition. *Right:* This resist was exposed for 22 s, which results in over exposure and bad definition of the Au.

Due to a break down of clean room equipment, one batch of cantilevers had to be left in PGMEA for 36 hours. This resulted in a very bad layer of Au, Figure (3.8). The fact that the Au is broken is because also the cantilever layer of the SU-8 has been affected by the PGMEA. It is not be possible to dissolve cross-linked SU-8 in PGMEA, but if exposed to the solvent for a prolonged time, it can be seen to have an effect. The SU-8 was probably not dissolved, but the PGMEA must have diffused into the structures, affecting the Au definition

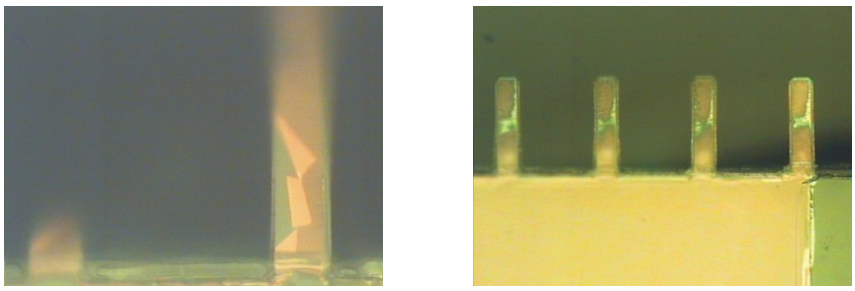

Figure 3.8: The wafer was left in PGMEA for too long during the lift-off which resulted in a very bad layer of Au. *Left:* 50X optical image of 200 µm long cantilever. *Right:* 20X optical image of 100 µm long cantilevers.

3.2.3 Support layer

As the cantilevers are so small and thin, they need a support structure so one will be able to handle them. This is spun in two stages of 160 µm layers of SU-8 with a final thickness of ∼310 µm. The two layers are exposed at the same time and structured together with a mask patterning 2000 µm x 3000 µm squares.

3.2.4 Develop and Release

Finally, the whole chip is developed in PGMEA and released from the wafer by a Cr etch. Once the chips are taken out of the Cr etch, they need to be rinsed in water as the etch is very sticky and acts as a glue once it has dried. It was this step that involved the greatest challenge in the whole fabrication sequence.

As the cantilevers are so small and thin, they are very sensitive to any mechanical damage. The SU-8 is hydrophobic and when the chips are taken out of the water bath, the surface tension of the water is so strong it bends the cantilevers. The cantilevers get completely bent and stick to the substrate and they do not rise back up again after drying, Figure (3.9).

It was discussed whether it would be the residual stress that was the cause of this bending but it was concluded it was not. Baking at 60 °C, and thereby gaining less thermal stress, may reduce the final bending of the cantilevers but not prevent the stiction as seen in Figure (3.8). This phenomenon arises because the cantilevers are so thin. Cantilevers with a nominally greater thickness of 2.4 µm would flip back to the original position upon drying.

It could also be determined that the direction of the cantilevers when the chips were taken out of the water bath determined the yield. Chips that were lifted out with the cantilevers downwards ended up with the cantilevers stuck to the top-side of the chip and if they were lifted out with the cantilevers upwards, the cantilevers got stuck to the side of the chip. Cantilevers stuck

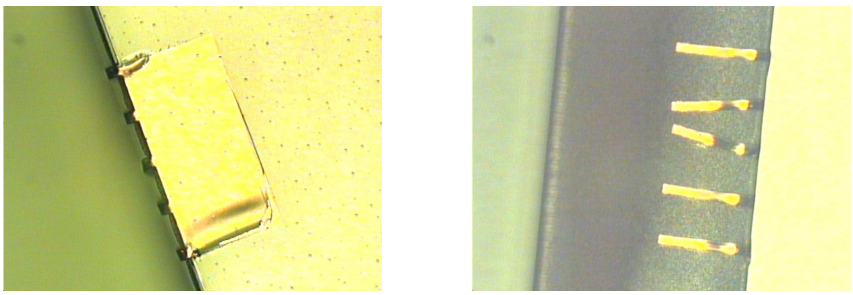

Figure 3.9: It was often seen that the cantilevers bent once they were picked out of the water bath following the Cr etch. *Left:* Top view of the chip. The cantilevers are bent downwards. *Right:* The chip has been placed vertically and the cantilevers can be seen to be stuck to the side.

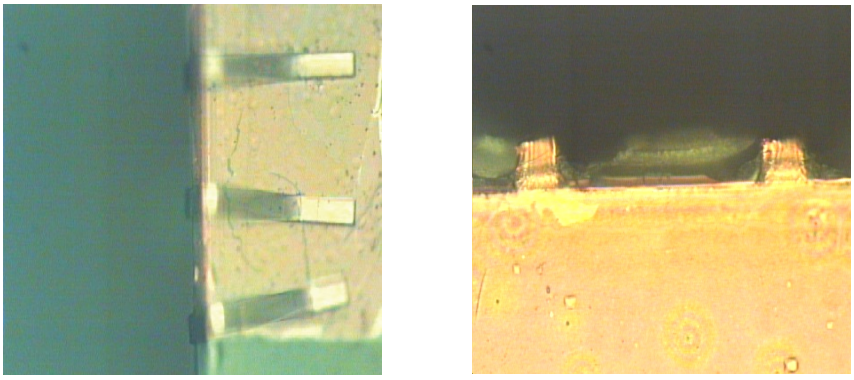

Figure 3.10: *Left:* These cantilevers were lifted up downwards in respect to the chip and are now stuck to the top. *Right:* These cantilevers were lifted up upwards in respect to the chip and are now stuck to the side .

to the top proved to be more likely to return to the original position than cantilevers stuck to the side of the chip, Figure (3.10). Ideally, the cantilevers should be lifted up pointing downwards but this proved to be very difficult when handling such small chips.

The longer cantilevers also had a tendency to stick to each other, Figure (3.11). The water in-between the cantilevers did not dry and the cantilevers were never released. Possibly, dipping the chips back into water would return the cantilevers to their original position, but the problem remains in removing them. One approach could be to leave the chips for the water to evaporate but probably though, the cantilevers would end up stuck to the side of the support as the water level slowly reduces.

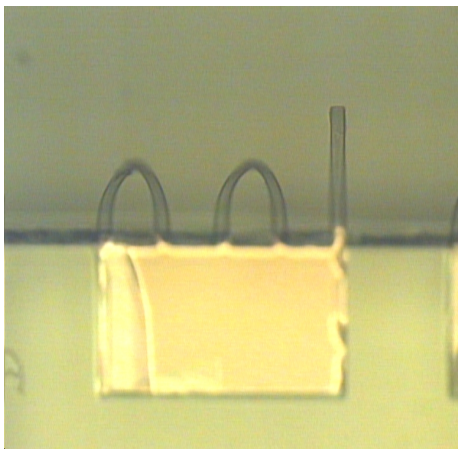

Figure 3.11: The longer cantilevers often stuck to each other.

3.3 Molecular detection

The cantilevers fabricated in this project have been developed as components of a device applicable for biochemical detection. These types of measurements with cantilevers can either be of static or dynamic kind, where the bending or change in resonance frequency of the cantilever is detected respectively. These cantilevers are intended for static measurements and the actual measurements carried out with them are described in Chapter 6.

3.3.1 Cantilever properties

The cantilevers fabricated consist of two different materials where the SU-8 is the major structural component covered by a 100 Å thick layer of Au. For the calculations below, only the SU-8 is considered as the Au thickness is negligible.

To characterise the cantilevers, the spring constant and resonance frequency needs to be known. The spring constant, k, of the cantilever is calculated from Equation (3.1).

$$k = \frac{Et^3}{4l^3}w \tag{3.1}$$

Where E is the Young's modulus of the cantilever material and t, l and w represents the thickness, length and width, respectively.

The resonance frequency in vacuum is calculated from

$$f_{res}^{vac} = \frac{1}{2\pi}\sqrt{\frac{E}{\rho_c}}\frac{t}{l^2} \tag{3.2}$$

Where ρ_c is the density of the cantilever material.
The resonance frequency in a fluid is found from

$$\frac{f_{res}^{fluid}}{f_{res}^{vac}} = \left(1 + \frac{\pi\rho w}{4\rho_c t}\right)^{-1/2} \tag{3.3}$$

Where f_{res}^{vac} is found from Equation (3.2), ρ is the density of the fluid, ρ_c is the density of the cantilever material and w and t are the width and thickness of the cantilever respectively [56].

The calculated cantilever properties are listed in Table (3.2).

Length (µm)	Width (µm)	Thickness (µm)	k (N/m)	f_{res}, vacuum (kHz)	f_{res}, air (kHz)	f_{res}, water (kHz)
200	20	1.6	0.013	14.5	14.4	4.3
200	20	2.4	0.043	21.8	21.7	7.8
100	20	1.6	0.101	58.1	57.7	17.3
100	20	2.4	0.342	87.2	86.8	31.0

Table 3.2: Characteristics of the fabricated cantilevers.

SU-8 is an attractive alternative to Si_3N_4 cantilevers commercially available for these types of measurements due to the cost reductions possible on fabrication and because of the much lower Young's modulus, which makes the cantilever more sensitive. The Young's modulus is a measure of the resilience of the material and the energy stored. SU-8 is more efficient for these types of detections, as it stores a less amount of the energy obtained from the measurements, available for the read-out.

3.3.2 Surface stress detection

To detect the surface stress induced on a cantilever surface, the bending of the cantilever is monitored. This is achieved by detecting the reflection of a weak laser beam from the back of the cantilever. The laser is detected by a photo-diode and any changes in the cantilever bending will change the position of the laser beam at the diode, Figure (3.12). The sensitivity of the deflection set-up is limited by thermal noise, the pointing stability of the laser and drift of the laser [21].

The surface stress difference between the two surfaces can be calculated from Stoney's formula, Equation (3.4).

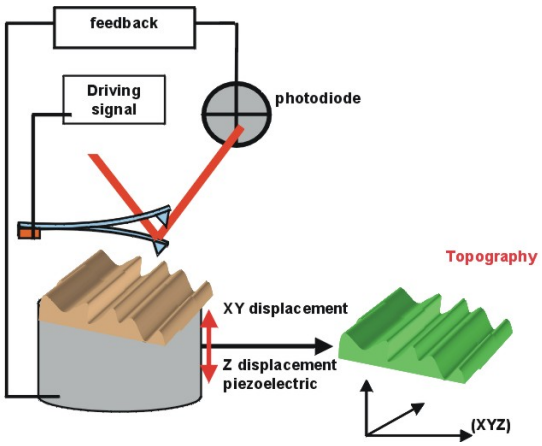

Figure 3.12: The laser light is reflected off the back of the cantilever and detected by a photo-diode. Any changes in the bending of the cantilever will result in a voltage change in the read-out due to the changed position of the laser spot at the photo-diode.

$$\frac{1}{R} = \frac{6(1-\nu)}{Et^2}\Delta\sigma \tag{3.4}$$

Where R is the radius of curvature, E and ν are the Young's modulus and Poisson's ratio of the cantilever material, t is the thickness of the cantilever and $\Delta\sigma$ is the uniform surface stress difference between the two cantilever surfaces [57].

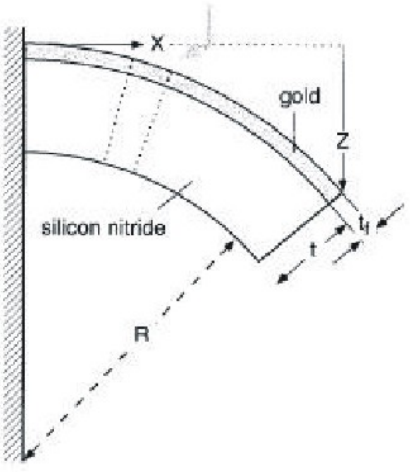

Figure 3.13: The radius of curvature, R, can be related to the bending of the cantilever, z, as Equation (3.5).

The radius of curvature is related to the displacement of the cantilever as seen in Figure (3.13) by Equation (3.5).

$$\frac{1}{R} = \frac{2z}{z^2 + l^2} \tag{3.5}$$

Where R is the radius of curvature, z is the displacement of the free end of the cantilever and l is the length of the cantilever [3].

By measuring the deflection at the end of the cantilever, Equation (3.4) and (3.5) can be combined to Equation (3.6) [20].

$$\Delta z = \frac{3(1-\nu)l^2}{Et^2}\Delta\sigma \tag{3.6}$$

To calibrate the cantilever, another cantilever with a known relation of bending versus applied force at the end point is used. The calibration cantilever is pushed down onto the measurement cantilever and the bending of the latter is observed for the application of a specified surface stress.

In the set-up used in Madrid for these measurements, deflections of 0.5 nm can be detected. By using these 1.6 µm thin and 200 µm long cantilevers, surface stress changes as small as 70 µN/m can be detected.

3.4 Summary

Cantilevers of both 100 µm and 200 µm length, 20 µm width and 1.6 µm thickness were successfully fabricated. They were also applied for DNA and pesticide measurements, as will be discussed in Chapter 6.

SU-8 is a very suitable material for these types of measurements. As seen above, Equation (3.6), the deflection of the cantilever for a specified surface stress applied scales as 1/E. The Young's modulus of SU-8 is approximately 30 times lower than that of Si which has until now been the conventional cantilever material. Thereby, the sensitivity for surface stress measurements would be much greater for cantilevers fabricated in SU-8, with the same dimensions.

The main problem in the fabrication sequence was the last step, the release of the cantilevers. Due to their small size and thickness, they are very sensitive to any external forces and easily deform. As SU-8 is a hydrophobic material, it proved hard to wash the cantilevers in water without them bending. A new technique should be developed for this. Possibly; the cantilevers could be washed by spraying small amounts water onto them, which could then evaporate. The best would be if the wet release could be completely

avoided and to achieve this, another release layer would need to be developed. For cantilevers with a thickness ∼2 µm, the release did not prove to be a problem and therefore no time was spent investigating different release techniques.

To decrease the stress induced during the PEB, another substrate material could be found with a value of α which would compare better to α_{SU-8}. In combination with using a different substrate, another release layer depending on a dry treatment could be developed. An interesting technique of using a self-assembled monolayer which can be removed by mechanical lift-off has been reported for SU-8 fabrication [58]. Alternative methods to the current release technique ought to be found and this would greatly increase the quality and yield of cantilevers from each wafer.

Chapter 4

Channel Chip

In this chapter, all work involved with the fabrication of the channel chip will be discussed. Firstly, in Section (4.1), fluid dynamics on the micro-scale will be discussed. In Section (4.2) the ideas behind the design of the chip will be followed and in Section (4.3) the steps involved in the fabrication are reported. In Chapter 6 the measurements done with the channels are described.

4.1 Fluid dynamics

Fluid dynamics on the micro-scale can be fairly complicated. With decreasing size of the channels, the ratio of surface area to volume increases and factors related to the surface area become dominating [59]. Here, the most important parts of fluid theory on the micro-scale will be presented and the sections will be run through fairly quickly.

In all theoretical calculations, characteristic values of water are used as mainly water based solutions are used in the measurements for which the channels are intended. In the theoretical derivations, the fluid is assumed to be an in-compressible Newtonian fluid; which water is.

4.1.1 Fluid flow

To be able to design a good chip for the intentions above, fluid dynamics on the micro-scale should be understood. There are three main characteristics of the fluid and the channels that initially need to be determined.

Firstly, the effect of gravity needs to be considered. The capillary length, Δc, determines whether the effect of the gravitational force needs to be included in the calculations, Equation (4.1). In calculations with capillarity of vertical channels, gravity is crucial. In this case, the channels are placed horisontally and gravity might be ignored, depending on the ratio of Δc to the channel height.

$$\Delta c = \left(\frac{\sigma_{lg}}{\rho g}\right)^{1/2} \tag{4.1}$$

Where σ_{lg} is the surface tension of the liquid-gas interface, ρ is the density of the fluid and g is the acceleration due to gravity.

For water, Δc has a value of 3 x 10^3 µm, which is far greater than the height of the channels designed here. Therefore, the effect of gravity can be ignored.

If the channels are very small, the continuum approximation does not hold and the Navier-Stokes equation, used to compute fluid flow on the macro-scale, don't apply [60]. The Knudsen number sets the regime of the flow [61].

$$Kn = \frac{\lambda}{l} \tag{4.2}$$

Where λ is the mean-free-path of the liquid and l the characteristic length scale.

For liquids, λ is approximately the intermolecular length L_{mol} (bond length) and for water this is $\sim$ 0.31 nm [61]. For $0 < Kn < 0.01$ the continuum approximation is applicable and the Navier-Stokes equations can be used. In these micro channels the Knudsen number is (0.31 nm)/(100 µm) $\sim 3.1 \times 10^{-6}$ and the flow is in the continuum regime. This means that the Navier-Stokes equation, Equation (4.3) and the no-slip condition[1] apply.

$$\rho\left[\frac{\delta u}{\delta t} + (\underline{u}\cdot\underline{\nabla})\underline{u}\right] = -\nabla p_0 + \mu\underline{\nabla}^2\underline{u} + f \tag{4.3}$$

Where ρ is the density of the fluid, p_0 is the capillary pressure, μ is the viscosity of the fluid and $\underline{u}$ is the velocity of the fluid.

Navier-Stokes equation is the force equation of a fluid. The first term on the right-hand-side of the equation represents the capillary pressure, the second term represents the shear viscosity and the third term represents any external forces acting on the fluid.

Thirdly, the type of flow needs to be determined. This is determined by the Reynolds number, *Re*, which is expressed as Equation (4.4). The flow can be either laminar or turbulent [8].

[1]The no-slip condition implies that the velocity of a viscous fluid is zero at a solid surface [60].

$$Re = \frac{\rho V R_H}{\mu} \qquad \text{where} \qquad V = \frac{\text{Flow rate}}{WH} \tag{4.4}$$

Where ρ is the density, μ is the viscosity of the fluid, V is the reference velocity, W and H is the width and height of the capillary respectively and R_H is the hydraulic parameter[2].

If the flow is laminar, two different fluids can flow next to each each other and only mix by diffusion. This is a slow process and in typical sized micro channels, the fluids can flow for over 1 cm without mixing [25]. For these channels, the flow should be laminar to prevent turbulence around the cantilevers, as this would increase the noise. Also, it could be an advantage to use laminar flow as each channel theoretically could be used for the entry of multiple fluids.

The flow rate of the channels should lie around 10 µL/min to make sure all liquid quickly runs through the system before evaporating. Substituting for V= 8.33 L/s/m^2 and the values of ρ and μ for water into Equation (4.4), with the restrain of $Re \leq 2000$ for laminar flow, it can be seen that the dimensions of the channel can be huge and still the flow will be of laminar kind. Thus, it is not the dimension of the micro channel that are the limiting factor upon achieving a low Reynolds number

In micro channels with laminar flow, Equation (4.3) reduces to the *Creeping Flow* equation, Equation (4.5) as the inertial forces are negligible and the effect of gravity can be ignored. Here, surface tension and the viscous force is only relevant.

$$\rho \frac{\delta u}{\delta t} = -\nabla p_0 + \mu \underline{\nabla}^2 \underline{u} \tag{4.5}$$

Where ρ is the density of the fluid, p_0 is the capillary pressure and μ is the viscosity of the fluid.

Now, it has been determined that the channels designed will be in the continuum regime, the flow will be laminar and the effects of gravity can be ignored.

4.1.2 Contact angle

The contact angle of a liquid, θ_c, on a surface is measured as the angle between the tangent of the contact line of the droplet and the surface, Figure (4.1).

[2]The hydraulic parameter, R_H, is the ratio of volume to surface area of the capillary.

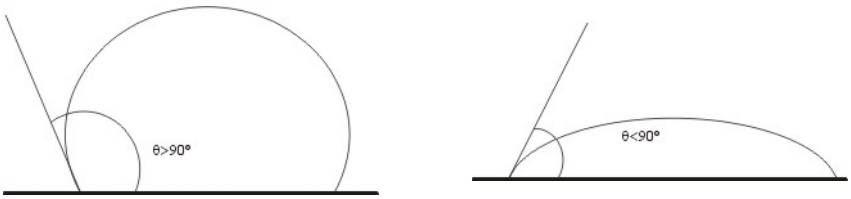

Figure 4.1: A low-energy surface is hydrophobic with θ_c >90°. A high-energy surface is hydrophilic with θ_c <90°.

The physical concept of the contact angle is found from Young's equation, Equation (4.6). The liquid places itself in such a way as to minimise the surface free energy between the three states.

$$\sigma_{sg} - \sigma_{sl} = \sigma_{lg} \cos \theta_c \tag{4.6}$$

Where σ_{sg}, σ_{sl}, σ_{lg} are the surface free energies for the solid-gas, solid-liquid and liquid-gas interfaces respectively and θ_c is the contact angle of the liquid on the surface [62].

If the surface is hydrophobic, $\theta > 90°$ and for $\theta < 90°$, the surface is said to be hydrophilic. Kim *et al.* have showed experimentally that the filling of liquids into capillarities is directly proportional to the contact angle, θ_c, of the liquid on the surface [63]. SU-8 is hydrophobic by nature but in Chapter 5 a method developed to render it hydrophilic is presented.

The contact angle can be of three types; *advancing*, *receding* and *static*. The angel at which the liquid moves forwards onto a surface as a droplet spreads is slightly different to the angle with which it recedes. The advancing contact angle is larger than the receding, they might differ by up till 10° [64]. The static contact angle is the angle used in Equation (4.6) and the experiments done in Chapter 5.

4.1.3 Capillarity

It is not desirable to incorporate any external pumping devices in the fabrication and it is desirable that the capillary force will be enough to flow the liquid through the system. The flow of liquid in a capillary occurs as a result of a pressure difference between two hydraulically connected regions of the liquid mass, and the direction of flow is such as to decrease this difference in pressure [63].

Several groups have done work on liquid flow in micro channels and mostly circular capillaries are investigated. However, it has been shown that when capillary flow occurs in square capillaries, the flow is initiated by liquid running along the corners of the capillary [63, 65]. The channels fabricated

on this chip are square and the Young-Laplace equation is expressed as Equation (4.7) for square capillaries.

$$\Delta p = \sigma \left(\frac{1}{R_1} + \frac{1}{R_2} \right) \tag{4.7}$$

Where R_1 and R_2 are the principal radii or curvature of the flow front shape.

As seen in Figure (4.2), the values of R_1 and R_2 can be substituted by Equation (4.8).

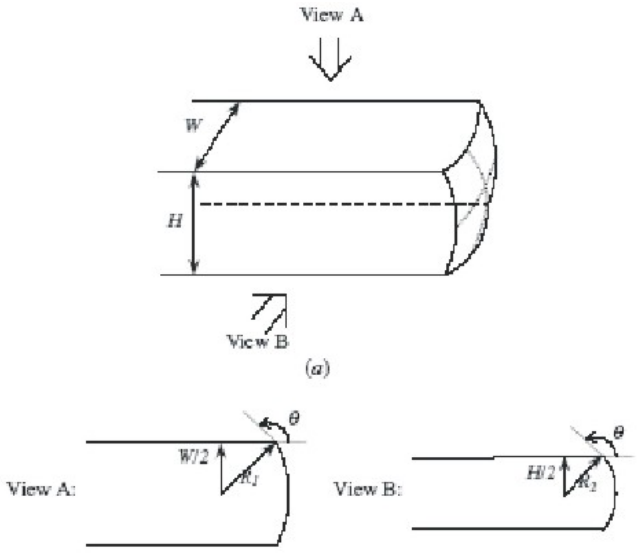

Figure 4.2: R_1 and R_2 are determined by the geometry of the micro channel [66].

$$R_1 = -\frac{W}{2\cos\theta} \qquad \text{and} \qquad R_2 = -\frac{H}{2\cos\theta} \tag{4.8}$$

Where W and H is the width and height of the capillary respectively.

This means that Equation (4.7) can be more simply expressed as Equation (4.9).

$$p = -2\sigma\cos\theta \left(\frac{1}{W} + \frac{1}{H} \right) \tag{4.9}$$

Where the pressure of the air in the cavity is set to zero.

For circular capillaries, Laplace's equation is expressed as

$$\Delta p = \frac{2\sigma_{lg}\cos\theta_c}{r} \tag{4.10}$$

Where Δp is the pressure difference between the two menisci, σ_{lg} is the surface energy at the liquid-gas interface, θ_c is the contact angle of the liquid on the urface and r is the radius of the capillary.

4.2 Design

These channels are intended to be used in sensitising the cantilevers for specific biochemicals. The idea is that solutions can be entered into a reservoir of the channel chip by hand, using a micro pipette, and by the use of a stable mechanical set-up with a micro-positioner, the cantilever chip can be put in position at specific measuring sites. The channel chip should therefore be large enough for easy handling by the human hand, but still incorporate small sites suitable for minimal liquid quantities for the cantilever treatments. This involves one of the major challenges in microengineering - to smoothly go from the macroworld and into the microranges.

4.2.1 Channel chip design

In the fabrication of the channel chip, no external pumping devices or complicated valves should need to be incorporated to simplify the fabrication and handling of the chip. The fluid should flow by the capillary force and reservoirs are placed at the entrance and exit of the channel with a small measuring site in the middle. Components to control the liquid flow have been fabricated and demonstrated, but the process of incorporating such devices usually makes the fabrication of the chip very costsome [67]. This prevents the chip from being disposable, which is an important property of a channel chip used in medical 'Point-of-care' devices. This might be one application of the chip.

Goedecke *et al.* have designed a simple and very useful set-up where the liquid is driven by evaporation from the waste reservoir [68].
Namasivayam *et al.* have reported on a similar solution, where they mimic the driving motor of trees and thereby generate a continuous flow [69]. Goedecke *et al.* manage to achieve flow rates of 2.25 mm/s (0.27 µL/min) which is well suitable for this type of application. However, to maintain this flow rate, a fan is needed at the waste reservoir to obtain an un-even evaporation rate over the liquid system. No such devices were desired in this design. Instead, the reservoirs were left open, as well as the measuring sites for the liquid to flow through the channels purely by capillarity.

It has been shown that bubbles have a great tendency to form and stay at sharp edges in micro channels [62]. To prevent any clogging due to bubbles, the bends of the channels were made smooth and no sharp corners were incorporated anywhere in the design.

The smallest volume required to accurately determine DNA assays is reported as 100 µL and a typical aqueous droplet, for example blood, is of a volume of 30 µL [70]. The intention was to design the reservoirs to hold a volume of 30 µL but as the thickness of the chips should only be around 200 µm, that volume was not possible in the designated area. Instead, the reservoirs were made to encompass a volume of 10 µL which could then be refilled easily for larger samples.

The place where the cantilevers should be introduced is called the measuring site. Preferably, all liquid passing through there should come in contact with the cantilevers, to reduce the amount of wasted liquid. The sites can however, not be made too small as positioning the cantilevers should still be straight forward. A size of 600 µm x 500 µm was decided.

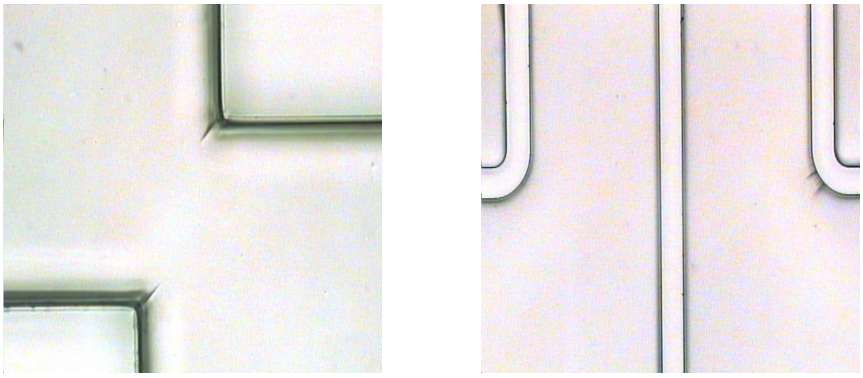

Figure 4.3: The stress in thick layers of SU-8 is seen as wrinkles in the corners. *Left:* The stress is often released in corners. *Right:* The stress can also typically be seen at the bends of the channels, but not every time.

It was seen that when cross-linking large areas of SU-8, the cross-linked polymer had a tendency to crack, due to the large build up of stress. Typical signs of released stress are seen in Figure (4.3). The concept of *stress barriers* was introduced by Chang *et al.* and was also applied in this design [71]. They show that by reducing the connected area of cross-linked SU-8 and separating it from the structures, cracking and wrinkling of the SU-8 can be avoided. This was taken into consideration and *stress holes* were included in the design. Ideally, the channels should only exist of thin walls separated by air to exclude the negative effect of stress. Lin *et al.* have used a technique of 'constant-volume-injection' method to achieve this, with very good results in reduction of stress [72]. This structure would not be very stable for handling

after the release off the Si wafer, and the stress holes were therefore used as a compromise. Both holes of 50 µm x 50 µm and 100 µm x 100 µm were used. It was carefully observed that the stress holes were not placed underneath the reservoirs nor the channels.

4.2.2 Mask design

For the fabrication of the channel chip, three masks were used. All masks were designed with the software L-Edit and fabricated as standard Cr/Glass masks.

The first mask was used to define the bottom layer. Stress holes of 50 x 50 μm^2 were incorporated, Figure (4.4). The stress holes were placed in groups of 308 and 378 in the center of the chip and in smaller groups of 60 and 170 on the sides. The dimensions of the whole chip were 30,000 µm x 35,000 µm.

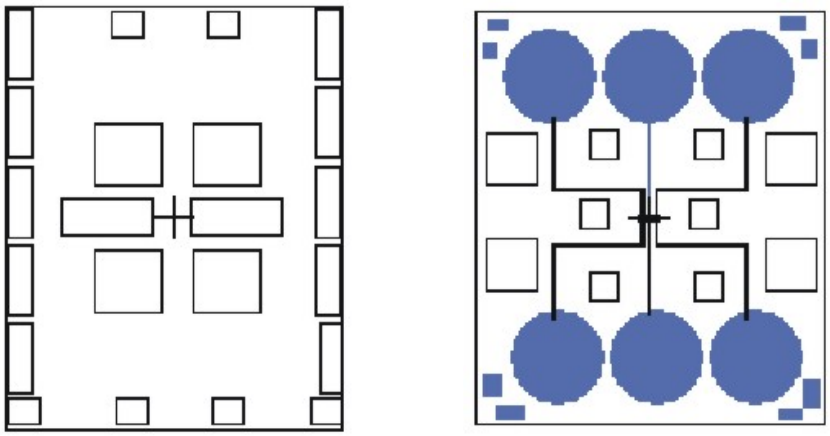

Figure 4.4: *Left:* The mask used to define the bottom layer of the channel chip. Each square seen represents a group of between 60-378 50 µm x 50 µm stress holes. *Right:* The mask used to define the walls of the reservoirs and the channels. The different sized square represents groups of 25 and 64 100 µm x 100 µm stress holes respectively.

Secondly, a mask needed to define the reservoirs and channel walls was used, Figure (4.4). In this layer, stress holes of 100 µm x 100 µm were added. They were placed in groups of 25 and 64 on the chip. The radius of the reservoirs is 0.4 cm and the width of each channel is 100 µm. Due to the large size of the reservoirs needed, only four chips could be fitted on every Si wafer. The reservoirs could be placed differently to reduce the size of every chip but the gain in available area was minimal and not sufficient to fit another chip. The outermost channels have a total length of 1.5 cm and the center channel is 7.7 mm long.

Lastly, a mask to close the channels was used, Figure (4.5). This mask

was not used every time. Instead of structuring the lids on the same wafer as the channels, the mask for the lids could be used in combination with the second mask on a separate wafer, to define a top layer. This layer could then be glued onto the bottom layer comprising the channels. The lids have a width of 300 µm and the center piece is 1700 µm wide. This is far wider than the channels, to simplify the aligning process.

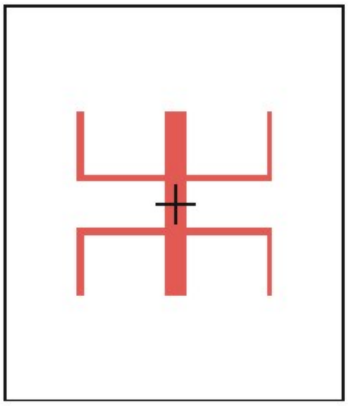

Figure 4.5: The mask used to define the lids of the channels. The lids have a width of 300 µm and the center piece is 1700 µm wide.

4.3 Fabrication sequence

Here, the fabrication sequence of the channel chip is described. In Figure (4.6) the cross-sectional structuring of the chip can be seen. The parameters for spin speeds, baking temperatures, baking times and exposure dosage for the SU-8 can be found in Chapter 2, where each step of SU-8 fabrication was described in detail.

4.3.1 Bottom layer

The bottom layer of the channel chip is spin-coated with SU-8 to a thickness of 10 µm. It is patterned by the mask in Figure (4.4). After the cross-linking, the bottom is developed and hard baked, to remove the un-exposed SU-8.

4.3.2 Walls

The walls of the reservoirs and channels is patterned from two thick layers of SU-8 2075 and structured with the mask in Figure (4.4).

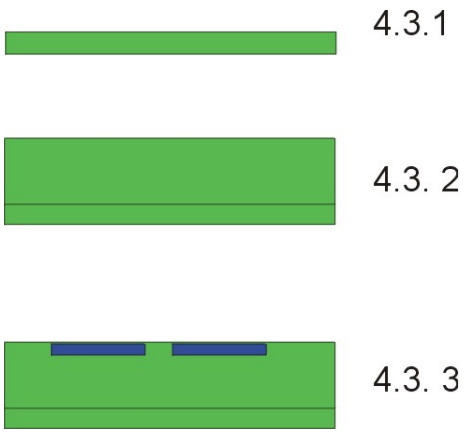

Figure 4.6: Side view of the fabrication sequence of the channel chip. The numbers correspond to the relevant sections.

4.3.3 Lid

To achieve a fast and continuous flow, the channels should be closed as capillaries. The closed structure of the channels is also good to minimise the evaporation of measuring solution before it reaches the measuring sites. Structuring SU-8 by standard UV lithography, the whole layer of resist will cross-link, due to the low optical absorption of the polymer, Figure (4.7). This obviously presents a problem for the fabrication of closed micro channels and different methods are used within the field of micro fluidics to overcome this obstacle.

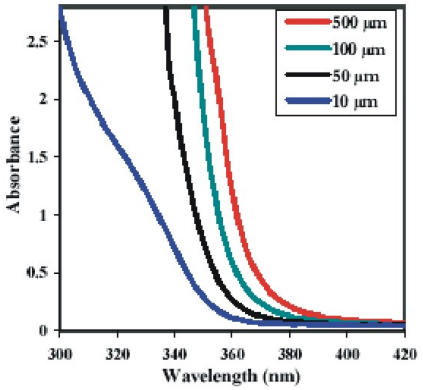

Figure 4.7: The low optical absorption of SU-8 in the near-UV spectra prevents the fabrication of overhanging structures.

The easiest and most intuitive method is to fabricate the micro channel in two steps, gluing the top layer to the bottom layer after developing the two. The top layer is often just made simply out of a glass wafer, possibly with drilled holes for the entering of liquids [73]. Another method is to cover the channels with another, more flexible material, as the resist Riston® [74]. The most common problem with the gluing technique is to achieve a fully enclosed junction, with no resulting leaks. Even the smallest opening will lead liquid from the channel and in-between the two layers. This could possibly disrupt the system.

To prevent this from happening, the lid of the micro channel should be fabricated in the same processing step as the defining walls. For this, electron beam (e-beam) lithography [75, 76] and proton beam exposure [77] have been demonstrated to be very successful, Figure (4.8).

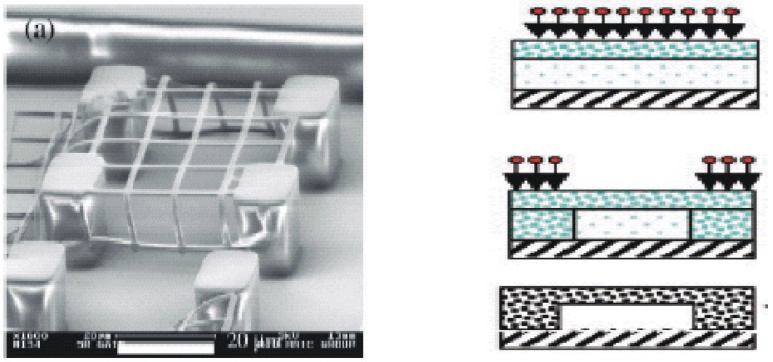

Figure 4.8: By the use of different lithography techniques, SU-8 can be structured with a defined top-wall thickness. *Left:* E-beam lithography can produce structures to a thickness of hundreds of nanometers [76]. *Right:* Proton beam techniques can produce SU-8 structures as thin as 5 µm [77].

Guérin *et al.* present different ways to achieve closed micro channels, one *fill process* and one *mask process*, Figure (4.9). There, a different material to SU-8 is used to either fill the structures which should be left open or to mask them, preventing the UV-light from cross-linking the underlying SU-8.

The methods mentioned above have all resulted in the successful fabrication of closed micro channels, but they are all rather complicated and often require expensive equipment. The approach taken in this project, was to try to mimic the results from Chuang *et al.* who have reported on closed micro channel fabrication by controlled UV-dosage exposure [47]. They use an anti-reflection coating in their work, but here a lower wavelength than 365 nm is used. The optical absorption of SU-8 drastically increases with a lower wavelength, Figure (4.7). By exposing the channels with the mask for the lids in an Aligner without the 365 nm filter, also light at lower wavelengths will be included, Figure (4.10).

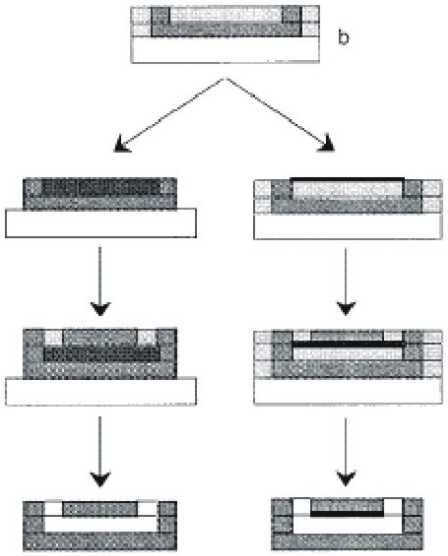

Figure 4.9: Schematic drawings of the *fill process* and the *mask process* for micro channel fabrication [43] *Left:* The filling material is removed after processing, leaving enclosed channels. *Right:* A layer of metal is used to mask the section which should not be exposed.

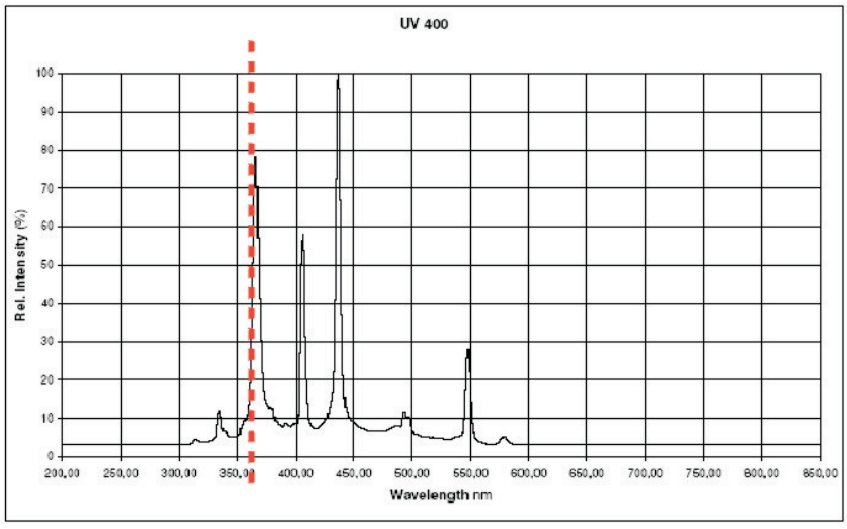

Figure 4.10: The wavelength spectra of the two Aligner lamps. The KS Aligner has a filter blocking out all light below 365 nm, marked with a red dotted line. The EVC Aligner does not have this filter.

SU-8 was spin-coated to a thickness of 360 µm and first exposed with the

mask of the cantilever support layer. Secondly, it was exposed in an Aligner (EVC) with the mask of the cantilever network for different energy dosages. The resulting thicknesses of the network top-wall are seen below in Figure (4.11).

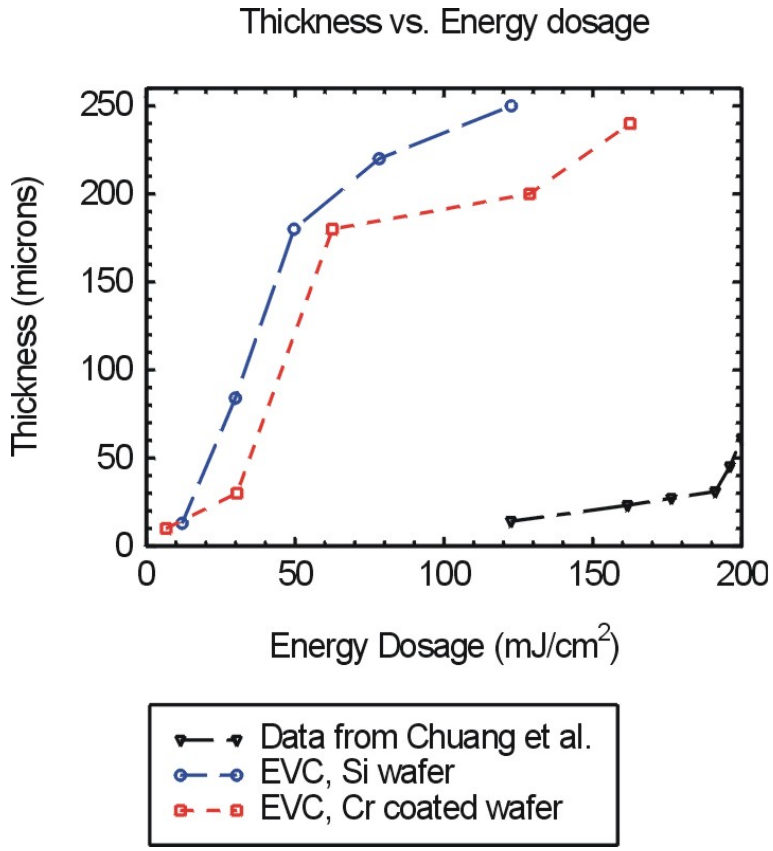

Figure 4.11: The variations in top-wall thicknesses with increased energy exposure using the EVC Aligner compared to the results from Chuang *et al.*.

It can be seen in Figure (4.11), that the resulting thicknesses differed when the SU-8 was structured upon a bare Si wafer or upon a Cr coated Si wafer. This is because also the reflected light has an effect on the cross-linking density. The reflectivity is found from Equation (2.1). The values of n are; n_{SU-8}=1.57, n_{Cr}=1.86, n_{Si}=6.01. From this we can calculate that a Cr coated Si wafer would only have 0.7 % of the induced light, which reaches the bottom of the SU-8, reflected, whereas a bare Si wafer would reflect 34 % of the same light.

The results from the UV-dosage exposure control experiments looked promising, but unfortunately other problems were encountered when they were applied to the small micro channel structures. One major problem

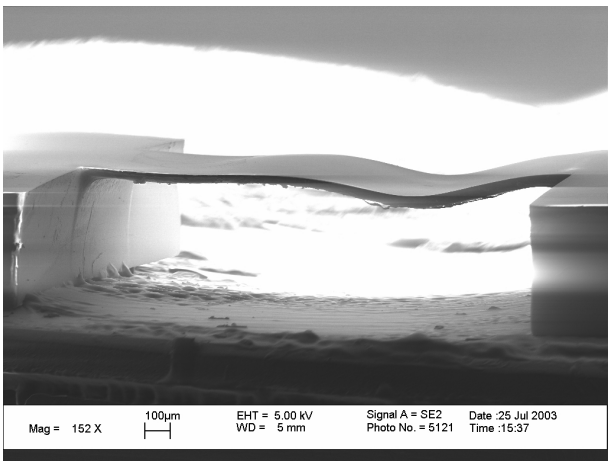

Figure 4.12: By only exposing the SU-8 structures to a low energy dosage, the thickness of the cross-linked top wall can be controlled.

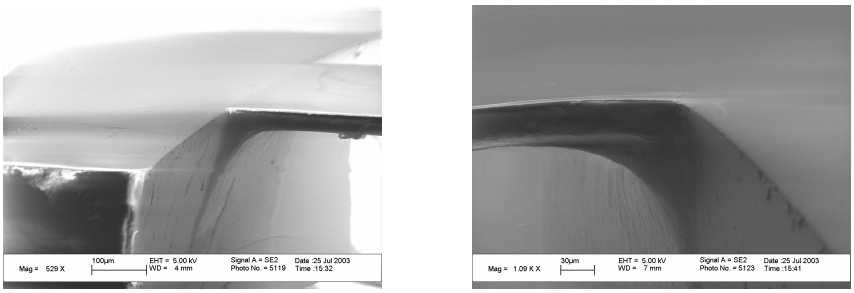

Figure 4.13: Due to diffraction off the cross-linked SU-8 support, straight corners are not achieved upon the second exposure.

was to develop the non-cross-linked SU-8 encapsulated in the channels. Guérin *et al.* and Tay *et al.* also point to this problem but they do manage to achieve fully developed structures [43, 77]. In this project, this was unfortunately not achieved due to the length and bending of the channel design, Figure (4.14).

The failure in developing the closed channel structures was probably a combination of the low viscosity of the SU-8 2075 used in the spin-coating, as well as the non-straight corner between the side wall and the lid, resulting from diffraction of the UV-light in the cross-linked SU-8 supports. In the exposure trials, the distance between the supports was 2000 µm but in the micro channels, the side walls are only separated by 100 µm. The small protrusion, which does not have a noticeable effect on the large scale, become crucial on the micro channel scale.

It is not fully understood how over-hanging structures can be obtained

by exposing the SU-8 to a light source without the 365 nm filter. Possibly, the shorter wave lengths have a cross-linking effect on the top layer of the SU-8, which in turn becomes less transparent to the light of $\lambda \geq 365$ nm and thereby preventing a full cross-linking.

It was later realised that the channels did not need to be closed to achieve a sufficiently fast flow of the measuring solutes.

4.3.4 Develop and Release

The closed micro channels never developed properly. If the structures were not closed, there was no problem to develop the reservoirs or channels as well as the measuring sites.

The channels were released from the Si wafer by a Cr etch. The release took over 48 hours due to the large surface area of the reservoirs.

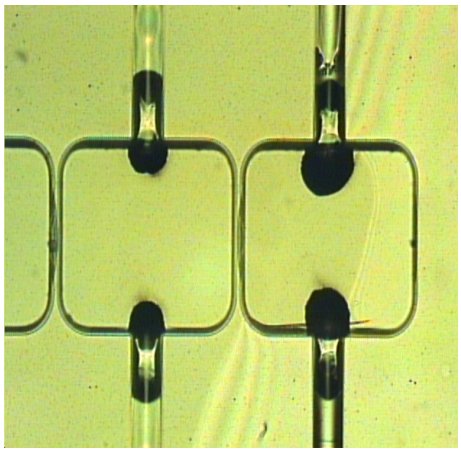

Figure 4.14: The enclosed SU-8 does not manage to come out of the closed channels.

4.4 Summary

The channel chips designed were successfully fabricated with open channels. No chips could be fabricated with closed channels, but in liquid flow experiments, it was realised that closed channels were not necessary to achieve a high flow rate.

As no chip like this had been fabricated previously, the dimensions needed were not known. The reservoirs were made to include a volume of 10 µL of solution but once fabricated and tested, it was realised the reservoirs could be much smaller as the amounts of detection solutes needed was much lower. This would mean the advantage that probably more chips could be fitted on every wafer during the fabrication.

Chapter 5

Surface Investigations

The chemical and mechanical properties of the material SU-8 have previously been studied in detail. The properites were listed in Table (2.1) in Chapter 2. On the other hand, the surface properties of SU-8 are not known at all. For example; the chemical structure, the surface roughness, the contact angle and the reactions with other chemicals. These properties have been studied and the results are presented below in this chapter.

In Section (5.1) the adhesion between SU-8 and materials commonly used in SU-8 fabrication are analysed. The adhesion between SU-8 and Au is investigated via bond strength measurements, done in collaboration with Associate Professor Bjarne Clausen at IPL, DTU.

In Section (5.3) the effects of different plasma treatments on SU-8 are investigated by the etch rate. AFM investigations were also done on plasma treated samples in collaboration with PhD student Maria Holmberg, Bioprobes group, DFM, DTU.

In Section (5.5) contact angle modifications are developed and in Section (5.6) XPS studies are done on the samples. The XPS measurements were done in collaboration with Institute Leader Ib Chorkendorff and Lab Technician John Larsen, ICAT, DTU.

5.1 Adhesion

Adhesion between two samples is a combination of physical, mechanical and chemical adhesion. The physical adhesion is due to Van der Waal's and hydrogen bonds forming between the two surfaces. Mechanical adhesion is mainly obtained due to friction between two non-smooth surfaces where the irregularities can interlock. Chemical adhesion originates from chemical bonds forming between the two surfaces, other bonds than for the physical adhesion [78].

This section will discuss the adhesion of SU-8 to itself, to the resist AZ5214E, to Si wafers and to metals, which are all relevant issues for this project. No specific problems have been experienced with the adhesion of subsequent SU-8 layers to existent ones nor with the adhesion between SU-8 and the resist AZ5214E. On the other hand, great difficulties have arisen when trying to make SU-8 stick to layers of metal as well as making metals stick to SU-8 and in parts of the fabrication process there have been problems with the adhesion of SU-8 to the Si wafers.

More detailed investigations of the adhesion between SU-8 and Au were carried out with pull-test experiments. These were carried out at The Institute of Manufacturing Engineering and Management (IPL) at DTU in collaboration with Associate Professor Bjarne Clausen.

5.1.1 Adhesion between SU-8 and SU-8

The fabrication of SU-8 chips is done in several steps where a new layer of SU-8 is spun onto already-present ones. This was described in detail in Chapter 2.

To achieve the desired thickness of the support layer for the cantilever chips, the last layer needs to be spin-coated in two stages. The two SU-8 layers are then exposed and structured simultaneously. On such occasions, the previous layer is still not cross-linked when the following layer is spin-coated. The two layers of SU-8 seem to diffuse together during the second soft bake and on no occasion in the processing did problems with this step appear. SEM images of a cantilever chip also shows there to be no visible division between the two layers, Figure (5.1).

Most commonly though, the new layer of SU-8 needs to be structured differently to the previous layer which means the first layer has already been cross-linked. When the support structure is spun onto the cantilevers, the cantilever layer has previously been cross-linked, developed and even hard baked. To increase the adhesion between the cross-linked and the new SU-8 layer, the wafer is treated to a plasma. The plasma asher is set to flow 240 sccm of oxygen and 40 sccm of nitrogen at a power of 400 W for 4 min. The plasma treatment results in an increase in surface energy and surface

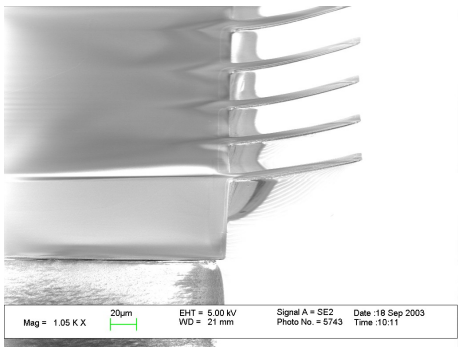

Figure 5.1: The support layer for the cantilevers is structured with two subsequent layers of SU-8. No division can be seen between them, they have fused together perfectly.

roughness, Section (5.3).

No problems appeared with this step either, but it has been seen to occur for other people in our group [39]. Ideally, the top of the lower SU-8 layer should never be fully cross-linked when a new layer of SU-8 is added. However, this cannot be achieved with standard top-side exposure equipment, as all exposed resist will cross-link during PEB.

Bond strength investigations have been done by other groups where they report on a value of a maximum bond strength of 14 MPa and 20.6 MPa respectively for SU-8 to SU-8 where the lower layer initially was cross-linked [79, 80]. Dellmann *et al.* have reported on a bonding surface energy of SU-8 as 0.43 $\mathrm{Jm}^{-2} < \gamma_s < 2.26\ \mathrm{Jm}^{-2}$ [37].

5.1.2 Adhesion between SU-8 and AZ5214E resist

A thin layer of the resist AZ5214E is used in the patterning of the Au covering the cantilevers. The resist is spun onto a developed and hard baked layer of SU-8. It has been known that for other resists, which are very hydrophobic, the AZ5214E resist has had a tendency to spin off the wafer due to very low adhesion but on no occasion in this processing did problems of this type appear.

5.1.3 Adhesion between SU-8 and Si wafers

The SU-8 is kept on Si wafers throughout the processing sequence and problems with this adhesion would be disastrous. In the process, the wafers are covered with a release layer consisting of 50 Å Cr, 500 Å Au and 500 Å layer of Cr. The wafer is left in a 200 °C oven for at least 2 hours prior to processing, to dehydrate the wafer and increase the adhesion. Only on one occasion was there a problem with the SU-8 structures starting to come

off the wafer. This happening proved rather to be a problem with the SU-8 layer not being fully cross-linked. On development, PGMEA was able to sneak in underneath and 'release' the structures. When the exposure dose was doubled, the problem did not persist.

When large structures are patterned, the adhesion proves crucial. On many occasions large amount of thermal/intrinsic stress can be seen to pull the structures off the wafer. The SU-8 layers stay together though, so it does not result in a breakage of the chips.

Other groups, who do not use the same release technique, have shown that a good rinse of a Si wafer with piranha solution (sulphuric acid:hydrogen peroxide, 3:1) and dehydration on a 200 °C hotplate for 20 min prior to processing is enough to achieve sufficient adhesion of SU-8 structures [73]. This method is easier but cannot be applied in this case, as the structures need to be separated from the processing wafer.

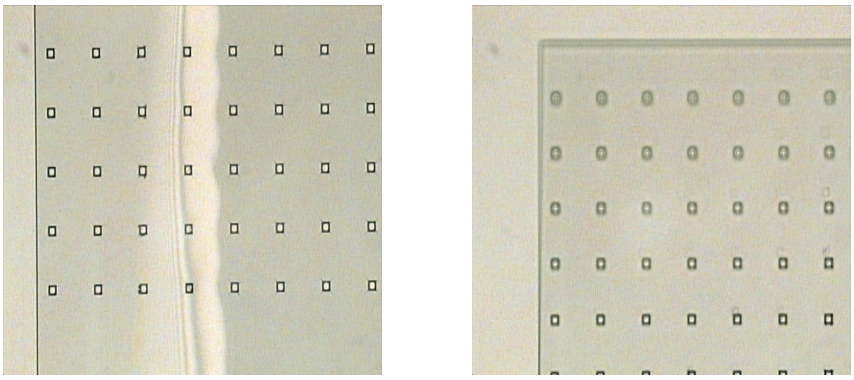

Figure 5.2: *Left:* The colour change underneath the SU-8 structure is PGMEA which has penetrated in between the SU-8 and the substrate. *Right:* The structures are lifted off from the substrate which can be seen as difficulties to focus over the whole area.

5.1.4 Adhesion between SU-8 and metal

In the fabrication of these chips, metals only need to be incorporated with the SU-8 structures in one step. The cantilevers are covered with a thin layer of Au to provide good reflection for the laser used for the detection and to make the two sides of the cantilever different from one another. The adhesion between SU-8 and metal is known to be very poor, especially in the case of Au. At the same time, Cr and Ti are often used as adhesion promoters. The answer to the different effects of these metals lies in their electronic configuration, Table (5.1).

Au is a metal with a very high electronegativity compared to the other metals mentioned. This can also be concluded from its closed electronic configuration where there is only one half-full atomic shell, the 6s shell,

Metal	Electronic configuration	Electronegativity (Pauling scaling)
Au	$[Xe]4f^{10}5d^{10}6s^1$	2.54
Ti	$[Ar]3d^2 4s^2$	1.54
Cr	$[Ar]3d^5 4s^1$	1.66
Al	$[Ne]3s^2 3p^1$	1.61
Si	$[Ne]3s^2 3p^2$	1.90

Table 5.1: The electronic configuration and electronegativity for some metals commonly used in the fabrication. For comparison also Si.

which makes the metal very inert. Cr and Ti, on the other hand, have fairly low values of electronegativity and their electronic configuration shows more open shells. Especially in the case of Cr, where all its outer shells, 3d and 4s, are half-full. Metals with many half-full atomic shells show a greater tendency to react with surrounding materials, Cr and Ti oxidise very easily for example. Adhesion is attained by Van der Waal's forces and electrostatic attractions and therefore more reactive compounds will provide better adhesion. Still, the adhesion of SU-8 with metal is bad but it's better in the case of Ti and Cr than for Au.

For the case where metal is deposited on SU-8, the resist is treated to a plasma just prior to the metal deposition. Standard recipe of 240 sccm oxygen and 40 sccm nitrogen at 400 W for 4 min is used. This increases the cleanliness, the energy and the roughness of the surface. All these factors are very important upon increasing adhesion. For the case of SU-8 being structured upon a layer of metal, the plasma treatment is not effective enough to increase the adhesion and rather an adhesion promoter is needed.

One example of adhesion promoter is Omnicoat, provided by MicroChem [28]. This material works both as a release layer and adhesion promoter, where it is easily stripped with an oxygen plasma. According to MicroChem 'Omnicoat is simply a dilute formulation of our PMGI (Polymethylglutarimide) resin. PMGI has excellent adhesion to almost any substrate when baked above 200 °C. The SU-8 is better able to bond to this resin than the substrate alone' [81]. Omnicoat was never used in this processing due to previous bad experiences with the product within the group. Omnicoat proved to be incompatible with the metal structuring step of the process [39].

5.2 Investigations of SU-8 and Au bond strength

No information could be found in literature and no work has been published on the adhesion between Au and SU-8. This is rather surprising as Au is the most common metal used in combination with the polymer. It is the closed electronic configuration of Au that makes it both desirable as a component

(high electrical conductivity and reflectivity) and difficult to work with.

To investigate the strength of this bond, pull-test experiments were performed. In the experiment, four samples were tested; one which had a monolayer of the molecule 4-AminoThiolPhenol (4-ATP) as an alternative adhesion promoter (A), one which had an intermediate layer of Omnicoat (B), one with a Ti adhesion layer (C) and one which had SU-8 patterned straight onto Au (D).

5.2.1 4-AminoThiolPhenol

4-AminoThiolPhenol (4-ATP), Figure (5.3), is investigated as an alternative adhesion promoter. Previous work in our group has shown Omnicoat to be incompatible with the metal lift-off step in the fabrication of SU-8 [39].

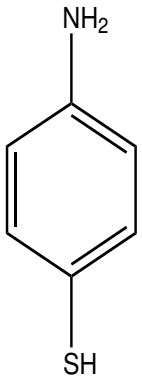

Figure 5.3: Chemical structure of the molecule 4-AminoThiolPhenol used in a mono-layer in the patterning of SU-8 on Au.

The molecule 4-ATP binds to the Au layer with the thiol group (–SH–) [82] and the opposite amine group ($–NH_2$) is commonly used to react with epoxy groups (–CH–O–CH_2–) [83]. Thereby the molecule is ideal to use as a monolayer in between SU-8 and Au and the bond strength is expected to increase drastically. The 4-ATP was diluted in absolute ethanol to a concentration of 10 mM.

5.2.2 Sample preparation

Four 4" $\langle 100 \rangle$ Si wafers were covered with a 50 Å layer of Cr to make sure the bond between the Au and the wafer was strong and would not break. The wafers were then coated with a 500 Å layer of Au, which the SU-8 was structured upon. The different wafers had different adhesion promoters between the Au and SU-8 which are described below.

A This wafer is soaked in 40 mL of 10 mM 4-ATP overnight to make sure the Au is covered with a complete monolayer. The wafer is taken directly from the Alcatel where the Au is deposited to make sure the surface is fresh and clean. The wafer and the solution are kept in an air-tight container and afterwards the wafer is rinsed in absolute ethanol to remove any excess 4-ATP molecules that are not properly bound to the Au.

B This wafer has a layer of Omnicoat as adhesion promoter. The Omnicoat is spun with a spin recipe in two stages; the first stage has a spin speed of 3000 rpm and an acceleration of 400 rpm/s followed by a spin speed of 5000 rpm and an acceleration of 600 rpm/s. The Omnicoat is baked for 2 min on a 120 °C hotplate.

C This wafer has a 20 Å layer of Ti deposited onto the Au straight after the deposition of Au.

D The final wafer was used as a reference and did not have any further treatments. The wafer was processed directly after the metal deposition, to prevent an oxide layer to form on the Cr.

After these different treatments, all wafers had a 10 μm layer of SU-8 2005 structured, details on the preparation can be found in Chapter 2. To increase the adhesion of the SU-8 to the epoxy-glue the wafers were treated to a plasma. Finally, the squares were cut with a diamond scriber.

The samples were glued between two 10 mm iron bolts with a 17 mm head diameter. Before the gluing, the heads of the bolts were planarised in a turning lathe. The samples were glued using epoxy-based two component glue (Super Epoxy, Loctite). A thin layer of prepared glue was spread on the head of one bolt and a small drop of the glue was placed on the Si surface of the sample. They were pressed into contact and left for 10 min for the glue to cure. Another thin layer of mixed glue was then spread onto the head of another bolt. This was placed heads-down on top of the previous bolt and it was made sure the two bolts were perfectly aligned and that the sample was placed horisontally. The bolts were left for at least 10 min for the second layer of glue to cure. When gluing the second bolt, no glue was placed on the SU-8 surface. Due to the very small thickness of the sample ($\sim$2 mm) it proved to be very easy to get too much glue which would then pour down the sides of the sample, leaving it useless for experiments. When the sample had been glued between the bolts, it was left for 12 hrs before the experiments were carried out, to make sure the glued bond had acquired full strength.

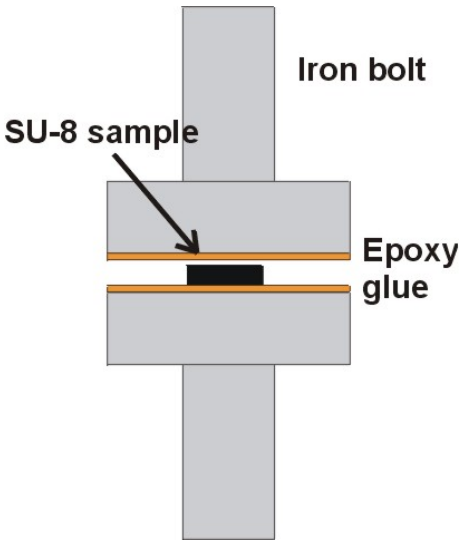

Figure 5.4: The SU-8 sample was glued in-between two iron bolts with epoxy glue. The dimensions are not to scale of this drawing.

5.2.3 Experimental details

The pull-test experiments were carried out on an Instron 1115 standard pull-testing machine at the Institute of Manufacturing Engineering and Management (IPL) at DTU. The samples were placed in between the two grippers of the equipment which are separated at a speed of 0.5 mm/min, whilst computing load-extension curves. The lowest mass range of 0-415 kg was chosen, as the bond is expected to be very weak.

It is very important that the samples were glued properly and that they were perfectly aligned as any non-vertical strain will have a negative effect on the final graphs. The measurements were carried out at room temperature. The breaking of the bond is observed as a drastic drop on the load-extension graph simultaneously plotted on the computer and as a snap. After the bond had broken, the samples were visually inspected to make sure it was actually the bond between the SU-8 and Au that broke.

5.2.4 Results

From the load-extension curves plotted from the pull-test experiments the bond strength can be calculated. Bond strength is calculated as the force per unit area the bond can stand before it breaks.

$$\text{Bond Strength} = \frac{m \times g}{A} \tag{5.1}$$

Where m is the breaking load, g is the acceleration due to gravity and A is the cross-sectional area.

Below typical data obtained can be seen, Figure (5.5). Here, the data from the sample treated with 4-ATP are shown and similar graphs were obtained for the other three samples as well. The pull-test experiments were carried out on two occasions. The first time twelve samples were prepared but data could only be obtained from one sample for each treatment. This was due to problems with the gluing and the preparation of the samples. On the second occasion, sixteen samples were prepared and this time the gluing procedures had been improved and more data could be obtained.

The analysis of the data could be more rigorous and one of the methods presented by B. Bilenberg could be used [84]. Due to limited time assigned for these investigations, a simple average was calculated on the obtained data and standard deviation was used as error analysis.

Sample	No. of samples	Bond strength (MPa)	Standard deviation (MPa)
A (4-ATP)	3	5.6	1.8
B (OmniCoat)	1	11.4	n/a
C (Ti)	3	5.2	1.7
D (Reference)	4	3.8	0.9

Table 5.2: Measured average bond strengths for the four different wafers investigated. The letters correspond to the respective treatments of the wafers.

5.2.5 Conclusion

In this investigation it was the structuring of SU-8 onto Au that was investigated. It is important to remember that the conditions for structuring Au onto SU-8 are slightly different. When the Au is deposited onto a layer of SU-8, a plasma treatment will usually be enough to make the bond sufficiently strong. For the case investigated here, this will not be enough.

The bond between SU-8 and Au was measured to have a strength of 3.8 ± 0.9 MPa. This is a very weak bond, as seen in the clean room work, compared to the reported bond strength value of 20.6 MPa between two layers of SU-8.

As can be seen from the results listed in Table (5.2) it is the Omnicoat that is the strongest adhesion promoter between SU-8 and Au, of the ones investigated. It can also be noted that no error is available for this adhesion promoter. This is because it was only possible to obtain bond strength

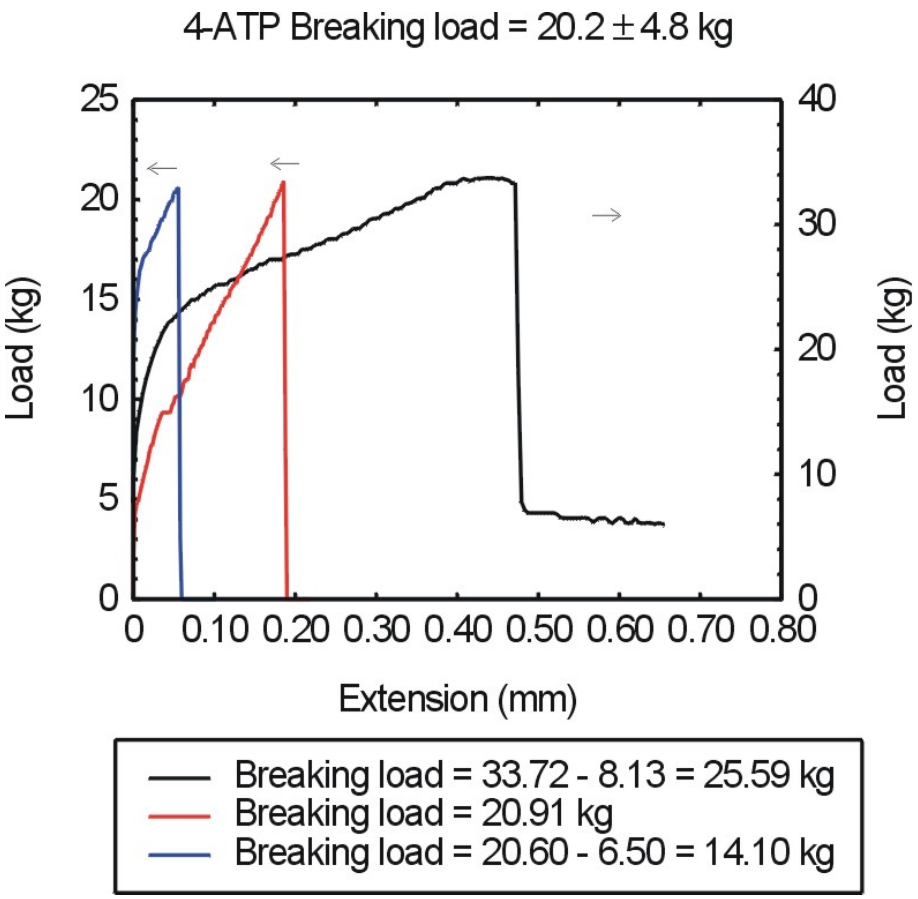

Figure 5.5: Typical load-extension graph combining all data obtained in the pull-test experiments. Bond strength of the samples is calculated from the breaking load.

data from one sample out of the seven samples prepared. It has been mentioned before that Omnicoat is not ideal for this process as it is incompatible with the metal structuring step of the process and this test also shows how unreliable Omnicoat can be to work with.

The bond strength of the samples treated with 4-ATP and Ti show a very close value. It can be argued that the Ti is easier to incorporate in the process as it is a much faster process and that it can be done in the same step as the Au is deposited. On the other hand, 4-ATP is more suitable as usually the spin-coated SU-8 should not cover the whole area. As seen above, Figure (5.6), if the Au should be exposed to the environment one might encounter difficulties.

In the case of the cantilevers fabricated in this project, the Au is deposited to make the cantilever surface easy to chemically sensitise and to provide good reflection of the laser spot. For the former, the Au needs to be the outermost layer and once the SU-8 has been structured and developed, the

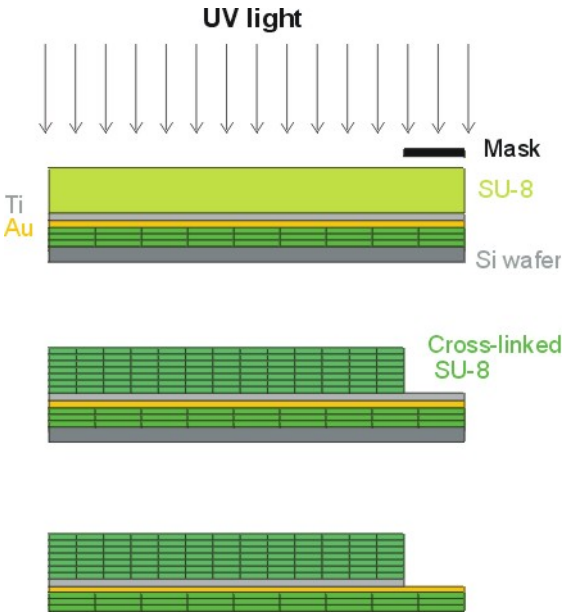

Figure 5.6: The Ti deposited as adhesion promoter between the SU-8 and Au needs to be etched in the final step to provide a naked surface of Au on one side of the cantilever.

adhesion promoter needs to be removed. Ti is etched in Hydrofluoric acid (HF) which is very dangerous to work with. HF might also have an effect on the Au deposited and the SU-8 structures. It has been seen experimentally that Au surfaces can be regenerated from thiol bonds with an UV/O_3 treatment [83] and it suggests that 4-ATP could easily be removed by the same treatment. Since it is easier to remove the 4-ATP, this is a much better option as an adhesion promoter when spinning SU-8 onto Au.

5.3 Plasma

In this section different plasma treatments of SU-8 will be discussed. Plasma treatment of the surface is commonly used before deposition of metal or a new layer of resist to increase the adhesion. Therefore, the effect of different plasma treatments were investigated with Atomic Force Microscopy (AFM).

5.3.1 Plasma treatment

A plasma is the fourth state of matter where the atoms have been torn apart and the constituent components exist separately [85]. In the cleanroom, the equipment available for plasma treatments are a plasma asher and reactive-ion etching (RIE). In this investigation only the plasma asher was used.

The plasma asher produces ionized species which are accelerated towards the substrate. A Faraday's cage surrounds the wafers and prevents the substrate from being bombarded by the ions. In the process, plasma treatments were used prior to depositing metal or a new layer of resist. The plasma was used as it increases the surface roughness and energy, which is very advantageous in the aspect of adhesion. Here, investigations were done to see if the expected and desired results were actually achieved. Oxygen, nitrogen, tetra-fluoro-carbon and argon plasmas were investigated.

The ions produced in a plasma asher are chemically reactive and when these react with the surface of the sample it can either result in volatile species that will be removed by the vacuum pump or it can leave the surface with a chemical modification [86]. It can be used to remove Omnicoat for example, or to make the surface of SU-8 change from hydrophobic to hydrophilic.

It was seen that when placing a wafer with partially non-cross-linked SU-8 in the asher and running it with 120 sccm of tetra-fluoro-carbon at 400 W for 4 min followed by 120 sccm of nitrogen at 200 W for 5 min that the top layer of the SU-8 cross-linked. It could easily be cracked open by a light tap of a pair of tweezers. The SU-8 was cross-linked due to the high temperature in the plasma asher and by the small amount of UV-light present.

5.3.2 Etching rates

We wanted to investigate the etch rate of SU-8 in different plasmas. SU-8 is very hard to remove once it is cross-linked. Therefore, we wanted to investigate the possibilities to use a plasma to etch it. To investigate the effects of the oxygen plasma, 1.7 µm structures of SU-8 2002 were used. To investigate the effects of tetra-fluoro-carbon plasma, structures fabricated to a thickness of $\sim$10 µm were used. The results are displayed below in Table

(5.3) and (5.6).

The different wafers were all treated to an oxygen plasma at 120 sccm for 1 min at different powers. The height of the structures was measured with the Tencor profilometer, on ten different positions, before and after the plasma treatments, Table (5.3). The etch rate of oxygen plasma was negligible.

Power (W)	Initial height (μm)	Final height (μm)	Etch rate (nm/min)
200	1.765 ± 0.014	1.725 ± 0.038	-39 ± 52
400	1.759 ± 0.029	1.732 ± 0.041	-27 ± 70
800	1.775 ± 0.017	1.763 ± 0.016	-12 ± 33
2000	1.739 ± 0.023	1.668 ± 0.061	-71 ± 84

Table 5.3: Etch rates for different effects of oxygen plasma treatment. It can be concluded that oxygen plasma does not have an etching effect on SU-8.

Three different wafers were all treated to a tetra-fluoro-carbon plasma at 120 sccm for 40 min at an effect of 1000 W. Due to safety regulations in the clean room, the plasma asher needs to be run with a cleaning program of 200 sccm of nitrogen at 1000 W for 5 min before the asher is opened. Therefore, one wafer was treated to this cleaning program only, so the effect of the tetra-fluoro-carbon plasma could be calculated. The height of the structures was measured with the Tencor profilometer before and after the plasma treatments, Table (5.6).

Plasma	Initial height (μm)	Final height (μm)	Etch rate (nm/min)
CF_4 + N_2	9.72 ± 0.14	11.90 ± 0.22	+0.55 ± 0.06
CF_4 + N_2	9.42 ± 0.11	10.23 ± 0.44	+0.20 ± 0.11
CF_4 + N_2	9.40 ± 0.11	10.49 ± 0.15	+0.27 ± 0.05
N_2	9.77 ± 0.11	9.68 ± 0.10	-18 ± 30

Table 5.4: Etch rates for different effects of tetra-fluoro-carbon plasma treatment. At first it was believed that the plasma had an effect of increasing the height of the SU-8 (shown values). Later it was realised it was actually the Si wafer that was being etched.

The results obtained indicate that tetra-fluoro-carbon plasma should *increase* the height of SU-8 structures. This finding is very non-intuitive and more investigations showed that it was not the SU-8 structures that increased in height but rather the Si wafer that was being etched. Etch rate of Si wafers with tetra-fluoro-carbon plasma in this plasma asher has been documented as 1 μm/min [87]. Those optimisations showed that also O_2 had to be mixed with the CF_4 plasma to obtain that high etch rate. Therefore, the etch rate of these wafers cannot be known. The tetra-flouro-carbon plasma has *some* effect on the SU-8, but it was not possible to determine what from these experiments. Therefore, the data displayed above does not

show neither the etch rate of SU-8 nor Si but rather the initial findings. It was concluded tetra-fluoro-carbon plasma could not be used as a dry etchant of SU-8 as the etch rate could not be determined.

5.3.3 Contact angle modifications

Different plasma treatments are commonly used to modify the contact angle, θ_c, of polymers [88, 89]. This is achieved by a chemical modification of the surface. In the case of SU-8, the epoxy groups present on the surface can be opened and reacted with the oxygen in the environment, leaving hydroxyl groups instead. This drastically decreases the contact angle from 90° down to about 3°. The treatment is not stable with time and instead a new approach was developed in this project, which is described in Section (5.5). In Table (5.5) the change in θ_c can be seen after 40 days after the samples have been treated to an O_2 plasma at different effects.

Power (W)	θ_c (°) Upon treatment	θ_c (°) After 40 days
200	3 ± 2	31 ± 11
400	3 ± 2	21 ± 6
800	3 ± 2	28 ± 9
2000	3 ± 2	31 ± 11

Table 5.5: Variations in θ_c with O_2 plasma treatment of SU-8 samples. Measurements of θ_c after 40 days show a large increase.

5.4 AFM Investigation

Atomic Force Microscopy (AFM) relies on the atomic interaction between a cantilever tip and the atoms of the surface. By scanning a tip and observing the laser light reflection off the back side of the cantilever, one can get a very good image of the surface.

AFM measurements were done on four SU-8 samples treated to different plasmas. The experiments were done at Danish Institue of Meterology (DFM) at DTU in collaboration with PhD student Maria Holmberg.

5.4.1 Sample preparation

Four 4" ⟨100⟩ Si wafers were spin-coated with SU-8 2002 to a thickness of 1.6 µm. Details on the fabrication can be found in Chapter 2.

After this, the different samples were all subjected to different plasma treatments. The Ar^+ plasma treatment was not done in the plasma asher but in the same machine as where metal depositions are carried out. This is

a great advantage to the other plasma treatments, as the substrate can be kept under vacuum throughout the process. Even a quick exposure to the atmosphere incorporates large amounts of contaminants.

Sample	Treatment
A	No further treatment
B	O_2 + N_2 plasma of 240 and 40 sccm respectively at 400 W for 4 min
C	Ar^+ plasma at 200 W for 4 min
D	Ar^+ plasma at 200 W for 4 min and 1000 Å Au deposited

Table 5.6: Treatment of the different SU-8 samples under investigation.

5.4.2 Experimental details

The samples were investigated by AFM with tapping mode using a Si sharpened tetrahedral tip (Olympus) with resonance frequency of 300 kHz and spring constant of 42 N/m.

5.4.3 Results

The 3D images generated by the software SPIP are displayed below. The average height along the x-axis is also shown. It can be seen that the SU-8 surface is very smooth and that all plasma treatments greatly increased the surface roughness.

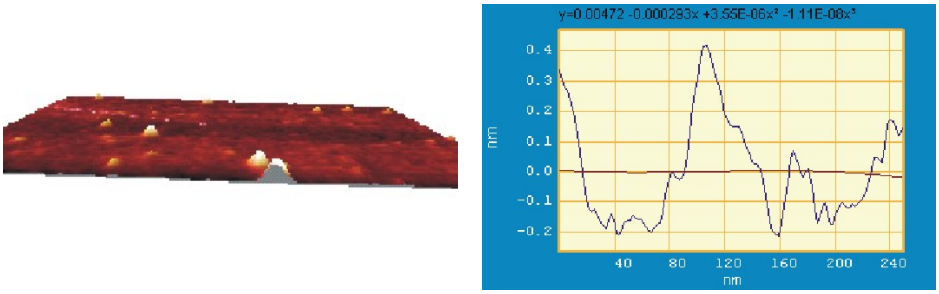

Figure 5.7: *Left:* 3D image of the SU-8 surface scanned over a 5 x 5 μm^2 area. The height of the peaks has been multiplied 10 times for clarity. *Right:* The average height over a 250 x 250 nm^2 area.

The surface of non-treated SU-8 is very smooth and the average height of the untreated SU-8 proved to be less than half a nanometer. This is expected as the size of the SU-8 monomer is only ∼2 nm. We only expect some unreacted epoxy groups at the surface and they have a height of ∼0.3 nm.

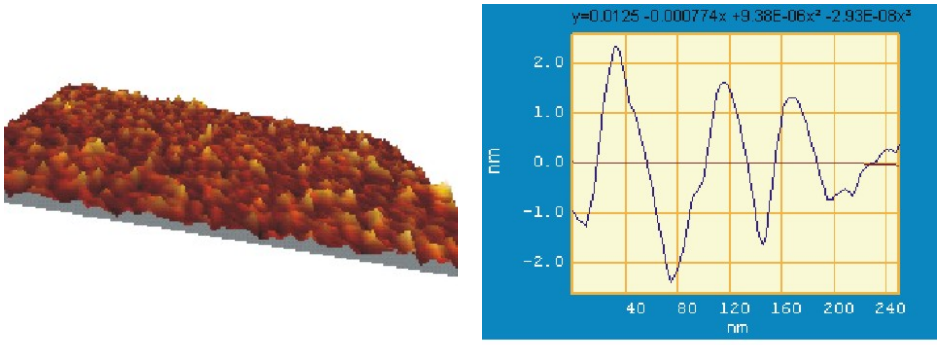

Figure 5.8: *Left:* 3D image of the O_2/N_2 plasma treated SU-8 surface scanned over a 5 x 5 μm^2 area. The height of the peaks has been multiplied 10 times for clarity. *Right:* The average height over a 250 x 250 nm^2 area.

After the O_2/N_2 plasma treatment it can be seen that the surface roughness has been greatly increased, ranging up to 2 nm. This would indicate that this plasma treatment have more than just chemical effects on the SU-8 surface and it actually induces mechanical scrubbing. It can be seen that the treatment is very even on the surface, there are no protruding peaks.

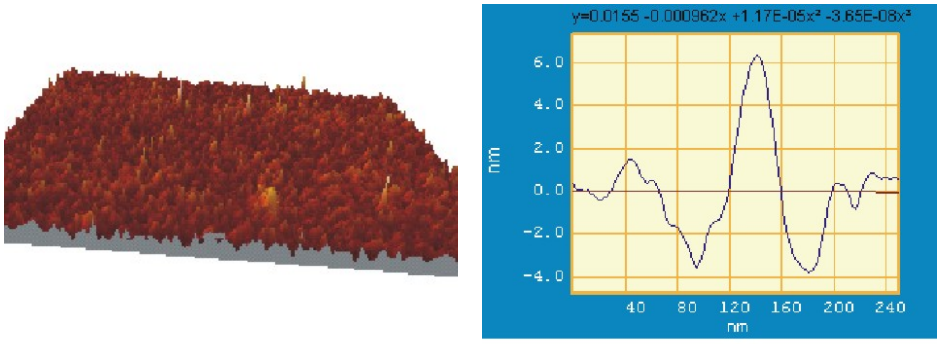

Figure 5.9: *Left:* 3D image of the Ar^+ plasma treated SU-8 surface scanned over a 5 x 5 μm^2 area. The height of the peaks has been multiplied 10 times for clarity. *Right:* The average height over a 250 x 250 nm^2 area.

The surface that has been treated with Ar^+ plasma shows even greater roughness than the O_2/N_2 plasma treated surface. Here, peaks of 6 nm are detected. Even though this plasma treatment was only run at half the effect, the roughness achieved was much more noticeable.

The final sample had the Ar^+ plasma treated surface covered with a 1000 Å layer of Au. This was done to investigate the abilities of the Au to *even out* the surface roughness. It was done as there have been problems with step-coverage of deposited Au in other processes [39]. It was seen that the Au did manage to regain the smooth surface of the original SU-8.

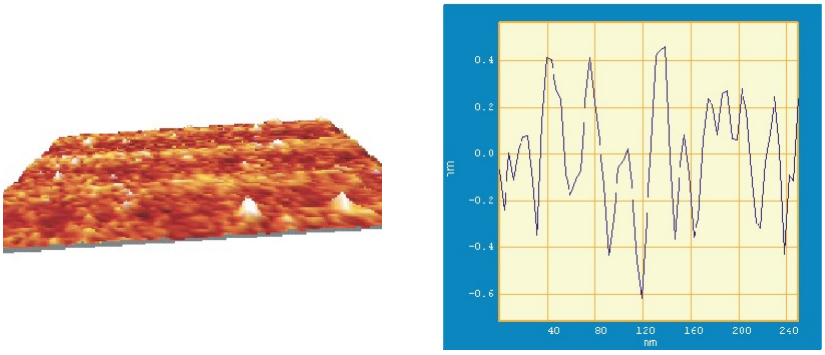

Figure 5.10: *Left:* 3D image of the Ar^+ plasma treated SU-8 surface after 1000 Å Au has been evaporated, scanned over a 5 x 5 μm^2 area. The height of the peaks has been multiplied 10 times for clarity. *Right:* The average height over a 250 x 250 nm^2 area.

5.4.4 Conclusion

In this section the effects of different plasma treatments were analysed; both by measuring the etch rate, contact angle and by AFM measurements. It was seen that neither the O_2 plasma nor the N_2 plasma had any etching effects on the SU-8. The effect of the CF_4 plasma was impossible to determined as it also etched the Si wafer.

Measurements on the contact angle showed that it decreased to 3° upon treatment to O_2 plasma but that it was not stable with time.

The AFM measurements on the SU-8 showed that the Ar^+ plasma had the greatest effect on the SU-8 surface, as expected. The surface roughness increase to ∼6 nm. It was interesting to determine the surface roughness of SU-8, which was only 0.5 nm, as no measurements have been done on this before. The increase in surface roughness after the O_2/N_2 plasma treatment was also good to confirm. This shows that the plasma treatments done, to increase the adhesion of the SU-8 to subsequent layers or metals, does not only have a chemical effect, but also a mechanical advantage. This treatment can lead to greater adhesion as a result of higher surface energy and surface area.

5.5 Ethanolamine treatment

The surface of SU-8 is hydrophobic after cross-linking, due to the presence of un-reacted epoxy groups. For the channels fabricated, the liquid should flow without the need for external pumps. To achieve this, the surface of the SU-8 must be made hydrophilic as to take advantage of the capillary force.

The conventional method of rendering polymer surfaces hydrophilic is to treat them to an O_2 plasma. The effects of plasma treatments are not stable with time and using a wet chemical treatment can include other advantages, such as (i) being able to treat structures where plasma cannot be used due to the design of the sample. There might be difficulties for the plasma to reach very small and closed channels; (ii) not getting any of the undesirable effects of the plasma treatment, such as etching; (iii) being able to determine exactly which areas that should be treated. Here a new approach is presented, which offers a permanent change of the contact angle by the use of the molecule Ethanolamine.

5.5.1 Ethanolamine

The molecule Ethanolamine is well suited for the intended purpose; at one end, it has an amine group (–NH_2–) which will react with the epoxy groups (–CH–O–CH_2–) on the SU-8 surface. At the other end of the molecule, there is an hydroxyl group (–OH), Figure (5.11). By making the molecule form a mono-layer on the SU-8 surface, the hydrophobic epoxy groups are 'substituted' with hydrophilic hydroxyl groups.

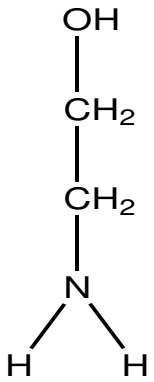

Figure 5.11: Chemical structure of the molecule Ethanolamine. The amine group (–NH_2–) reacts with the epoxy group (–CH–O–CH_2–) on the SU-8 surface.

The proposed reaction of this treatment is based on the fact that amine groups are commonly employed within biochemistry to react with epoxy groups [83]. By letting the molecule Ethanolamine react with the epoxy

groups, the surface chemistry of SU-8 changes from hydrophobic to hydrophilic with the replacement of the epoxy group with two hydroxyl groups. The reaction is analysed with X-ray induced photoelectric spectroscopy (XPS) in Section (5.6) and the results obtained indicate the proposed reaction to be the actual process.

5.5.2 Sample preparation

SU-8 samples were prepared to a thickness of 160 µm and structured into 5 mm x 7 mm squares. Exact details on the fabrication sequence can be found in Chapter 2.

Ethanolamine (Sigma Aldrich) was dissolved in Sodium Phosphate buffer at pH 7.6 to a concentration of 100 mM.

5.5.3 Experimental details

The contact angle, θ_c, was measured on the samples throughout the process. The first time it was measured was just after cross-linking. θ_c was measured on twenty different spots on the wafer, where the SU-8 was cross-linked. After development in PGMEA, θ_c was again measured on twenty different spots. After this, the wafer was left in Cr etch to release the SU-8 structures.

The SU-8 squares were divided into four batches of five square samples each. The contact angle was measured twice on each side of every SU-8 sample, leaving a total of twenty values of θ_c of each batch. The samples were then soaked in 10 mL of 100 mM Ethanolamine for different periods of times: 5 min, 10 min and 20 min at 50 °C in an air-tight container. The samples were dried in a flow of N_2. At this point the contact angle was again measured twenty times for each batch. To make sure the Ethanolamine was strongly bound to the SU-8 surface and not just unspecifically adsorbed, the samples were washed in Sodium Phosphate buffer in ultra sound for 10 min. Afterwards the contact angle measurements were repeated. The value of θ_c was measured 20 days later to get an indication of reliance of the treatment.

A sample of PolyMethylMethAcrylate (PMMA) was also subjected to the Ethanolamine treatment and washing in ultra sound as a reference.

5.5.4 Results

In Figure (5.12) the variations in θ_c with the different treatments can be seen. The different steps have been marked with numbers corresponding to the following treatments;

1. Initially SU-8 is hydrophobic with a contact angle of 90°.

2. The value of θ_c does not change significantly after development in PGMEA, which is expected.

3. After release of the structures from the Si wafer, the measured value of θ_c was $50 \pm 2°$.

4. After the Ethanolamine treatment, the contact angle is decreased even further. It can be seen that the sample treated for 10 min shows the largest reduction.

5. No noticeable change in θ_c occurs after washing in ultra sound, indicating a strong bond between Ethanolamine and SU-8.

6. The contact angle is measured again, 20 days after the initial experiments. None of the samples have had their contact angle increased back to the initial value after this period of time. Again, the sample treated for 10 min shows the lower value in θ_c.

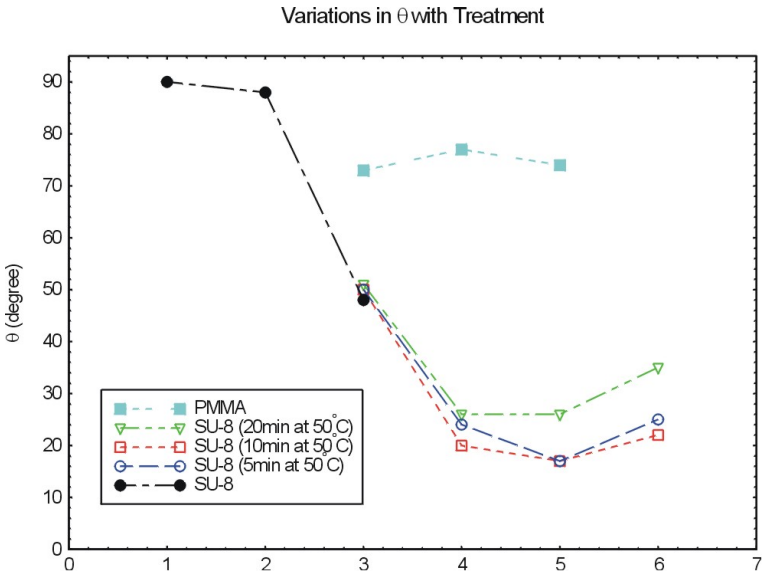

Figure 5.12: Variations in θ_c with the different steps in the Ethanolamine treatment. The treatment with Ethanolamine is necessary to obtain a low enough value of θ_c.

After the release of the SU-8 samples from the Si wafer, the value of θ_c is decreased by 40°. The Cr layer is etched by Ceric Ammonium Nitrate (CAN) in Acetic Acid in which the wafer is left over-night. CAN is know to act as a catalyst in the breaking of epoxy rings especially in the presence of Acetic Acid [90, 91]. The reaction taking place here is analogous to an O_2 plasma treatment, where the epoxy rings are opened and react with oxygen from the environment. Due to limited amount of catalyst, this reaction reaches an equilibrium before all epoxy rings have been opened, resulting in a final contact angle of 50°. By supplying the solution with *unlimited* amount of

catalyst the contact angle could theoretically be reduced further. CAN is not a desirable molecule to work with as it is hazardous for the human and corrosive and Ethanolamine is therefore used instead for the desirable further reduction in θ_c.

It is seen that soaking the samples for 10 min results in the greatest reduction in θ_c. It is not fully understood why soaking the samples for 20 min does not result in a greater decrease. When the samples were left in the solution overnight, no reduction at all was seen. This supports the idea that there is an optimal time for the treatment of 10 min. The samples treated for 10 min show the least increase in contact angle after 20 days, yet again showing 10 min being the optimal time of treatment. Possibly, the solution of Ethanolamine diffuses into the SU-8 polymer upon prolonged exposure, but this is only an proposition and it has not been investigated experimentally.

The slight increase in contact angle after 20 days is probably due to contaminating molecules from the environment. The contact angle is very dependent on the chemical composition of the surface and any foreign molecules adsorbed will change the value in θ_c.

5.5.5 Conclusion

To achieve a continuous flow of liquid in the channel system, the surface of SU-8 needs to be made hydrophilic. To achieve this, the SU-8 samples were treated to Ethanolamine. C.-L. Wu *et al.* have reported on a permanent modification of the contact angle of SU-8 by mixing the resist with another polymer before cross-linking [92]. This would form a co-polymer with a value of θ_c of 55° upon cross-linking. It is seen that the above treatment with Ethanolamine results in an even greater reduction in θ_c.

Samples of SU-8 were treated to a solution of Ethanolamine and it was determined that a treatment at 50 °C for 10 min was optimal to reached a value of θ_c low enough to support liquid flow in the channels, after release from the Si wafer.

PMMA was also treated to the same procedure but as PMMA does not contain any epoxy-groups on the surface, no reduction was seen in the contact angle of this sample. PMMA was chosen as a reference as many micro channel systems of today are fabricated in this polymer. It is clearly seen that the contact angle of PMMA is much greater than that of chemically treated SU-8.

5.6 XPS

X-ray induced Photoelectron spectroscopy (XPS) of SU-8 was carried out at the Interdisciplinary Research Center for Catalysis (ICAT) at DTU. The aim of the measurements was to determine the chemical composition of the surface of cross-linked SU-8. We also wanted to show that when Ethanolamine reacts with SU-8, it is through the binding of the amine group of the former to the free epoxy groups of the latter. Measurements of this type on SU-8 have never been published before.

The chemical structure of SU-8 is explained in detail in Chapter 2 and the purpose and chemistry of the reaction with Ethanolamine is analysed in Section (5.5). Here, I shall only be concerned with the physics of XPS and the analysis of the acquired data. The measurements were done in collaboration with Institute leader Ib Chorkendorff and Laboratory Technician John Larsen.

5.6.1 Theory

In XPS one relies on the photoelectric effect. X-rays are shone onto the sample surface and the energy spectrum of the emitted electrons is analysed. First, the X-rays are generated when electrons emitted from a heated cathode are accelerated through a high potential difference. In this set-up a 12 kV potential difference is applied and the cathode is heated with 200 W. The accelerated electrons hit a metallic anode and by the *reverse* photoelectric effect the X-rays are generated. Many metals are suitable as anode *eg.* Si, Ag, Ti and Cr, but usually Mg or Al is preferred, due to the narrow line width in their energy spectra, which provides greater accuracy in the final results. The energy of the Mg K_α line is 1253.6 eV and for the Al K_α line it is 1486.6 eV and their Full-Width-at-Half-Maxima (FWHM) are 0.70 eV and 0.85 eV respectively. In these XPS scans the Mg anode was mostly used, but one overview scan was also done using the Al anode, Figure (5.14).

The X-rays are shone onto the surface of the sample under investigation and by the photoelectric effect, valence electrons are emitted from the material.

The kinetic energy of the electrons is expressed as

$$E_{kin} = h\nu - E_B - \phi \tag{5.2}$$

Where h is Plank's constant, ν is the frequency of the X-rays, E_B is the binding energy of the electrons in the sample under investigation and ϕ is the work function of the sample.

The value of the constants are fed into the software and the equation is plotted as a function of E_B in the energy spectra. By observing the positions of the peaks in these spectra, one can find the electron configuration of the surface elements; which in turn tells us about their chemical compositions. For electrons with energy in the range of 50-1000 eV, the mean-free-path is only a few atomic layers [93]. This ensures that only electrons emitted from the top 10 nm of the sample manage to escape. The SU-8 monomer has an approximate size of 2 nm x 2 nm which means that also some information of the bulk material is included in the results.

The measurements are done on a set-up from Physical Electronics Industries, USA equipped with a X-ray source, sample holder and a Φ 550 analyser. The analyser is a Double-Pass Cylindrical Mirror analyser (CMA) which consists of two cylindrical mirror analysers placed in combination, Fig. (5.13). An electron multiplier is mounted at the exit.

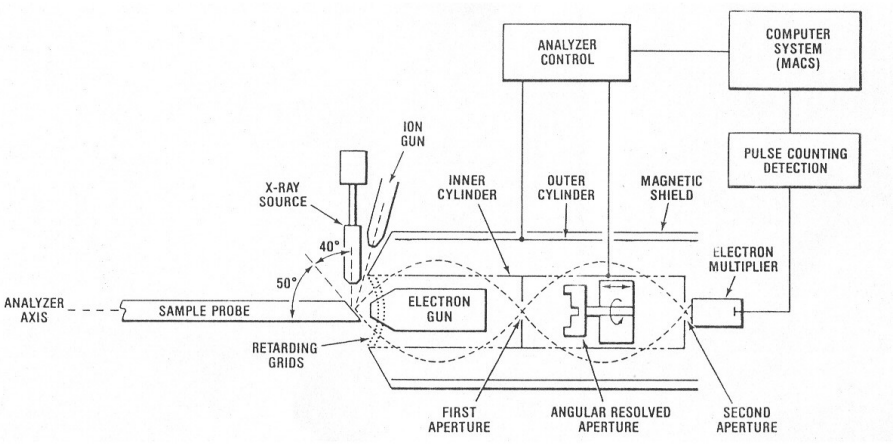

Figure 5.13: The Φ 550 analyser used in these measurements with the additional set-up.

The pass energy is determined by the potential difference of the two cylinders where the inner cylinder is held at earth. Only electrons with appropriate energy in relation to the pass energy can exit at the end and be detected. Setting the equipment to a higher pass energy results in a higher signal-to-noise ratio, but also in a lower accuracy. A lower pass energy results in a reduced signal-to-noise ratio, but also in a reduction of the line width, which increases the detailed amount of information one obtains. Therefore, one usually first scans the sample at a fairly high pass energy to get a chemical overview and later one scans a more narrow region at a lower pass energy to obtain more specific information.

The energy distribution of the detected electrons follows Gaussian statistics. By fitting a Gaussian curve to the experimental data, one can find the

binding energy of the valence electron. If the element exists in more than one form on the surface, the experimental data will be the convolution of more than one Gaussian function, one for each electrical configuration. The analysis programs Origin 6.0 and Matematica 4.2 were used to analyse the data. The position of the 1s peak for most elements is known in literature so the experimentally obtained values can be compared and confirmed. Due to the fact that we are observing organic molecules, which easily charge, a slight shift of 3-5 eV is seen in the spectra used below for the analysis [93]. The X-ray source in this set-up is not monochromatic and this results in at least one satellite peak for every element. These can be seen close to the 1s peak. Also, Auger lines appear in the spectrum. The Auger lines arise from the fact that there are two anodes but only one is being used at a time. Some electrons generated from the cathode will hit the other anode, generating X-rays. These lines are shifted by 233 eV if the other anode is used, Figure (5.14).

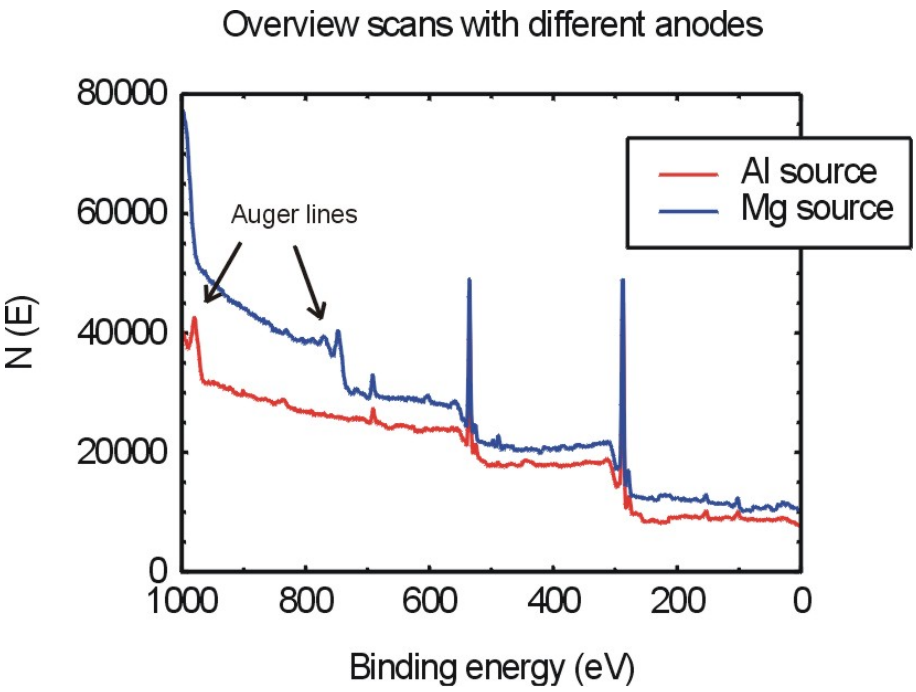

Figure 5.14: Overview scans done with Mg and Al anode plotted together. The Auger lines are shifted by 233 eV. The signal is weaker with the Al anode, therefore the use of the Mg anode is more common.

5.6.2 Sample preparation

Samples of SU-8 were prepared on a 4" ⟨100⟩ Si wafer which was first covered with 50 Å of Cr, 500 Å of Au and 500 Å of Cr. The metals did not serve a particular purpose. A 1.6 µm layer of SU-8 2002 was spin-coated onto the wafer and details on the preparation can be found in Chapter 2. Finally, the wafer was sawed into 10 mm x 15 mm squares by LabTechnician Helle Vendelbo Jensen at MIC.

For the second set of experiments, SU-8 was prepared with the same procedures but after PEB it was submerged in 50 mL of 100 mM Ethanolamine and left for 20 hours. The wafer was rinsed in ethanol to remove the excess Ethanolamine and dried in a stream of N_2 and finally diced into squares. These samples were then investigated in the same manner with the XPS and the two spectra were compared.

5.6.3 Experimental details

Before the actual measurements can start, the software and equipment need to be properly calibrated. This is achieved by bombarding the sample surface with 2 keV electrons, observing the spectrum of the elastically scattered electrons and calibrating the software. Meanwhile, the sample surface is observed on a screen (SEM effect) and it can be noted that the bombardment leaves marks on the SU-8 surface, which remain with time. Whether these are only apparent or physical is unclear.

The sample is mounted in the lock and when a pressure of 10^{-6} mbar is established, it is mechanically inserted into the measuring chamber. It is possible to establish a Ultra High Vacuum (UHV) in the chamber with a pressure of 10^{-11} mbar but as these measurements do not contain reactive components and the sample already has been exposed to the atmosphere, it is not necessary to establish such a low pressure. These measurements were carried out at 10^{-9} mbar.

The analyser can be set to detect electrons at an angle of 90° or 12° to the surface. The former method gives a picture of the chemical composition of about 10 nm into the bulk of the sample. The latter (so-called glanzing) shows the top mono-layers only. We are interested in a chemical reaction occurring at the surface, and thus we use glanzing data for our analysis. The SU-8 monomer has an approximate size of ∼2 nm x 2 nm, which means it is very hard to observe the surface epoxy-groups only, so information from the bulk of the material is included in the data. The Ethanolamine molecule has a length of ∼0.6 nm and assuming this is attached straight onto the SU-8

surface, still the bulk will be seen in the results.

5.6.4 Results

Initially an overview scan ranging from 1000-0 eV with a pass energy of 50 eV is done to get data on the chemical composition of the sample. It is done with the Mg anode, Figure (5.15). The major peaks are attributed to oxygen and carbon, as expected. There can also be seen traces of Si as remains of dust from the sawing. F and Sb are also present in small amounts, as these are components of the photoinitiator, as discussed in Chapter 2. Calculations done by the software, determined that carbon makes up 70 % of the SU-8 and oxygen only 20 %, which is an expected result.

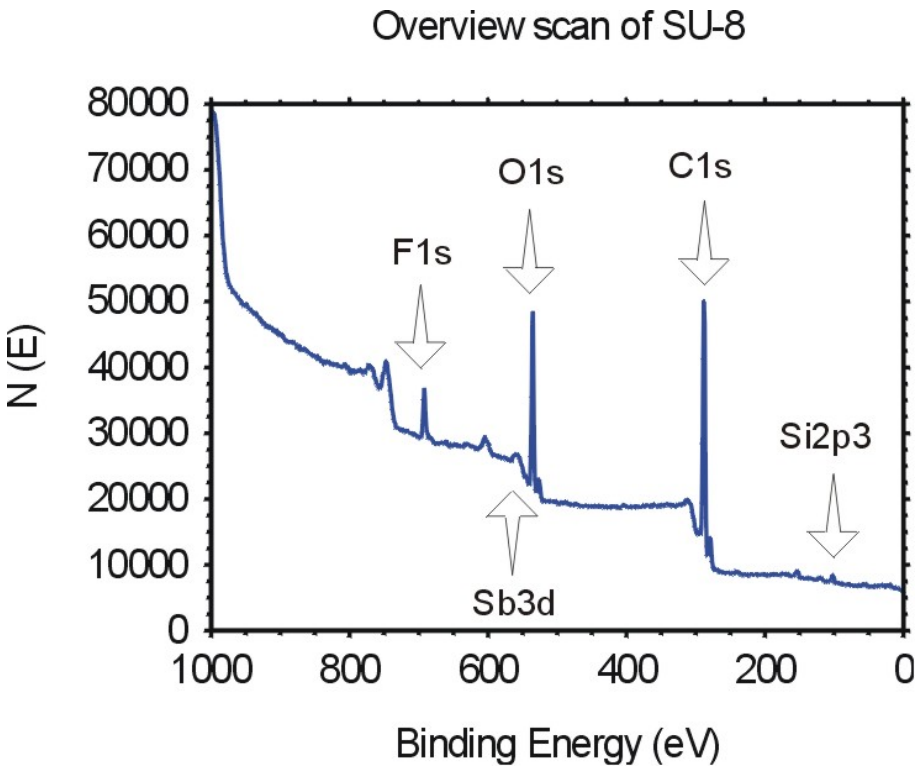

Figure 5.15: Overview scan of cross-linked SU-8 using the Mg anode with a pass energy of 50 eV.

Secondly, more detailed scans were done over the oxygen 1s and carbon 1s peaks. They were scanned with a pass energy of 25 eV, Fig. (5.16).

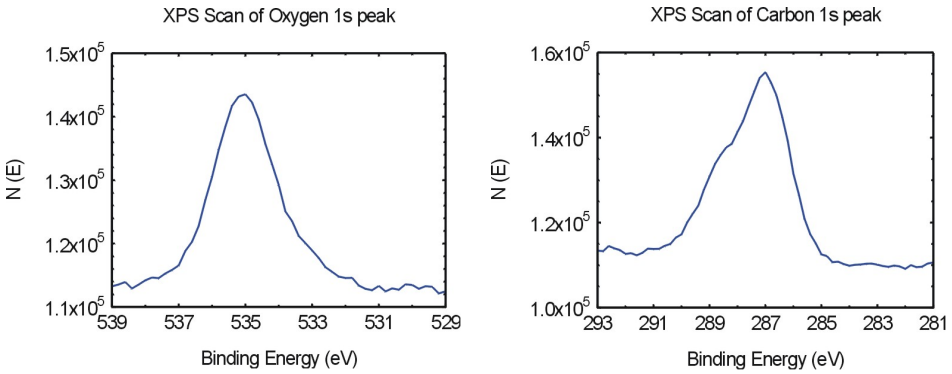

Figure 5.16: More detailed scans done on the oxygen 1s and carbon 1s peaks.

After this scan was done, the sample holder was exchanged and glanzing scans of the surface was done, which were to be used for the analysis. During glanzing scans, much less information is obtained and the pass energy needs to be increased again. Narrow scans over the oxygen 1s and carbon 1s peaks were done with a pass energy of 50 eV, Figure (5.17).

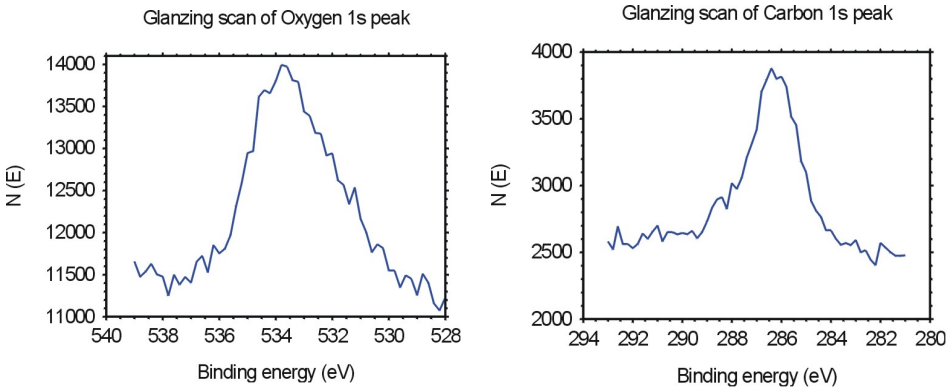

Figure 5.17: Glanzing scans done on the oxygen 1s and carbon 1s peaks. The energy range was scanned over 300 times at a pass energy of 50 eV to obtain reliable results.

The same procedures were repeated for the sample treated with Ethanolamine. Initially an overview scan ranging between 1000-0 eV was done with a pass energy of 50 eV, Figure (5.18). The signal generated in this measurement is lower than in the one represented by Figure (5.15). Here, N from the Ethanolamine can be detected and F is present to a lower degree. F is a component of the photo-initiator with an in-homogenous distribution in the sample, therefore it is not surprising that the amount detected differs between the two samples. The N detected also generates a very small signal, which is expected as it is present only on the surface to a small degree and the overview scan plots the composition of the sample a few nm into the bulk, measured from the surface.

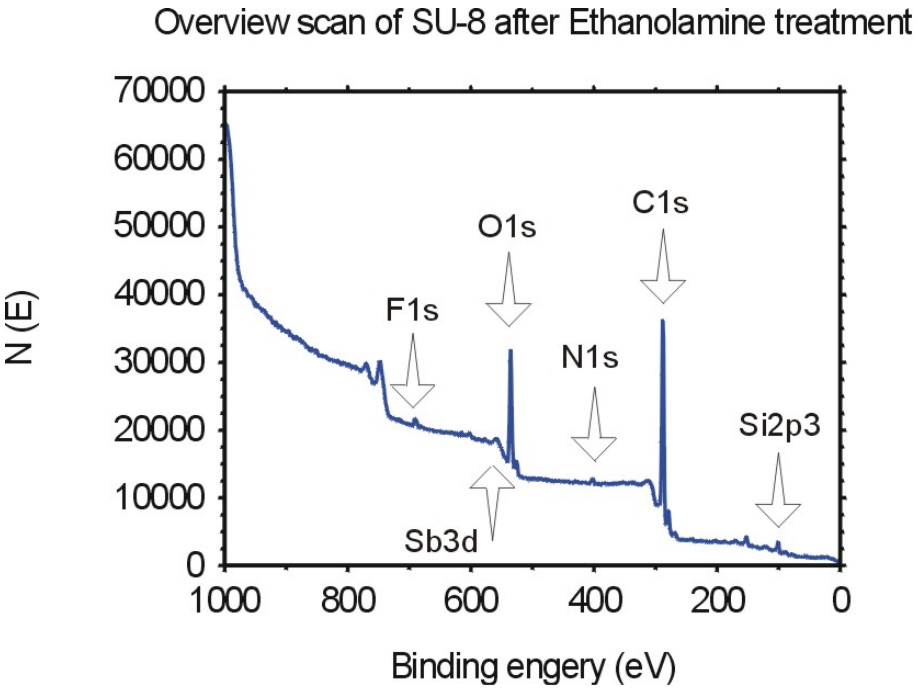

Figure 5.18: Overview scan of the cross-linked SU-8 surface with a pass energy of 50 eV after treatment to 100 mM Ethanolamine. The same elements as in Figure (5.15) are present, with the addition of nitrogen.

The oxygen 1s and carbon 1s peaks were then scanned in more detail with a pass energy of 25 eV, Figure (5.19). Following this, glanzing scans were done over the same peaks with a pass energy of 50 eV, Figure (5.20).

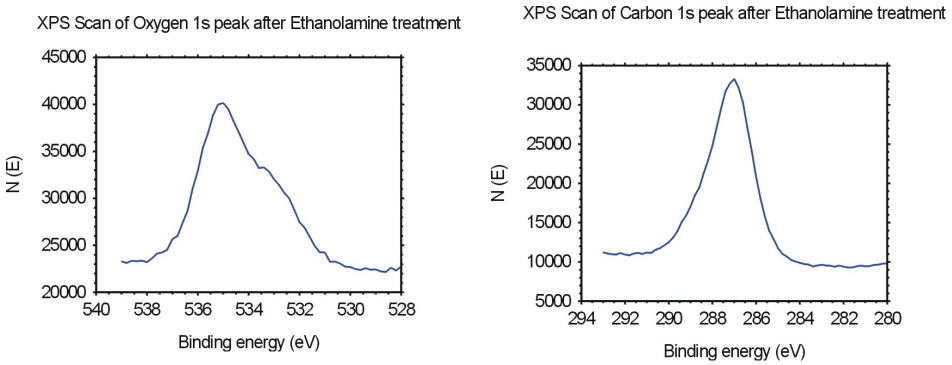

Figure 5.19: More detailed scans done on the oxygen 1s and carbon 1s peaks after the sample has been treated with Ethanolamine.

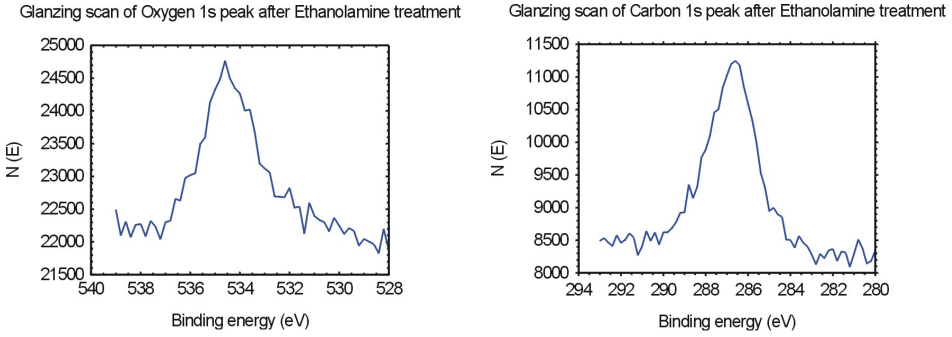

Figure 5.20: Glanzing scans done on the oxygen 1s and carbon 1s peaks after the sample has been treated with Ethanolamine.

5.6.5 Analysis of data

The peaks are governed by the Gaussian distribution and by trying to fit Gaussian functions to the data, one can determine in how many configurations the element exist. By observation we see that the data obtained does not fit to a single Gaussian. Equation (5.3) is iterated in Matematica and an extra term is added for every new function, until a good fit is obtained. All Matematica work was done by PhD student Rodolphe Marie in the Bioprobes group, MIC, DTU.

$$N(E) = \alpha \times \left(\frac{1}{\sqrt{2\pi}\sigma} e^{\frac{-(x-a)^2}{2\sigma^2}} \right) + \dots \tag{5.3}$$

Where α is a parameter regulating the height of the peak, σ is the full width at half maximum (FWHM) and a is the proposed position of the peak.

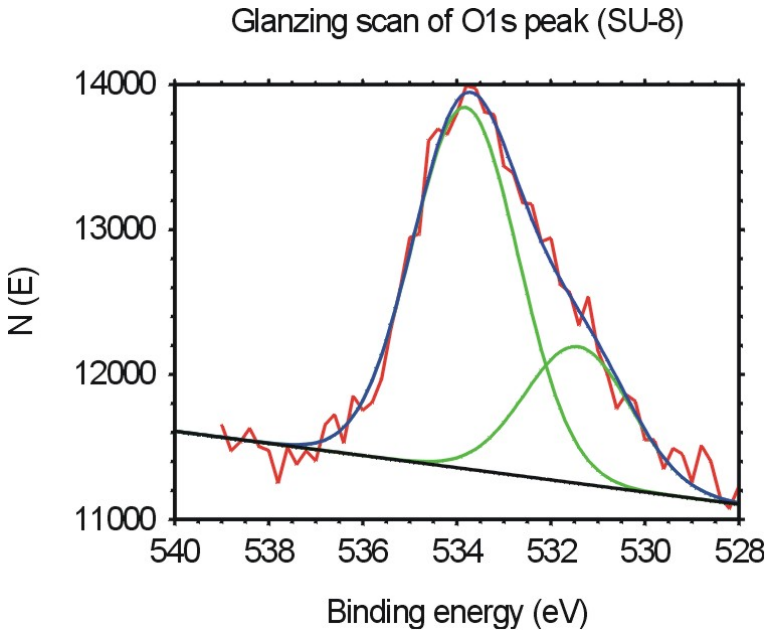

Figure 5.21: Glanzing scan of the oxygen 1s bond on the SU-8 surface shows the presence of oxygen in two chemical states. The blue line represents the convolution of the green Gaussians fitted. The red line is the data obtained.

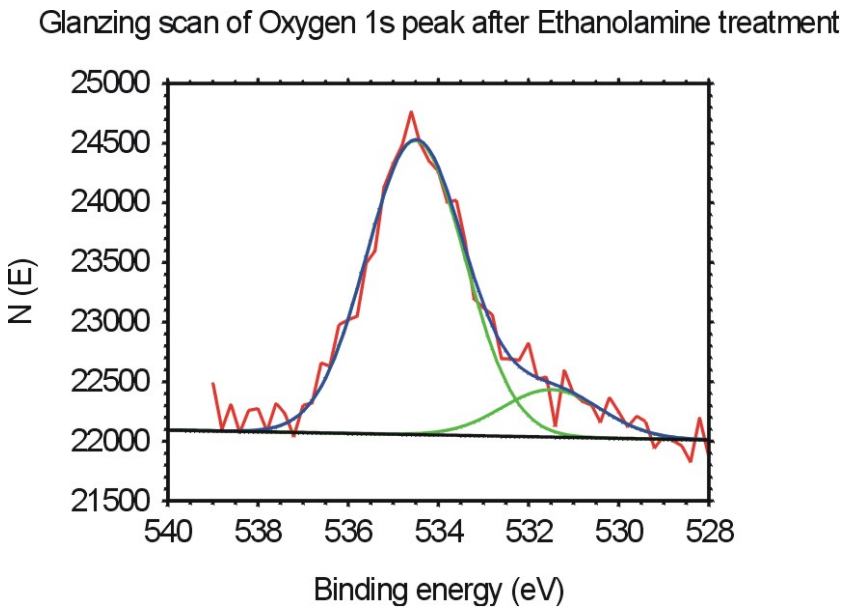

Figure 5.22: Detailed glanzing scan of oxygen 1s peak on the SU-8 surface after the Ethanolamine treatment. The blue line represents the convolution of the green Gaussians fitted. The red line is the data obtained.

The analysis with Matematica of the oxygen 1s peak shows that it exists as a convolution of two Gaussian peaks, Figure (5.21). The energies are positined at 533.8 eV and 531.4 eV. From Figure (2.1), the expected result would be to find oxygen in *three* states;

- –CH–O–CH_2–; oxygen is present in the epoxy group on the surface. This configuration is called the epoxy state.
- –CH_2–O–aromatic carbon ring; oxygen is present in the back-bone of the polymer. This state is called the aromatic state.
- –CH_2–OH; oxygen is also present in this configuration in the back-bone. This state is called the hydroxyl state.

From literature the position of the aromatic state is found to be 534.9 eV and the hydroxyl state is at 532.4 eV [94]. The position of the epoxy state is at 533.8 eV [95]. The range in energy of the states from data is 2.3 eV, which agrees well with the energy shift of the measured states, Figure (5.23).

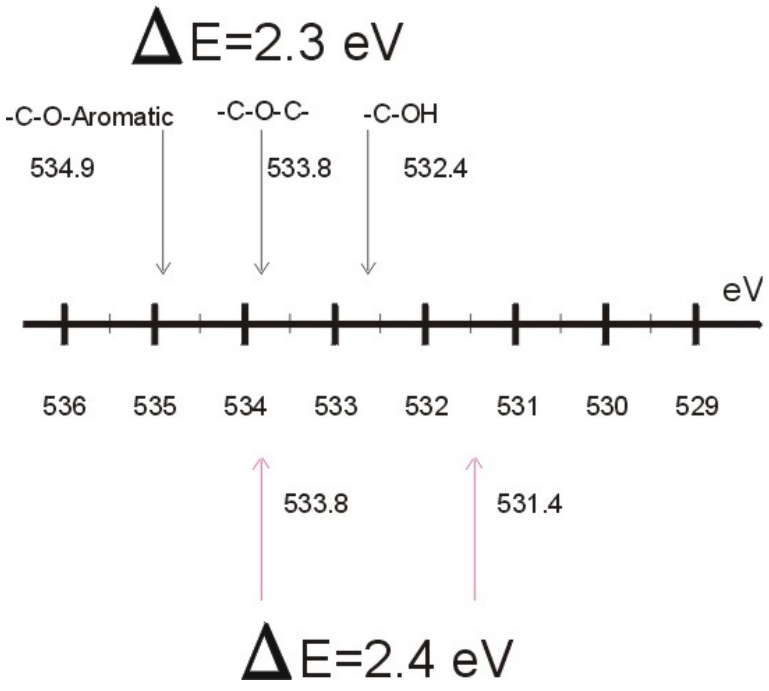

Figure 5.23: It can be seen that the observed spectra has been shifted.

It is assumed that the measured spectra has been shifted by -1.2 eV, compared to literature. The 533.8 eV peak is attributed to the aromatic state and the 531.4 eV peak to the hydroxyl state. It is assumed that the signal from the epoxy state is too weak to be detected in these measurements

and that it should lie in-between the aromatic and the hydroxyl state. The ratio of the aromatic state to the hydroxyl state is approximately 3.

From the spectra obtained after the SU-8 surface has been treated with Ethanolamine, Figure (5.22), one peak at 534.5 eV and one peak at 531.5 eV are observed. The ratio between the two peaks has been increased to 6 and the range in energy of these states has been increase to 3 eV. It can be seen that the 531.5 eV peak compares well to the previously detected 531.4 eV peak, and it represents the hydroxyl state. The 534.5 eV peak does not correspond so well to the 533.8 eV peak, indicating that there has been a change in the configurations of the oxygen. From the observation that the range in energy has been increased it is determined that the middle epoxy state has disappeared, which is the expected chemical reaction taking place. It is not clear why the ratio of the aromatic to the hydroxyl state *increases* after the Ethanolamine treatment, when there should be more hydroxyl groups present.

A detailed scan of the carbon 1s peak and analysis with Matematica shows that the best fit could be obtained with carbon in four electrical states on the SU-8 sample, Figure (5.24). In the SU-8 monomer, carbon exists in at least *six* different states, as strictly speaking the carbon atoms involved in the aromatic ring are in different chemical configurations, Figure (2.1). Unfortunately the data available is not detailed enough to separate these since there is only a marginal difference in energy between them. The four peaks detected are positioned at 290.8 eV, 288.2 eV, 286.2 eV and 284.3 eV. From literature it is know that the –CH_2–CH_2– bond has an energy of 285.0 eV and the aromatic carbons should be represented by a peak of 0.6 eV lower value [96]. Thereby, we determine that the 286.2 eV peak represents the aromatic carbon in the SU-8 structure. This is also the largest peak and it agrees well as the aromatic carbon is the prevailing chemical configuration in SU-8. It can be seen that even this spectrum has been shifted, but this time by +1.8 eV.

The peaks for –CH_2–CH_2–, –CH_2–H and –CH_2–O– are all very close and cannot be distinguished in this plot. They are represented by the 288.2 eV peak. The epoxy state is seen at 290.8 eV. The peak at 284.3 eV we cannot account for.

The glanzing scan of the Carbon 1s peak after the treatment of Ethanolamine can only be fitted with three Gaussians, Figure (5.25). The peak at 290.8 eV has disappeared, showing the disappearance of the epoxy state. Instead, the peak incorporating the –CH_2–CH_2–, –CH_2–H and the –CH_2–O– states has increased in amplitude. This means also the –CH_2–NH– state is represented in the data. The σ of the peaks varies slightly, as they are convolutions of several peaks. Would they have represented only one, σ would have remained constant, as the life time is an intrinsic property of every element.

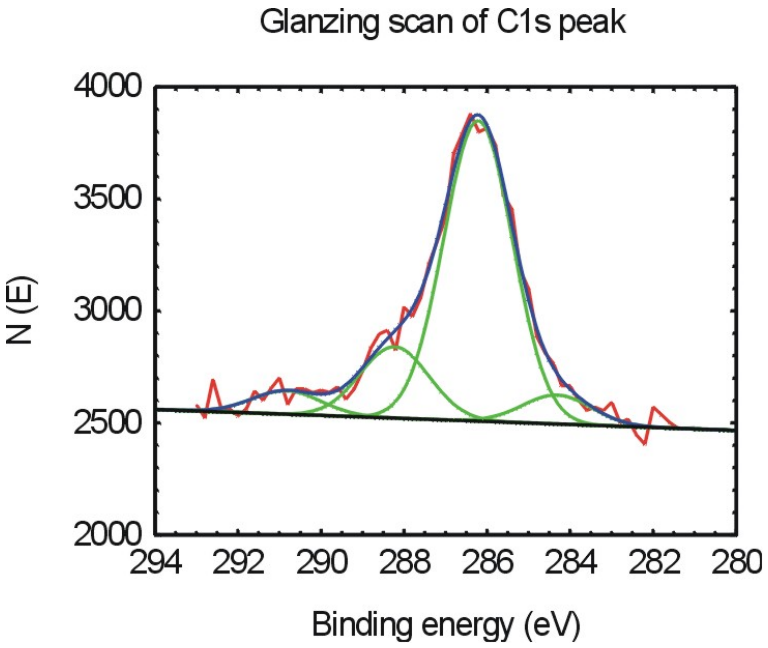

Figure 5.24: Glanzing scan of the carbon 1s bond shows the presence of carbon in four chemical states. The blue line represents the convolution of the green Gaussians fitted. The red line is the data obtained.

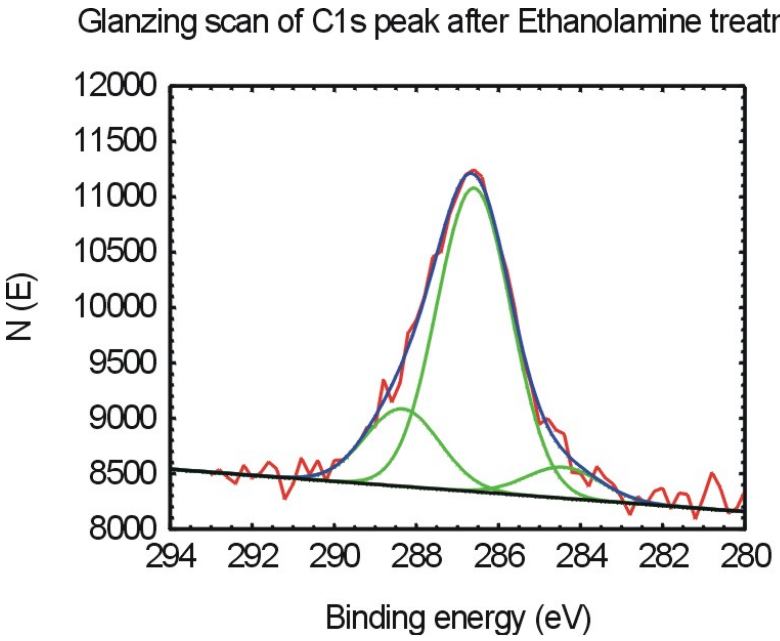

Figure 5.25: Glanzing scan of the carbon 1s bond after the Ethanolamine treatment. The blue line represents the convolution of the green Gaussians fitted. The red line is the data obtained.

5.6.6 Conclusion

The XPS experiments done here are a good start, but not nearly finished. To be able to analyse the surface of SU-8 properly, one would most likely need a synchrotron X-ray source. This is because the peaks of the constituent elements are so close in their spectra.

The results do give an indication that the expected chemical reaction is taking place. For example, the glanzing scan of the carbon 1s peak shows a good fit with four Gaussians on the SU-8 surface, but only three peaks fit after the Ethanolamine treatment. This could represent the disappearance of the epoxy groups. The value of the binding energy of the disappearing peak is ∼291 eV and it is assumed this represents the epoxy state of carbon.

In the glanzing spectra of the oxygen 1s bonds, no peaks are disappearing, but there is a prominent increase in energy range of the peaks. This could well show the disappearance of one bond and thereby more defined peaks.

5.7 Summary

These experiments carried out to investigate the surface of SU-8 have all been very informative. Still, they all have to be developed further to provide the exact information required.

The bond strength data for example, shows how weak the SU-8 to Au bond is and also shows that one can obtain a better adhesion with different adhesion layers. The molecule 4-ATP is offered as an alternative to provide a better adhesion.

The plasma investigations show that O_2/N_2 or CF_4 plasmas do not serve as good etching plasmas for SU-8, but a combination plasma of O_2 ad CF_4 has been reported to provide an etch rate of 1 µm/s [97].

The AFM investigations showed a large increase in surface roughness upon treatment with Ar^+ plasma of the SU-8. An average surface roughness of 0.5 nm was found of non-treated SU-8, which shows the polymer to be very smooth.

Treatment of SU-8 to Ethanolamine showed to decrease the contact angle to 20°. This induces flow in the micro channels and measuring sites of the chip. Such flows were not possible when the value of θ_c was higher. XPS studies were done to show the chemical reaction between the amine group of the Ethanolamine and the free epoxy groups on the SU-8 surface.

Chapter 6

Measurements

In this Chapter, the measurements done with the two chips fabricated will be presented. The cantilevers have been used for detection of DNA and the antibody of the pesticide Carbaryl. The DNA was detected both with fluorescence measurements and with the more advanced optical read-out for surface stress measurements. The channels were used in combination with the cantilevers for the fluorescence measurements. The flow rate has also been studied qualitatively with the channels, but no equipment or techniques were available for quantitative analysis of the flow rate.

The measurements with the cantilevers are presented in Section (6.1) and the measurements with the channels are described in Section (6.2). Finally, the studies will be summarised in Section (6.3).

6.1 Cantilever measurements

The principle of using cantilevers for biochemical detection was described in Chapter 3. Here, the measurements done and results obtained will be presented.

All measurements were carried out by Dr. M. Calleja at CNM-CSIS, Madrid, in co-operation with the Optoelectronics and Nano mechanics Biosensor group.

6.1.1 Characterisation of the cantilevers

First, the resonance frequency of the 200 µm and 100 µm long cantilevers was determined, both in air and in liquid. The obtained results compare very well with the expected frequencies from theory, Table (3.2). For the measurements, the cantilevers are actuated by thermal noise.

The calibration of the set-up was done. For this, the photo-diode used to detect the reflected laser beam is moved by hand a specified distance and the change in signal is observed. This gives information on the relation between

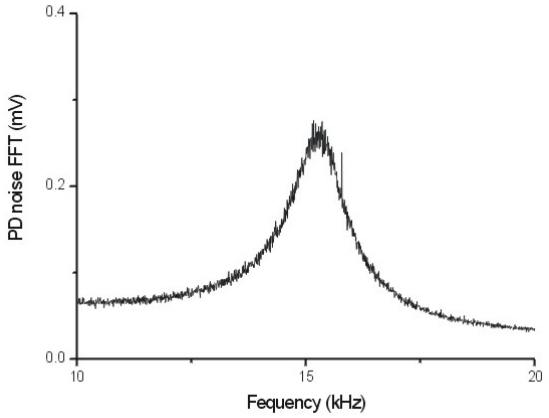

Figure 6.1: The resonance frequency of the 200 µm long cantilevers in air was found to be 15.3 kHz.

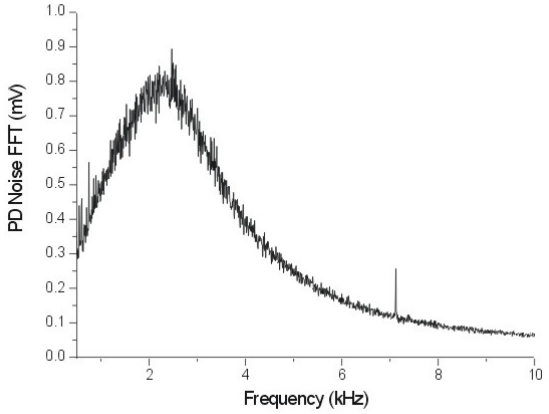

Figure 6.2: The resonance frequency of the 200 µm long cantilevers in liquid was determined as 2.3 kHz.

change in position of laser spot to change in voltage. Later, this change in voltage is related to bending of cantilever by Equation (6.1). A change in voltage of 1 V corresponds to a bending of 4 nm of the cantilever.

$$\frac{z}{x} = \frac{L}{2d} \tag{6.1}$$

Where z is the bending of the cantilever, x is the displacement of the spot at the photo-diode, d is the distance between the laser spot on the cantilever and the photo-diode and L is the length of the cantilever.

The cantilevers fabricated later in the process were only covered with a 100 Å layer of Au and the sensitivity of those was greatly increased to previous attempts with cantilevers covered with 200 Å of Au. All cantilevers used for the subsequent measurements were covered with 100 Å of Au. It proved to be much easier to work with cantilevers with a thin layer of Au. The aligning procedure of the laser was much faster and the definition of the laser spot was better. Also, the drift of the laser was lower, which is due to the reduced heating effect of the thinner Au layer. The drift of these cantilevers was only 0.04 V/min.

6.1.2 Ethanolamine treatment

As discussed before, one of the problems when working with SU-8 as a detection system is that the surface is hydrophobic. For cantilever measurements, this means that the cantilevers try to avoid the introduced liquid and easily stick to the substrate, rendering them useless. Also, there is a tendency for air bubbles to form and stick to the areas surrounding the cantilevers and interfering with the measurements. To overcome these problems, the cantilevers were treated with Ethanolamine. The chemical reaction of Ethanolamine and the investigations of optimal treatment are described in detail in Chapter 5.

The Ethanolamine should bind only to the SU-8 and thereby not interfere with the Au surface. One problem that could arise is that the Ethanolamine adsorbs to the Au surface, leaving less available sites for the molecules under detection to bind. A DNA immobilisation measurement was done with a Si_3N_4 cantilever after treatment to Ethanolamine and it can be seen that the signal generated is still strong, Figure (6.3). The introduced DNA binds to the Au side of the cantilever and creates a signal out-put. The introduction of Mercaptohexanol (MCH) displaces un-specifically bound DNA and binds on the available sites, generating a new signal. The introduced Ethanolamine does not seem to have had a noticeable effect on the Au.

6.1.3 DNA detection

In these DNA measurements, single-stranded DNA (sDNA) was immobilised on the Au surface of the cantilever. The DNA binds to the Au surface via a thiol bond. The binding of the sDNA would result in a downward

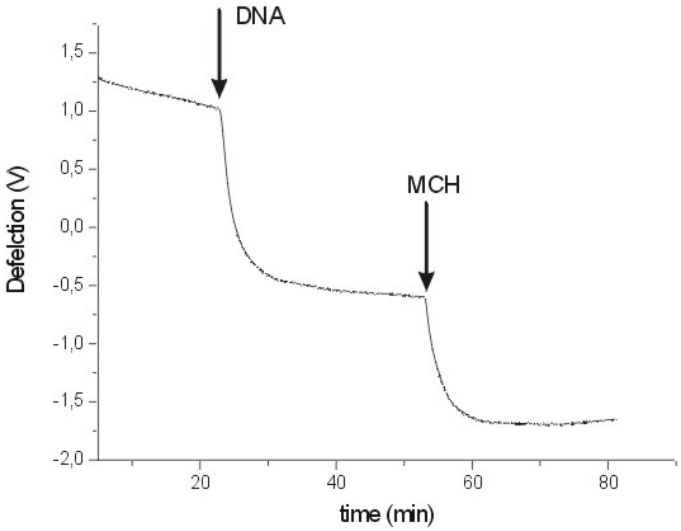

Figure 6.3: This Si_3N_4 cantilever has been treated to Ethanolamine before the measurement. The signal generated is slightly lower than expected, but still well defined.

bending. Following, Mercaptohexanol (MCH) was introduced. MCH is a spacer molecule often used in DNA detection to make the DNA molecules more accessible for hybridisation [98]. MCH can displace any un-specifically bound DNA but is not strong enough to displace specifically immobilised DNA as the thiol bond employed is very strong. Complimentary strands of DNA (cDNA) were then introduced and the hybridisation of the DNA was observed. The hybridisation is expected to generate a slight upward bending of the cantilever, but not returning it to the initial position [17]. Approximately 7 min after the introduction of a new solution, the measuring chamber was re-flowed with buffer.

The initial attempts to measure the immobilisation of DNA, were done without cleaning the cantilevers prior to measuring. Attempts had been made to clean the cantilevers in the plasma asher with a standard O_2/N_2 plasma, but the cantilevers were badly harmed by this. Therefore, no steps to clean the cantilevers were taken at the initial stage. As can be seen, the signal obtained was very small and noisy and hard to interpret, Figure (6.4).

During these measurements, it was found that a better signal was obtained from the laser by focusing through the SU-8 layer and therefore the chips were turned up-side-down in the measuring chamber. This explains why the deflection signal has been reversed in Figure (6.4). Generally, the cantilever is bent downwards upon a surface stress change, but here the deflection signal is seen to increase. It was later concluded that the signal was better

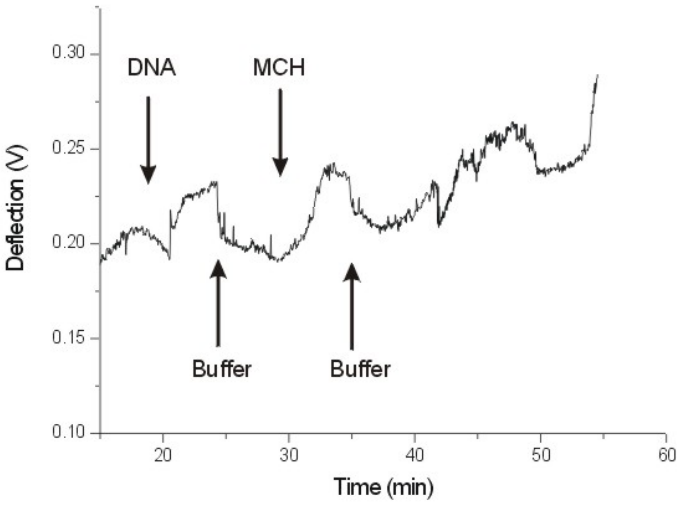

Figure 6.4: This cantilever had not been cleaned prior to measuring. The chip has been turned up-side-down, which explains the mirrored signal out-put.

when focusing through the SU-8 because that side of the Au was the cleaner one.

DNA was immobilised at a concentration of 10 nM. MCH was introduced at a concentration of 1 mM. The signal generated from the binding of both DNA and MCH is very low and the molecules are easily washed away when the buffer is entered into the chamber.

A cleaning procedure was developed as such; first the cantilevers were immersed in trichlorethylen, followed by acetone, followed by ethanol, followed by DI water. Then the cantilevers were washed with piranha (7:3 sulphuric acid:hydrogen peroxide) for 4 s and rinsed in water. Finally they were dried in a stream of N_2. The piranha had been allowed to cool down to room temperature before it was used to clean the cantilevers. After this cleaning procedure the above experiment was repeated and a much stronger signal was generated, confirming the importance of a clean Au surface for the immobilisation, Figure (6.5).

The signal for the DNA hybridisation is very small and impossible to discriminate from the noise. Therefore, it is very important to use reference cantilevers. In Figure (6.6) the drift of the laser in the measurement in Figure (6.5) has been subtracted. It can still be seen that the signal generated is too low to be conclusive. By the use of reference cantilevers, also the noise could have been subtracted and the signal might have been possible to decipher.

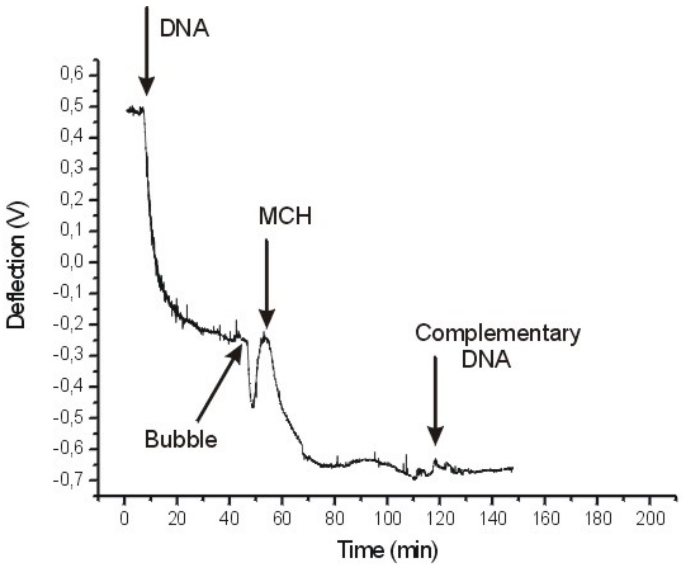

Figure 6.5: This cantilever had undergone the above cleaning procedure and a signal of 750 mV was generated for the immobilisation of 10 nM DNA. This time, there was no need to focus the laser through the SU-8. The introduction of the complementary DNA did not result in a strong signal.

6.1.4 Pesticide detection

The pesticide under investigation is Carbaryl, which is used as a general pesticide to control over 100 species of insects; for example insects which prey on fruit and crops, as well as on poultry, livestock and pets [99]. The pesticide is too small to be detected directly with this technique, as the binding on a surface would only generate a very small surface stress. Instead, *competitive immuno-assay* needs to be applied. This is a rather complicated method, involving several steps. The pesticide is bound to another protein, ovoalbumin (OVA), forming a hapten[1]. The antibody of the hapten is a monoclonal antibody manufactured at the Bioengineering Laboratory LIB-UPV, Valencia, which can be detected by the set-up.

The preparation of the immuno-assay is a process in three steps and all stages were successfully accomplished.

1. First, by introducing a solution of mecaptoundecanoic acid in ethanol into the measuring chamber the Au on the cantilever gets a thiol group attached to it. This allows the binding of the hapten.

[1]This is the name of the combined Carbaryl and OVA protein.

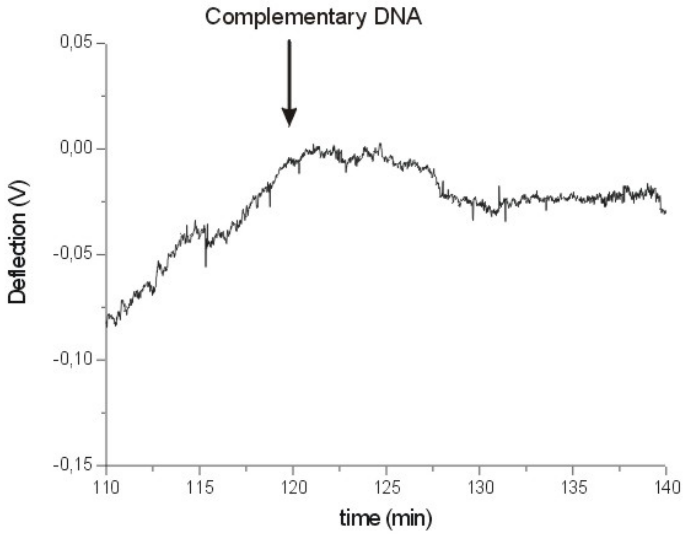

Figure 6.6: The signal from the DNA hybridisation is too small to be detected. By the use of a reference cantilever, the noise can be subtracted and the hybridisation signal discriminated.

2. The measuring chamber is then flowed with etyl dimetyl carbamide (EDC) and H-hydroxysuccinide (NHS) in water. This is done to stabilize the thiol layer.

3. Last, the hapten is introduced into the measuring chamber. Then, the cantilever has been sensitised.

A solution containing antibodies is then introduced. The antibodies will react with the haptens, resulting in a bending of the cantilever. If the Carbaryl is present in the solution, the antibodies will bind to these instead, and not to the cantilever, and thereby no signal will be generated from the cantilever. This is the principle of *competitive immuno-assay.*

Measurements need to be done to control every step of the preparation for the final immuno-assay. It was started with immobilising the hapten on the cantilevers and introducing the antibody, Figure (6.7).

A control experiment was done, to make sure the signal generated from the above measurement was not due to an un-specific reaction, Figure (6.8). Buffer is introduced into the measuring chamber approximately 7 min after the introduction of the different antibodies. The signal generated from the specific binding is twice that of the unspecific binding.

Attempts were made to complete the competitive immuno-assay by introducing a solution containing both the pesticide and the antibody of the

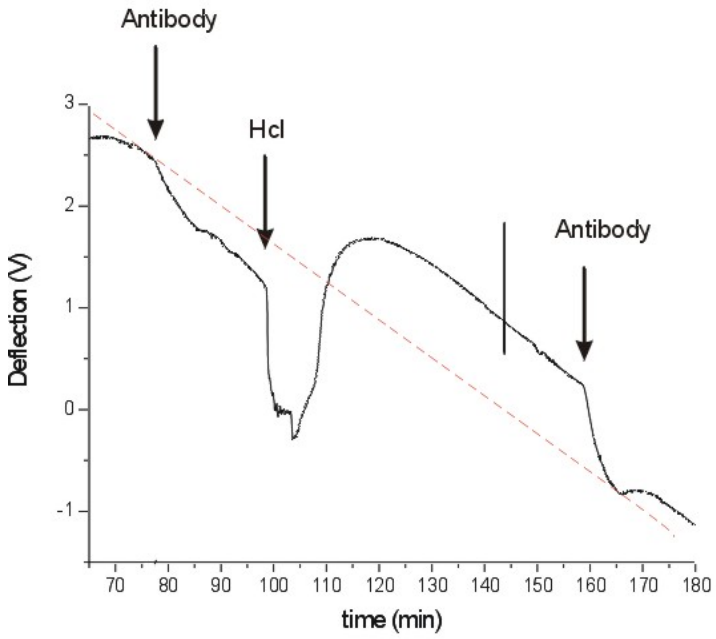

Figure 6.7: The antibody can be washed away with 0.1 M HCl, leaving a regenerated layer of the hapten. The reaction can be repeated on the same cantilever for several cycles. The red line represents the drift of the laser signal.

pesticide.The results were not conclusive since the un-specific absorption was introducing too much noise in the signal.

6.2 Channel measurements

In Section (6.2.1), attempts are made to show the dependence on the contact angle of the SU-8, though it was never possible to exactly determine the rate of liquid flow in the channels. The channels were also used in combination with the cantilevers to show the function of sensitising the cantilevers. This was done by un-specific binding of DNA labelled with fluorescence markers, which is described in Section (6.2.2).

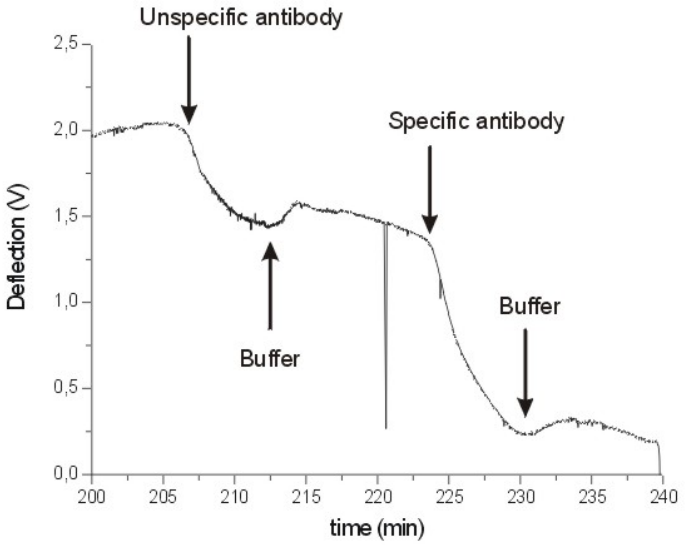

Figure 6.8: To make sure that the observed signal is generated as a result of a specific binding, a control experiment is done.

6.2.1 Liquid Flow

The contact angle of cross-linked SU-8 is just around 90°. The contact angle is a very sensitive parameter and is influenced by external factors such as surface roughness. In some of the channels, liquid was seen to flow through the channels but very slowly. However, the liquid never managed to enter and exit the measuring sites even if it could flow through the channels.

Upon releasing the channel chip from the wafer, the value of θ_c decreased to 50° but the liquid entered in the reservoir still does not manage to flow through the measuring sites, Figure (6.9).

It is crucial for the channel chip to serve its purpose that it manages to lead the liquid into the measuring sites. By reducing the contact angle further, down to 20° by treating the channels to Ethanolamine, the liquid can be seen to quickly flow into and out of the sites. In Figure (6.10) the middle and right-most reservoir can be seen to be filled with liquid. The picture was taken during the experiment described in Section (6.2.2) where the channel chip was used.

6.2.2 Sensitising of cantilevers

The channel chip is intended be used in combination with the cantilever chip, to sensitise them for specific chemical bindings. It was seen in Section (6.1.4) that molecules can also bind un-specifically to a surface. In this experiment,

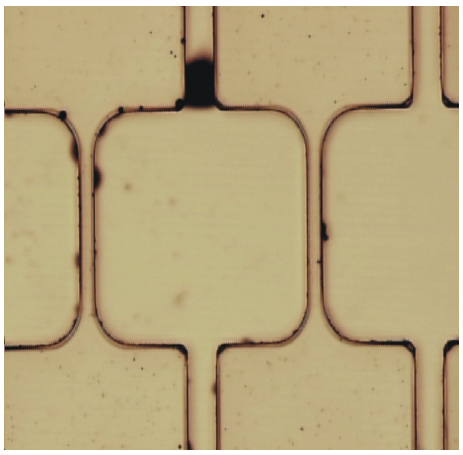

Figure 6.9: The contact angle is $\sim 50^{\circ}$ and the liquid does not enter into the measuring sites.

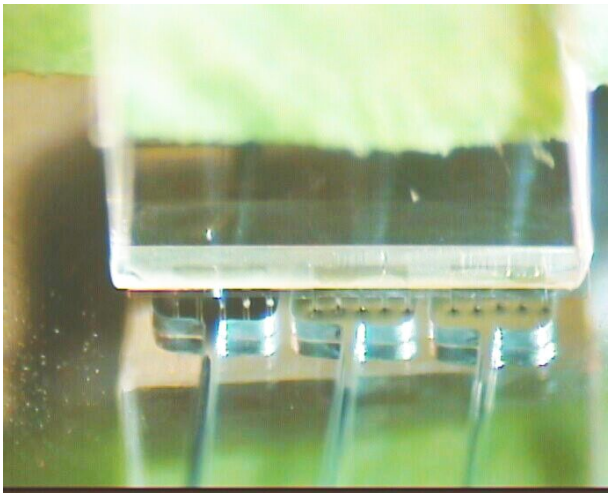

Figure 6.10: Once value of θ_c has been reduced sufficiently, the liquid can enter the measuring sites.

advantage has been taken of the latter fact, to show the importance of the first. On each chip there are three groups of cantilever arrays constituting of five cantilevers each. By sensitising two groups differently and leaving the third non-treated, they can be used to detect two different molecules in a solution simultaneously. At the same time, there is one group of cantilevers to be used for reference.

A micro-positioner was used to move the cantilever chip into position with the channel chip after the channels had been treated with Ethanolamine to achieve a low contact angle.

The first group of cantilevers was treated to 20 µL of 50'mer long DNA, diluted in DI water to a concentration of 1 µM (Sigma Aldrich). The DNA was labelled with a Cy3 fluorescent marker. The solution was deposited into the reservoir by the use of a micro-pipette and in Figure (6.11) the liquid can be seen at the measuring site.

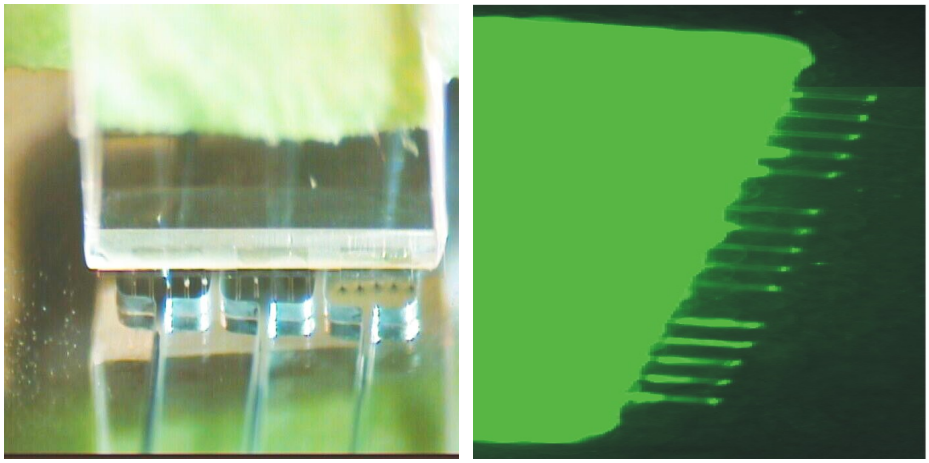

Figure 6.11: *Left:* The solution passed through the measuring site, binding un-specifically to the cantilevers. *Right:* It is clearly seen that it was the first group of cantilevers that was labelled with the Cy3 marker.

The middle group of cantilevers was treated to 10 µL of 25'mer long DNA, diluted in DI water at a concentration of 1 µM (Sigma Aldrich). As the needed amount of solution was un-known to achieve the best results, a less amount was used for the second occasion. This DNA was labelled with a Cy5 fluorescent marker and the experiment can be seen in Figure (6.12).

The third group of cantilevers was not treated in any way, as to be used as a reference group. The chip was rinsed in DI water for a few minutes and scanned in a fluorescent scanner (Array Workx, Applied Precision). Different filters were used for the two scans as to be able to differ the two markers. Thick layers of SU-8 are self-fluorescent, which is why the chip support is also seen to glow.

From the results it is seen that the cantilevers labelled with the specific marker scanned for, show a significant higher fluorescence than the other cantilevers, Figure (6.11) and (6.12). This shows the successful sensitisation of that particular array of cantilevers.

6.3 Summary

The cantilevers fabricated proved to be easy to work with. They were stabilising fast once introduced into a liquid environment and a good laser spot

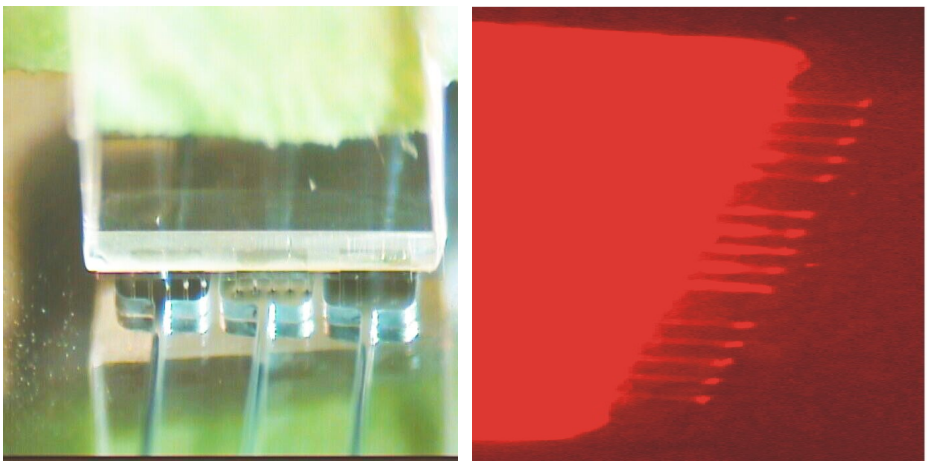

Figure 6.12: *Left:* The solution passed through the measuring site, binding un-specifically to the cantilevers. *Right:* It is clearly seen that it was the middle group of cantilevers that was labelled with the Cy5 marker.

reflection was achieved. Comparing to the conventional Si_3N_4 cantilevers used, the drift measured was much lower; 0.04 mV/min compared to 13 mV/min. This is a great advantage of the SU-8 cantilevers.

The cantilevers were used to detect the immobilisation of DNA onto the Au surface of the cantilever, generating a strong significant signal. The hybridisation of the complementary strand could not be detected, but it has proved to be very difficult to measure this reaction even with standard Si_3N_4 cantilevers, unless reference cantilevers are used. The antibody of the pesticide Carbaryl was successfully detected and could well be distinguished from an unspecific biding of another monoclonal antibody.

The aim of the project was to fabricate and to be able to measure from an array of cantilevers. This was achieved in the fluorescence measurements of DNA by un-specific binding when the cantilever chip was used in combination with the channel chip. For the measurements with the optical read-out, the read-out from several cantilevers is under development.

It was possible to show the intended purpose of the channel chip, as specific labelling was achieved on different cantilever arrays.

Chapter 7

Conclusion & Outlook

The cantilever chip with both 100 µm and 200 µm long and 1.6 µm thin cantilevers was successfully fabricated. There were prevailing difficulties with obtaining perfectly aligned cantilevers and no actual chip with three perfect arrays was fabricated. Still, the chips fabricated proved to function well as seen from the results of the measurements in Chapter 6.

The channel chips were also successfully fabricated but the original idea of keeping closed channels proved to be unnecessary. With a decreased contact angle of the SU-8 channel walls, fast liquid flow was still obtained. The chip could be used to show the concept of sensitising the cantilevers and the results from these experiments are seen in Chapter 6.

The fabrication of the two chips involved many hours in the clean room and, though they may seem straight forward, both processes proved to be full of challenges. The process sequence of SU-8 is not well understood as it is such a new material on the market and further work is definitely needed to fully understand the influence of all process parameters. Also, working with the cross-linking of polymers will always include a large number of experimental errors as the exact locations and behaviors of the monomers cannot be controlled.

Many surface properties of SU-8 were investigated and via AFM measurements, it could be concluded that the surface of the cross-linked polymer is smooth, with an average surface roughness of less than 0.5 nm. The etch rate of different plasma treatments were investigated and the resulting increases in surface roughness after such treatments were measured with AFM.

The bond strength between SU-8 and Au was investigated and the influence of different adhesion promoters were analysed. The molecule 4-ATP was proposed as an alternative adhesion promoter, increasing the SU-8/Au bond from 3.8 to 5.6 MPa. Another new wet chemical treatment of SU-8 was presented, where the contact angle of the polymer surface was greatly reduced. SU-8 was treated to Ethanolamine which reduces the contact angle by form-

ing a mono-layer on the SU-8 surface. This increases the capillary pressure of the micro channel system and induces a fast liquid flow throughout the whole system. The treatment proved to be stable with time and thereby offers a great alternative to conventional O_2 plasma treatments. The chemical reaction of Ethanolamine and SU-8 was studied with XPS measurements and the results indicate on the validity of the assumed chemical reaction.

Finding a new release layer for SU-8 fabrication is an interesting challenge for the future work. As mentioned in Chapter 2, the stress generated from the mis-match of the thermal expansion co-efficient between SU-8 and Si wafers is of major concern in the processing.

A new interesting approach to using cantilevers for biochemical detection has been taken by T.P. Burg *et al.* where they have integrated a sub-nanoliter fluidic channel in a suspended micro cantilever [100]. The approach is mainly interesting because it allows for dynamic measurements with cantilevers of molecules in liquid samples. Until now, only static measurements have been used for detection involving solutes, due to the high damping of liquids.

The work done here shows the possibilities of using cantilevers fabricated in polymer for biochemical detection systems and with further knowledge and advances of the processing techniques of SU-8, the thickness of the cantilevers can be reduced even further resulting in more sensitive cantilevers. The micro channel system proved to be useful and suitably designed. It could be used in sensitising the cantilever for specific biochemicals. This system is only intended to be used for the preparations of the cantilevers and is therefore a multiple-use system. In the future, another disposable micro channel system could be designed to be used in combination with the cantilever chip during the actual measurements. Below, Figure (7.1), an image is shown where the cantilever chips is placed lying on the channel chip to demonstrate the combined use of the two chips.

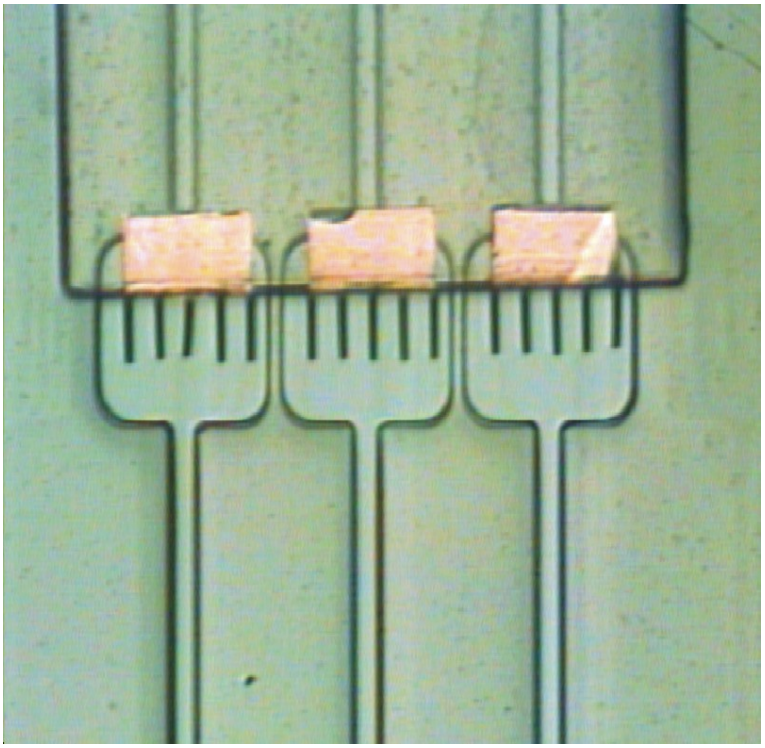

Figure 7.1: An optical image of the cantilever chip placed on the channel chip. For the actual measurements the cantilevers will be placed inside the measuring sites as seen on the front page of the Thesis.

Bibliography

[1] G. Binning *et al.*: 'Atomic Force Microscope', *Physical Review Letters*, 56(9):930-933, 1986

[2] T.R. Albrecht *et al.*: 'Microfabrication of cantilever styli for the atomic force microscope', *Journal of Vacuum Science and Technologies A*, 8(4):3386-3396, 1990

[3] R. Raiteri *et al.*: 'Measuring electrochemically induces surface stress with an Atomic Force Microscope', *Journal of Physical Chemistry*, 99:15728-15732, 1995

[4] E. Forsén *et al.*: 'Dry release of suspended nanostructures', *Submitted to MNE Conference Proceedings*, 2003

[5] Z. Davies *et al.*: 'Monolithic integration of mass sensing nanocantilever with CMOS circuitry ', *Sensors and Acuators A*, 105:311-319, 2003

[6] R. Berger *et al.*: 'Surface stress in the self-assembly of alkanethiols on gold', *Science*, 276:2021-2024, 1997

[7] P. Rasmussen: 'Cantilever-based Sensors for Surface Stress Measurements', *PhD Thesis*, MIC - Institute of Micro and Nanotechnology, Danmarks Tekniske Universitet, 2003

[8] J. Thaysen: 'Cantilever for Bio-Chemical Sensing Integrated in a Microliquid Handling System', *PhD Thesis*, MIC - Institute of Micro and Nanotechnology, Danmarks Tekniske Universitet, 2001

[9] H.P. Lang *et al.*: 'The Nanomechanical NOSE', *IEEE*, :9-13,1999

[10] T. Thundat *et al.*: 'Detection of mercury vapor using resonating microcantilevers', *Applied Physics Letters*, 66(13):1695-1697, 1995

[11] J.K. Gimzewski *et al.*: 'Observation of a chemical reaction using a micromechanical sensor', *Chemical Physics Letters*, 217:589-594, 1994

[12] M.K. Baller *et al.*: 'A cantilever array-based artificial nose', *Ultramicroscopy*, 82:1-9, 2000

[13] H.-J. Butt: 'A sensitive method to measure changes in the surface stress of solids', *Journal of Colloid and Interface science*, 180:251-260, 1996

[14] G.Y. Chen *et al.*: 'Resonance response of scanning force microscopy cantilevers', *Review of Scientific Instruments*, 65(8):2532-2537, 1994

[15] G. Wu *et al.*: 'Origin of nanomechanical cantilever motion generated from biomolecular interactions', *PNAS*, 98(4):1560-1564, 2001

[16] www.protiveris.com

[17] J. Fritz *et al.*: 'Translating biomolecular recognition into nanomechanics', *Science*, 288:316-318, 2000

[18] R. Raiteri *et al.*: 'Micromechanical cantilever-based biosensors', *Sensors and Actuators B*, 79:115-126, 2001

[19] M. Calleja *et al.*: 'Polymeric cantilever arrays for biosensing applications', *Sensor Letters*, 1:1-5, 2003

[20] S.J. O'Shea *et al.*: 'Atomic force microscopy stress sensors for studies in liquids', *Journal of Vacuum Science and Technologies B*, 14(2):1383-1385, 1996

[21] G. Meyer *et al.*: 'Erratum: Novel optical approach to atomic force microscopy', *Applied Physics Letters*, 53:2400-2402, 1988

[22] A. Manz *et al.*: 'Minituarized Total Chemical Analysis Systems: a Novel Concept for Chemical Sensing', *Sensors and Actuators B*, 1:244-248, 1990

[23] F. Fujii: 'PDMS-based microfluidic devices for biomedical applications', *Micrelectronic Engineering*, 61/62:907-914, 2002

[24] J.P. Brody *et al.*: 'Diffusion-based extraction in a microfabricated device', *Sensors and Actuators A*, 58:13-18, 1997

[25] A.D. Stroock *et al.*: 'Chaotic Mixer for Microchannels', *Science*, 295:647-651,2002

[26] J.M. Shaw *et al.*: 'Negative photoresists for optical lithography', *IBM J. Res. Develop.*, 41:81-94, 1997

[27] G. Genolet *et al.*: 'Soft, entirely photoplastic probes for scanning force microscopy', *Review of Scientific Instruments*, 70:2398-2401, 1999

[28] www.microchem.com

[29] L. Dellmann *et al.*: 'Fabrication process of high aspect ratio elastic and SU-8 structures for piezoelectric motor applications', *Senosrs and Actuators A*, 70:42-47, 1998

[30] G. Voskerician *et al.*: 'Biocompatibility and biofouling of MEMS drug delivery devices', *Biomaterials*, 24:1959-1967, 2003

[31] H. Lorentz *et al.*: 'Mechanical Characterization of a New High-Aspect-ratio Near UV-Photoresist', *Microelectronic Engineering*, 41/42:371-374, 1998

[32] S. Arscott *et al.*: 'Terahertz time-domain spectroscopy of films fabricated from SU-8', *Electronics Letters*, 35:243-244, 1994

[33] C.-H. Lin *et al.*: 'Micro capillary electrophoresis chips integrated with buried SU-8/SOG optical waveguides for bio-analytical applications', *Sensors and Actuators A*, 107:125-131, 2003

[34] H. Lorentz *et al.*: 'High-aspect-ratio, ultrathick, negative-tone near-UV photoresist and its applications for MEMS', *Sensors and Actuators A*, 64:33-39, 1998

[35] M. Despont *et al.*: 'High-aspect-ratio, ultrathick, negative-tone near-UV photoresist for MEMS applications', *IEEE, Conference Proceedings*, pp. 518-522, 1997

[36] H. Lorentz *et al.*: 'SU-8: a low-cost negative resist for MEMS', *Journal of Micromechanics and Microengineering*, 7:121-124, 1997

[37] L. Dellmann *et al.*: 'Fabrication process of high aspect ratio elastic structures for piezoelectric motor applications', *IEEE, Proceedings of Transducers*, pp. 641-644, 1997

[38] H.S. Khoo *et al.*: 'Mechanical strength and interfacial failure analysis of cantilevered SU-8 microposts', *Journal of Micromechanics and Microengineering*, 13:822-831, 2003

[39] A. Johansson: 'Cantilever platform for biowire', *Master Thesis*, MIC - Institute of Micro and Nanotechnology, Danmarks Tekniske Universitet, 2002

[40] C. Luo *et al.*: 'A New Method to Release SU-8 Structures Using Polystyrene for MEMS Applications', *Transducers Conference Proceedings, 2002*, pp. 168-171

[41] R. Feng *et al.*: 'Influence of processing conditions on the thermal and mechanical properties of SU-8 negative photo resist coatings', *Journal of Micromechanics and Microengineering*, 13:80-88, 2003

[42] N.C. Labianca *et al.*: *Elec. Soc. Proc.*, 95(18):386, 1993

[43] L.J. Guérin *et al.*: 'Simple and low cost fabrication of embedded microchannels by using a new thick-film photoplastic', *IEEE Conference Proceedings of Transducers*, pp. 1419-1421, 1997

[44] G. Genolet: 'New photoplastic fabrication techniques and devices based on high aspect ratio photoresist', *PhD Thesis*, École Polytechnique Fédérale de Lausanne, Lausanne, 2001

[45] J. Zang *et al.*: 'Characterization of the polymerization of SU-8 photoresist and its applications in miro-electro-mechanical systems.', *Polymer Testing*, 20:693-701, 2001

[46] P.J. Ross: 'Taguchi techniques for quality engineering: Loss function, Orthogonal experiments, Prarmeter and Tolerance design', McGraw-Hill, New York 1996

[47] Y.-J. Chuang *et al.*: 'A novel fabrication method of embedded microchannels by using SU-8 thick-film photo-resist', *Sensors and Actuators A*, 103:64-69, 2003

[48] Y.-J. Chuang *et al.*: 'Reduction of diffraction effect of UV exposure on SU-8 negative thick photo-resist by air gap elimination', *Microsystem Technologies*, 8:308-313, 2002

[49] C. Beuret *et al.*: 'Microfabrication of 3D multidirectional inclined structures by UV lithography and electroplating', *Proceedings of IEEE International Workshop on Micro Electro Mechanical System, Oiso, Japan*, pp. 81-85, 1994

[50] H. Sato *et al.*: 'A novel fabricaion of in-channel-3D micromesh structures using maskless multi-angle exposure and its microfilter application.', *Conference Proceedings, IEEE*, pp. 223-226, 2003

[51] Y.-K. Yoon *et al.*: 'Integrated vertical screen microfilter system using inclined SU-8 structures', *MEMS Conference Proceedings, IEEE*, pp. 227-230, 2003

[52] M. Han *et al.*: 'Fabrication of 3D microstructures with inclined/rotated UV lithography', *Conference Proceedings, IEEE*, pp. 554-557, 2003

[53] M.J. Madou: 'Fundamentals of Microfabrication', 2nd edition, CRC Press, 2002

[54] O. Hansen: 'Stoney's Formula', *Teaching material*, MIC - Institute of Micro and Nanotechnology, Danmarks Tekniske Universitet, 2000

[55] T.W. Madsen & M.E. Larsen: 'Production of cantilevers in SU-8 polymer', *3-week-course report*, MIC - Institute of Micro and Nanotechnology, DTU, 2003

[56] J.E. Sader: 'Frequency response of cantilever beams immersed in viscous fluids with applications to the atomic force microscope', *Journal of Applied Physics*, 84(1):64-76, 1998

[57] G.G. Stoney: 'The Tension of Metallic Films Deposited by Electrolysis', *Proceedings of the Royal Society of London*, 82(553):172-175, 1909

[58] B.J. Kim *et al.*: 'A self-assembled monolayer-assisted surface microfabrication and release technique', *Microelectronic Engineering*, 57/58:755-760, 2001

[59] Z.-Y. Guo *et al.*: 'Size effect on single-phase channel flow and heat transfer at microscale', *International Journal of Heat and Fluid Flow*, 24:284-298, 2003

[60] J.N Pfahler: 'Liquid Transport in Micron and Submicron Size Channels', *PhD Thesis*, University of Pennsylvania, 1992

[61] M. J. Jensen: 'Bubbles in microchannels', *Master Thesis*, MIC - Institute of Micro and Nanotechnology, Danmarks Tekniske Universitet, 2002

[62] M.J. Jensen *et al.*: 'The clogging pressure of large bubbles in microchannel contractions', *Sent for publication to Phys. Rev. E*, 2003

[63] E. Kim *et al.*: 'Imbibition and Flow of Wetting Liquids in Noncircular Capillaries', *Journal of Physical Chemistry B*, 101(6):855-863, 1997

[64] P.G. de Gennes: 'Wetting: statics and dynamics', *Reviews of Modern Physics*, 75(3):827-863, 1985

[65] M. Dong *et al.*: 'The Imbibition and Flow of a Wetting Liquid along the Corners of a Square Capillary Tube', *Journal of Colloid and Interface Science*, 172:278-288, 1995

[66] D.S. Kim *et al.*: 'Micro-channel filling flow considering surface tension effect', *Journal of Micromechanics and Microengineering*, 12:236-246, 2002

[67] S. Shoji *et al.*: 'Microflow devices and systems', *Journal of Micromechanics and Microengineering*, 4:157-171, 1994

[68] N. Goedecke *et al.*: 'Evaporation driven pumping for chromatography application', *Lab on a Chip*, 2:219-223, 2002

[69] V. Namasivayam *et al.*: 'Transpiration-based micropump for delivering continuous ultra-low flow rates', *Journal of Micromechanics and Microengineering*, 13:261-271, 2003

[70] K.E. Petersen *et al.*: 'Toward Next Generation Clinical Diagnostic Instruments: Scaling and New Processing Pardigms', *Clinical Diagnostic Instruments*, :71-79, 1998

[71] H.-K. Chang *et al.*: 'UV-LIGA process for high aspect ratio structure using stress barrier and C-shaped etch hole', *Sensors and Actuators A*, 84:342-350, 2000

[72] C.-H. Lin *et al.*: 'A new fabrication process for ultra-thick microfluidic microstructures utilizing SU-8 photoresist', *Journal of Micromechanics and Microengineering*, 12:590-597, 2002

[73] R.J. Jackman *et al.*: 'Microfluidic systems with on-line UV detection fabricated in photodefinable epoxy', *Journal of Micromechanics and Microengineering*, 11:263-269, 2001

[74] M.O. Heuschkel *et al.*: 'Buried micro channels in photopolymer for delivering of solutions to neurons in a network', *Sensors and Actuators B*, 48:356-361, 1998

[75] E.A. Shields *et al.*: 'Electron-beam lithography for thick refractive optical elements in SU-8', *Journal of Vacuum Science and Technologies B*, 21(4):1453-1458, 2003

[76] V. Kudryashov *et al.*: 'Grey scale structures formation in SU-8 with e-beam and UV', *Microelectronic Engineering*, 67/68:306-311, 2003

[77] F.E.H. Tay *et al.*: 'A novel micro-machining method for the fabrication of thick-film SU-8 embedded micro-channels', *Journal of Micromechanics and Microengineering*, 11:27-32,2001

[78] T. Nielsen: 'Nanoimprint Lithography', *Master Thesis*, MIC - Institute of Micro and Nanotechnology, Danmarks Tekniske Universitet, 2003

[79] B. Bilenberg *et al.*: 'PMMA to SU-8 Bonding for Polymer Based Lab-on-a-chip Systems with Intergrated Otics', *Eurosensors Conference Proceedings, 2003*

[80] C.-T. Pan *et al.*: 'A low-temperature wafer bonding technique using patternable materials', *Journal of Micromechanics and Microengineering*, 12:611-615, 2002

[81] E-mail from MicroChem.

[82] W.A. Germishuizen *et al.*: 'Dielectrophoretic manipulation of surface-bound DNA', *Nanobiotechnnology Conference Proceedings*, pp. 54-58, 2003

[83] Conversation with PhD student Rodolphe Marie, Bioprobes Group, MIC - Institute of Micro and Nanotechnology, Danmarks Tekniske Universitet

[84] B. Bilenberg: 'Technology for Integrated Optics on Lab-on-a-chip Microsystems', *Master Thesis*, MIC - Institute of Micro and Nanotechnology, Danmarks Tekniske Universitet, 2003

[85] H.D. Young & R.A. Freedman, 'University Physics', 9th edition, Addison-Wesley, New York, 1996

[86] S.D. Senturia: 'Microsystem Design', Kluwer Academic Publishers, 2001

[87] Optimisations of Si etch rate with CF_4 plasma by Jack Jonsman, MIC - Institute of Micro and Nanotechnology, Danmarks Tekniske Universitet

[88] B.-L. Johansson *et al.*: 'Characterization of Air Plasma-Treated Polymer Surfaces by ESCA and Contact Angle Measurements for Optimization of Surface Stability and Cell Growth', *Journal of Applied Polymer Science*, 86:2618-2625, 2002

[89] S.A. Pirzada *et al.*: 'Plasma Treatment of Polymer Films', *Society of Vacuum Coaters, Conference Proceedings*, pp. 301-306, 1999

[90] N. Iranpoor *et al.*: 'Ceric Ammonium Nitrate, an Efficient Catalyst for Mild and Selective Opening of Epoxides in the Presence of Water, Thiols and Acetic acid', *Tetrahedron*, 47:9861-9866, 1991

[91] N. Iranpoor *et al.*: 'Ceric Ammonium Nitrate: a Mild and Efficient Reagent for Conversion of Epoxides to β-Nitrato Alcohols', *Tetrahedron*, 51:909-912, 1995

[92] C.-L. Wu *et al.*: 'SU-8 hydrophilic modification by forming Copolymer with Hydrophilic Epoxy Molecule', *μTAS Conference Proceedings*, pp. 1117-1120, 2003

[93] I. Chorkendorff: 'The XPS and AES Method for Surface Analysis in Material Science', Physics Department, Technical University of Denmark, 1994

[94] B.V. Crist: 'Handbook of Monochromatic XPS Spectra', Wiley, 2001

[95] N. Völcker *et al.*: 'Functionalization of Silicone Rubber for the Covalent Immobilization of Fibronectin', *Journal of Materials Science: Materials in Medicine*, 12:111-119, 2001

[96] J.F. Watts *et al.*: 'Segregation and Crosslinking in Urea Formaldehyde/Epoxy Resin: a Study by High-resolution XPS', *Journal of Electron Spectroscopy and Related Phenomena*, 121:233-247, 2001

[97] P.M. Dentinger *et al.*: 'Removal of SU-8 photoresist for thick film applications', *Microelectrinoc Engineering*, 61/62:993-1000, 2002

[98] M. Holmberg *et al.*: 'Hybridisation of Short DNA Molecules Investigated with *in situ* Atomic Force Microscopy', *Ultramicroscopy*, 97:257-261, 2003

[99] http://pmep.cce.cornell.edu/profiles/extoxnet/carbaryl-dicrotophos/carbaryl-ext.html

[100] T.P. Burg *et al.*: 'Suspended microchannel resonators for biomolecular detection', *Applied Physics Letters*, 83(13): 2698-2700, 2003